

FACULTY OF ENGINEERING
DEPARTMENT OF ELECTRICAL ENGINEERING (ESAT)
MICAS - Microelectronics & Sensors
Kasteelpark Arenberg 10 box 2440
B-3001 HEVERLEE, BELGIUM
tel: +32 16 321130
info@esat.kuleuven.be
www.esat.kuleuven.be



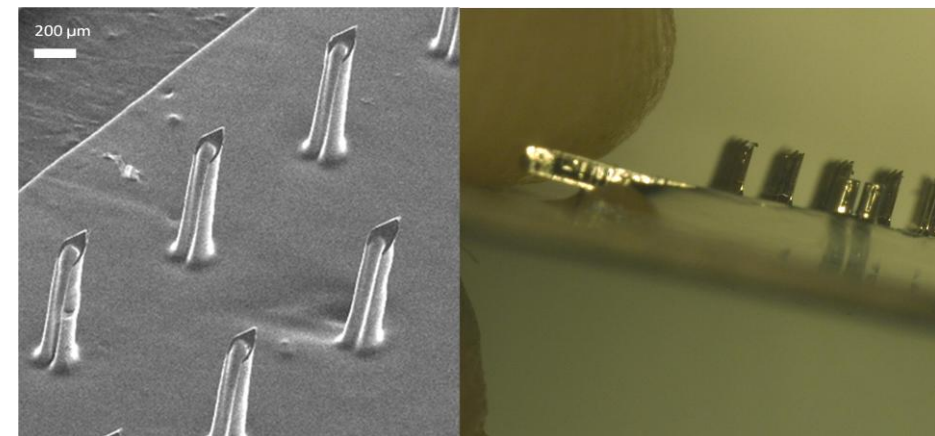
Buddhadev PAUL
CHAUDHURI

KU LEUVEN

ARENBERG DOCTORALSCHOOL
FACULTY OF ENGINEERING

A POLYMER-BASED TRANSDERMAL DRUG DELIVERY SYSTEM USING MICRONEEDLES

Buddhadev PAUL CHAUDHURI



Promotors:
Prof. Dr. R. Puers
Prof. Dr. C. Van Hoof

Dissertation presented in partial
fulfillment of the requirements for the
degree of Doctor of Engineering



The author, popularly known as “Buddha” among his friends, peers and supervisors, hails from India where he completed his Electronics and Communications engineering from the famed Vellore Institute of Technology. He then pursued a Dual Masters of Science program in Microsystems Engineering at Ecole Supérieure d’Ingenieurs en Electrotechnique et Electronique (ESIEE), Paris (France) and Nanyang Technological University (NTU), Singapore. Following this, he commenced his Ph.D. at IMEC / KULeuven in the area of biomedical microsystems. His other areas of interest include powerMEMS, microbatteries and microrobotics. Apart from research, he takes active interests in a host of diverse activities such as Latino dancing, golf, writing poetry, playing tennis, cooking and participating in business plan competitions. He is also currently the Social Chair of the PhD Society Leuven. For any queries, he can always be reached at buddhadevpc@gmail.com.

ISBN 978-94-6018-616-5
D / 2012 / 7515 / 147

A POLYMER-BASED TRANSDERMAL DRUG
DELIVERY SYSTEM USING MICRONEEDLES

December 2012

December 2012



KATHOLIEKE UNIVERSITEIT LEUVEN
FACULTEIT INGENIEURSWETENSCHAPPEN
DEPARTEMENT ELEKTROTECHNIEK
AFDELING ESAT – DIVISIE MICAS
Kasteelpark Arenberg 10, B-3001 Leuven, België

A POLYMER-BASED TRANSDERMAL DRUG DELIVERY SYSTEM USING MICRONEEDLES

Jury:

Prof. Dr. Y. Willems, *Chair*
Prof. Dr. R. Puers, *Promotor*
Prof. Dr. C. Van Hoof, *Promotor*
Prof. Dr. J. Van Humbeeck, *Secretary*
Prof. Dr. C. Bartic
Prof. Dr. V. Preat (Université catholique de Louvain)
Dr. C. O'Mahony (Tyndall National Institute, Ireland)

Dissertation presented in partial
fulfillment of the requirements for
the degree of "Doctor in de
Ingenieurswetenschappen"
by:

Buddhadev PAUL CHAUDHURI



In collaboration with

imec vzw

Interuniversitair Micro-Elektronica Centrum vzw
Kapeldreef 75
3001 Leuven, Belgium

December 2012

Cover: The left picture shows an SEM image of an array of fabricated polymer microneedles with sharp, bevel-shaped tips with slits running through their entire lengths. The microneedles are standing out-of-plane on a platform made of the same material, and are about 600 μm in height. For more details see Figure 4.40.

The right picture depicts the author holding the fabricated array of microneedles between his index finger and thumb, the relative heights of the microneedles w.r.t. the author's index finger thickness can be made out here. For more details, see Figure 5.21.

© 2012 Katholieke Universiteit Leuven – Faculty of Engineering,
Arenberg Doctoraatsschool, W. de Croylaan 6, 3001 Heverlee, België

Alle rechten voorbehouden. Niets uit deze uitgave mag worden vermenigvuldigd en/of openbaar gemaakt worden door middel van druk, fotokopie, microfilm, elektronisch of op welke andere wijze ook zonder voorafgaandelijke schriftelijke toestemming van de uitgever.

All rights reserved. No part of the publication may be reproduced in any form by print, photoprint, microfilm, electronic or any other means without written permission from the publisher.

ISBN 978-94-6018-616-5
D / 2012 / 7515 / 147

काममय एवायं पुरुष इति।

स यथाकामो भवति तत्क्रतुर्भवति।

यत्क्रतुर्भवति तत्कर्म कुरुते।

यत्कर्म कुरुते तदभिसंपद्यते॥

*kāmamaya evāyaṃ puruṣa iti |
sa yathākāmo bhavati tatkratur bhavati |
yatkratur bhavati tat karma kurute |
yat karma kurute tad abhisampadyate //*

English translation of above Sanskrit quote:

*You are what your deep, driving desire is
As your desire is, so is your will
As your will is, so is your deed
As your deed is, so is your destiny*

~ Brihadaranyaka Upanishad 4.4.5

*To the giants on whose shoulders I have stood thus far,
To the heads that guided me in raising the bar,
The hearts that sustained my lows, helping me cope,
To the celestial powers for granting me might and hope!*

Abstract

Transdermal drug delivery is one of the alternative routes for delivery of drugs in order to circumvent the first-pass metabolism of the gastro-intestinal (GI) tract. “Microneedles”, which is the object of this research, forms one of the several methods for transdermal drug delivery. Of the several advantages that microneedles offer over the other available methods, a primary one is its lack of restriction on the molecular size of the drug being delivered. Thus, large molecule drugs can be delivered which is not possible with many of the other methods. It can be made by low-cost processes on a large scale and its usage could be relatively simple by a patient, compared to other methods.

In this research, a mosquito’s fascicle has been the original source of inspiration. Subsequently, the designed microneedle tip is bevel-shaped like that of the mosquito. The state-of-the-art research in microneedles is reviewed and the gap in the research defined. Thus, the objective of this work is to design and fabricate out-of-plane, high-aspect ratio, hollow, polymer microneedles with sharp tips on a platform by following a step-by-step monolithic fabrication approach comprising moulding and photolithography techniques. The structural material selected for making the microneedles and its adjoining platform, is an epoxy-based photopatternable polymer called SU-8. Essentially, SU-8 is moulded on a pre-etched Si mould and patterned by UV radiation to form the microneedle shafts and the base platform. Thus, no Deep Reactive Ion Etching (DRIE) techniques are employed here. A novel anti-reflective coating of Cr-black is used here for the first time to prevent internal cross-linking of the microneedle bore. Innovative shapes of microneedle tips and cross-sections together with the achieved high-aspect ratio structures and sharp tips, sets this work apart from other similar works performed in the field.

Further, tests and characterizations on the fabricated microneedle arrays shows that the microneedles are quite strong (average compressive failure force of about 235 mN per microneedle while skin insertion force for microneedle of similar dimensions is about 100 mN) in spite of their high-aspect ratio design. The hollow lumens of the microneedles are also continuous through the thickness of the platform resulting in openings on the rear side of the platforms. A basic though novel applicator has been designed for integration with the fabricated microneedles. Using this, it was demonstrated by a microfluidic test that the microneedles are open throughout their entire shaft lengths. Furthermore, preliminary cytotoxicity

tests performed on the fabricated microneedle arrays strongly indicate that the structural material SU-8 used here is non-toxic.

Contact Author: *buddha@imec.be*

Samenvatting

Het toedienen van medicijnen doorheen de huid is één van de mogelijkheden om vertering van hiervoor gevoelige stoffen in het gastro-intestinaal systeem te vermijden, wat bij orale inname een probleem kan zijn.

Eén van de mogelijkheden om doorheen de huid toe te dienen is met behulp van micronaaldjes, het onderwerp van deze thesis. Dit biedt verschillende voordelen tegenover andere methoden, zoals pijnloosheid en het niet onderhevig zijn aan een beperking op de moleculegrootte van het toegediende geneesmiddel. Dit is vaak een probleem bij andere methoden. Verder is fabricatie in grote hoeveelheden relatief goedkoop en is het gebruik eenvoudig.

De micronaaldjes gepresenteerd in dit onderzoekswerk zijn geïnspireerd door het de naald van de steekmug, en heeft een ontwerp met o.a. gelijkaardige afschuining.

In dit werk wordt eerst de stand der techniek op het gebied van micronaald fabricatie en mogelijke verbeteringen besproken. Het doel van het onderzoek wordt dan scherpgesteld: het fabriceren van slanke, scherpe, holle polymeer micronaaldjes op een platform met behulp van lithografische technieken die goed opschalen.

Het geselecteerde materiaal is het fotopatroneerbaar epoxy SU-8. In essentie komt het fabricatieproces neer op het lithografisch patroneren van SU-8 op een silicium mal, die uitgeëtste holtes bevat die de scherpe bovenkant van de micronaaldjes definiëren. Het gebruik van een chromium zwart anitreflectieve laag is geïntroduceerd om ongewenste patronen, bijvoorbeeld het opvullen van de holle naaldjes, ontstaan door reflecties tijdens SU-8 lithografie te vermijden.

Door de vernieuwingen op fabricatiegebied waardoor zeer grote hoogte-breedteverhoudingen en scherpes mogelijk werden bij lithografische fabricatie en innovatief ontwerp werd de stand der techniek verbeterd.

Tijdens tests bleken de micronaaldjes voldoende sterk (breekspanning rond de 235 mN per naaldje) ondanks het slanke en hoge profiel. Stromingstests bewijzen verder de goede werking van de gefabriceerde naaldjes, en het ontbreken van blokkeringen. Tenslotte wijzen eerste testen op cytotoxiciteit uit dat het gebruikte materiaal niet toxisch is.

Preface & Acknowledgement

It gives me immense pleasure to write this section, a penultimate stage before my public defence. The fact that I'm already here means that the past four years have simply rushed by and only in hindsight can I say that it has been the most exhilarating roller-coaster ride of my life so far! I must state here that what started off as an attempt to create a “wearable fore-warning system for blockage of arteries using microsystem technology” based on a feed-back based system, gradually got channelled into “microneedles-on-patch”. Literature reviews showed that indeed this had been an active area of research for about a decade. So the path of selecting a research topic within this increasingly crowded field was as arduous as navigating a complex maze. Nevertheless, a suitable research problem was identified and the unmet need defined. Now, when I look back at the time of commencing this research, I realize how naive I had been about underestimating the challenges involved in this work, how I had thought that mimicking nature would be so much simpler. Indeed, nature does boast of some of the most advanced and amazing engineering examples, which continue to inspire the scientist in me till date.

However, I'm happy that I have been finally successful in accomplishing my research goal and that the microneedles fabricated have met the target specifications set out initially. Of course, this would not have been possible without the help of a few people who I shall proceed to thank here. First and foremost, I should like to thank my promotors, Prof. Bob Puers and Prof. Chris Van Hoof for their unstinted support during my entire tenure of the PhD. I express my sincerest gratitude to Bob for being willing to be my promotors and having faith in me and my abilities, especially when the research results were below expectations, for guiding me throughout from beginning till end systematically, and for bearing with my “last-minute-deadline shifting” actions. This work, in its present form, certainly wouldn't have been possible without Bob's constant guidance. In the same breath, I thank Chris for providing the necessary encouragement and critique of my work, for believing in me, for advising me whenever I needed it most and for according me ample opportunities to attend international conferences to broaden my exposure. Thank you so much, both Bob and Chris – you were like the sun and water needed for me, the plant, to grow and flower!

If they were the sun and water, Dr. Frederik Ceysens was the oxygen without which I would have surely not survived. Frederik, my daily supervisor-cum-mentor-cum-friend with whom I enjoy a fantastic working relationship, supported me throughout and helped me brainstorm for

solutions on problems and issues faced. His ever enthusiastic spirit, clarity of thinking, zeal for research and immense patience never failed to inspire me. Besides Frederik, I am thankful for the extensive help and support I have received from the entire MICAS team, especially, Martin, Wen, Tiannan, Philippe, Grim, Pieter, Michel, Tony, Noella and Thomas.

I am really grateful to Piet de Moor and Kris Baert of IMEC for firstly selecting me to do a PhD here at IMEC / KULeuven. I thank Piet for our discussions during my initial starting phase. I also take this opportunity to thank Herc Neves for providing me great motivation and for the very interesting application-based discussions for the microneedles. Next, a sincere word of gratitude for Mario Gonzalez, Kris Vanstreels and Myriam Van de Peer for assisting me with the mechanical tests and subsequent analysis. In this regard, I would also like to thank Tiannan Guan for helping me with the mechanical measurements at the Mechanical Engineering department. I shall not hesitate to thank my colleagues and former colleagues at IMEC who have always supported me in my research efforts: Francois Iker, Antonio la Manna, Philippe Soussan and the entire team comprising Thibault Boisson, Ziyang Wang, Anne Jourdain, Inge de Preter, Carine Gerets, Goedele Potoms and Wenqi Zhang. I also wish to thank Thomas Hantschel for providing me constant encouragement in my work and for his words of advice at the critical moments. A special word of thanks especially for my friend and colleague, Arno Aarts, for the very interesting discussions, technical insights and brain-storming sessions over coffee. I also greatly appreciate the invaluable time spent in enlightening discussions and arguments with another friend and colleague, Cristina de Joncheere, for trying to sharpen my entrepreneurial skills and business acumen. In a nutshell, I thank all my colleagues at IMEC and at MICAS in ESAT, KULeuven who have in some way or the other helped me bring my research to its present form. I once again am immensely grateful to IMEC for providing the financial support for this research, as well as to KULeuven ESAT-MICAS for providing me the support and facility to work at the MICAS cleanroom. All fabrication pertaining to this research was performed at the ESAT-MICAS cleanroom.

Needless to state, this PhD wouldn't have been the same without the unstinted support of my two dearest friends – Arindam Mallik and Gunjan Mandal – my support and lifelines during the most trying times. The lunches and the delectable dinners cooked by them infused the additional punch during this period. I also thank my dear friend Hithesh Gatty and Shubham Dutta Gupta for the very memorable times spent in my initial years of the PhD, Swaroop-*da* for taking on the role of my first personal mentor and Subhendu-*da* for advising me on the general principles of a PhD life, Sandip-*da*, Papiya-*di*, Gouri-*da* and Mitali-*di* for the mouth-watering free

lunches peppering my PhD life. I am also immensely grateful to my friends Sandeep Sangameswaran and Kamesh Mahadevan for the much needed practical tips and invaluable advice during the arduous process of writing this thesis. This acknowledgement would not be complete without a special word of thanks for my couple friend, Ashesh and Munia, for their untiring hospitality, generous open dinner invites and the endless *addas* over *chai*.

Finally, my heartfelt gratitude to my beloved family - my parents and brother, for supporting me in my endeavour to pursue my dreams, living in distant Belgium, thousands of miles away from home in India. And, last but certainly not the least, my humble obeisance at the lotus feet of my Preceptor and the Almighty without whose divine blessings, none of this might have been accomplished.

Buddhadev Paul Chaudhuri
December 11, 2012
Leuven, Belgium

Table of Contents

ABSTRACT	V
SAMENVATTING.....	VII
PREFACE & ACKNOWLEDGEMENT	IX
TABLE OF FIGURES.....	XV
LIST OF TABLES	XXIII
1 INTRODUCTION.....	1
1.1 TRANSDERMAL DRUG DELIVERY	2
1.1.1 A brief introduction	2
1.1.2 Types of transdermal drug delivery.....	4
1.1.3 Brief design considerations w.r.t. skin structure.....	5
1.1.4 Why microneedles?	6
1.2 RESEARCH GOAL	8
2 MICRONEEDLE THEORY, PRIOR ART & APPLICATIONS.....	9
2.1 WORKING PRINCIPLE – DIFFERENT ARCHITECTURES	10
2.2 PRIOR ART RESEARCH IN MICRONEEDLES	13
2.2.1 Solid microneedles.....	13
2.2.2 Solid coated microneedles	17
2.2.3 Solid dissolvable microneedles.....	18
2.2.4 Hollow microneedles	19
2.3 APPLICATIONS	23
3 DESIGN.....	27
3.1 DESIGN INSPIRATION	28
3.2 DESIGN OBJECTIVES	29
3.3 CHOICE OF STRUCTURAL MATERIAL	31
3.3.1 Material considerations.....	31
3.3.2 Final Choice of Material - SU-8	31
3.3.3 Properties of SU-8.....	32
3.4 MECHANICAL DESIGN.....	33
3.4.1 Individual Microneedle	33
3.4.2 Microneedle Array (MNA).....	38
4 PROCESS DESIGN & FABRICATION	41
4.1 INTRODUCTION TO THE PROCESS.....	42
4.2 GOALS & CHALLENGES OF THE PROCESS	43
4.3 A FUNDAMENTAL PRINCIPLE OF FABRICATION	45
4.4 BASIC PROCESS DESIGN	48

4.4.1	<i>A basic principle of SU-8</i>	48
4.4.2	<i>The basic process flow</i>	48
4.4.3	<i>Basic process: discussion, issues and results</i>	49
4.5	INTERMEDIATE PROCESS DESIGN	61
4.5.1	<i>Introduction to tip sharpening</i>	61
4.5.2	<i>Tip sharpening design – principle of moulding</i>	61
4.5.3	<i>Process flow incorporating tip sharpening</i>	62
4.5.4	<i>Intermediate process: results, issues and discussion</i>	68
4.6	ADVANCED PROCESS DESIGN	73
4.6.1	<i>The platform – what? why?</i>	73
4.6.2	<i>Fabrication options for platform layer</i>	73
4.6.3	<i>Advanced Process Design: Results, Issues & Discussion</i>	74
4.7	FINAL OPTIMIZATION OF THE PROCESS	81
4.7.1	<i>Resolving vital issues</i>	81
4.7.2	<i>Final process flow</i>	85
4.7.3	<i>Final results from optimized process: a discussion</i>	88
4.8	CONCLUSION	94
5	DEVICE TESTS & CHARACTERIZATION	97
5.1	MICRONEEDLE TESTING	98
5.1.1	<i>Mechanical tests</i>	98
5.1.2	<i>Microfluidic test</i>	115
5.1.3	<i>Preliminary biological tests</i>	119
5.2	CONCLUSION	120
6	CONCLUSION & FUTURE WORK	125
6.1	KEY CONTRIBUTIONS	126
6.2	CONCLUDING REMARKS	127
6.3	FUTURE WORK	128
6.3.1	<i>Broad issues</i>	128
	APPENDIX I: LIST OF ABBREVIATIONS	135
	APPENDIX II: LIST OF SYMBOLS	137
	APPENDIX III: LIST OF PUBLICATIONS	139
	APPENDIX IV: CURRICULUM VITAE	141
	BIBLIOGRAPHY	143

Table of Figures

FIGURE 1.1: FIRST PASS METABOLISM AFFECTING A DRUG. [COURTESY: NATURE REVIEWS]..... 3

FIGURE 1.2: CROSS-SECTION OF THE HUMAN SKIN STRUCTURE COMPARING THE DIFFERENT METHODS OF TRANSDERMAL DRUG DELIVERY. [IMAGE COURTESY: NATURE REVIEWS IMMUNOLOGY (5)] 3

FIGURE 1.3: (A) ALZA'S FENTANYL IONTOPHORESIS PATCH, TRADENAME IONSYS; (B) APPLICATION OF TRANSPHARMA RF-MICROCHANNEL TECHNOLOGY-BASED VIADERM SYSTEM TO SKIN; (C) POLYMEDICAL DERMOJET INJECTOR USING LIQUID JET INJECTION. 7

FIGURE 2.1: DIFFERENT MECHANISMS OF TRANSDERMAL DRUG DELIVERY USING MICRONEEDLE ARRAYS. (A) SOLID MICRONEEDLES USED FOR ONLY PRE-TREATMENT OF SKIN, AFTER WHICH DRUG IS APPLIED. (B) SOLID MICRONEEDLES, DRUG-COATED – DRUG REMAINS INSIDE SKIN AFTER NEEDLE WITHDRAWAL. (C) RESORBABLE MICRONEEDLES ENCAPSULATED WITH DRUG REMAINS INSIDE SKIN EVEN AFTER WITHDRAWAL. (D) HOLLOW MICRONEEDLES THROUGH WHICH DRUG IS INJECTED, DRUG REMAINS INSIDE SKIN AFTER NEEDLE WITHDRAWAL. [SOURCE: INT. J. PHARMA(12)] 10

FIGURE 2.2: (A) SOLID GLASS MICRONEEDLE WITH BEVEL-SHAPED TIP, 900 μM TALL (16); (B) QUARTZ MICRONEEDLE "LANCET"(17); (C) AN ARRAY OF QUARTZ MICRONEEDLES FOR SKIN ALLERGY TEST (17)..... 14

FIGURE 2.3: EXAMPLES OF FABRICATED SOLID MICRONEEDLES. (A)(32); (B)(33); (C) (34); (D) (35); (E) (36); (F) (20); (G) (37); (H) (38); (I) (39); (J) (29); (K) (40); (L) (41)..... 16

FIGURE 2.4: SEM IMAGE OF FABRICATED CERAMIC MICRONEEDLE ARRAYS - INDIVIDUAL MICRONEEDLE LENGTH OF 300 μM AND WIDTH OF 100 μM, AND A TIP DIAMETER OF ABOUT 5 μM (42). 17

FIGURE 2.5: EXAMPLES OF COATED SOLID MICRONEEDLES. A & B: (48); C (42); D & E: (46); F: (33); G & H:(49); I & J: (50); K & L: (51) 18

FIGURE 2.6: EXAMPLES OF DISSOLVABLE MICRONEEDLES COMPOSED OF WATER SOLUBLE POLYMERS AND BIODEGRADABLE POLYMERS. A: (52); B:(65); C (55); D: (62); E: (66); F: (67); G: (68); H: (69) 19

FIGURE 2.7: EXAMPLES OF FABRICATED HOLLOW MICRONEEDLES OF SI, METAL AND POLYMER MATERIALS. A: (87); B: (88); C: (77); D: (89); E: (90); F:(91); G: (75) H: (92); I(93); J:(76); K: (94)..... 22

FIGURE 2.8: AN EXTENSIVE FLOWCHART OF THE WIDE RANGE OF APPLICATIONS OF MICRONEEDLES. 24

FIGURE 3.1: (A) THE MOSQUITO MOUTH, LABIUM (SHEATH) AND FASCICLE (NEEDLE); (B) CLOSE-UP VIEW OF MOSQUITO FASCICLE TIP; (C) DIGITALLY ENHANCED IMAGE OF FASCICLE ENCLOSED IN LABIA.[SOURCE: (104)] 28

FIGURE 3.2: A 3-D REPRESENTATION OF THE ENVISAGED FABRICATED SINGLE, HOLLOW, TRIANGULAR CROSS-SECTION MICRONEEDLE ON A PLATFORM. NOTE THE SIMILARITY OF THE ANGLED TRIANGULAR TIP TO THE BEVEL-SHAPED TIP OF THE ACTUAL MOSQUITO. ALSO TO BE NOTED IS THE SHARP TIP ARISING FROM THE VERTEX OF THE TRIANGLE ITSELF AND IS A NATURAL BENEFIT OF THE CHOSEN GEOMETRY. 30

FIGURE 3.3: (A) SU-8 COATED ON A GLASS SUBSTRATE EXPOSED VIA A MASK TO UV RADIATION; (B) ARRAY OF HAR MICRO-PILLARS FORMED AFTER CROSS-LINKING BY UV EXPOSURE AND SUBSEQUENT DEVELOPMENT [SOURCE:(114)] (B) MOLECULAR STRUCTURE OF BISPHENOL A NOVOLAK EPOXY CONTAINED IN SU-8.{SOURCE: (114)(115)}. 33

FIGURE 3.4: A CROSS-SECTION OF THE DESIGNED MICRONEEDLE. BOTH THE TRIANGLES ARE ISOSCELES WITH EACH HAVING THE HEIGHT AND BASE AS INDICATED..... 34

FIGURE 3.5: VARIOUS MICRONEEDLE CROSS-SECTIONS THAT WERE DESIGNED. THE RED DOT IN THE CENTRE OF EACH SHAPE INDICATES ITS CENTRE OF GRAVITY (C.G.) WHILE THE X-X¹ AND Y-Y¹ AXES ARE ALSO DENOTED. (A) SOLID CIRCULAR (SC) (B) HOLLOW CIRCULAR (HC) (C) C-SHAPED (CS) (D) HOLLOW TRIANGULAR WITH TRIANGULAR CROSS-SECTION (HTTC) (E) HOLLOW TRIANGULAR WITH CIRCULAR CROSS-SECTION (HTCC) (F) HOLLOW BEVEL-SHAPED (HB) (G) HOLLOW-SLIT BEVEL-SHAPED (HSB). [NOTE: FIGURES NOT DRAWN TO SCALE] 35

FIGURE 3.6: COMPARISON OF THE DIFFERENT MOMENTS OF INERTIAS OF THE DESIGNED MICRONEEDLES IN THIS WORK. 37

FIGURE 3.7: AN INDIAN SAINT OF A HIGH MONASTIC ORDER, PERFORMING PENANCE ON A BED OF NAILS IN VARANASI IN 1907. THIS IS THE "FAKIR-BED EFFECT" WHEREIN THE FAKIR IS NOT HURT BY THE BED OF NAILS. 39

FIGURE 4.1: CROSS-SECTION OF TWO BASIC ARCHITECTURES REALISED IN THIS WORK: 1) HOLLOW MICRONEEDLES STANDING ON SOLID PLATFORM, 2) HOLLOW NEEDLES ON A PLATFORM WITH OPEN BORES COINCIDING WITH HOLLOW LUMENS OF MICRONEEDLES. 42

FIGURE 4.2: GRAPHICAL 3-D REPRESENTATION DISTINGUISHING BETWEEN IN-PLANE AND OUT-OF-PLANE FABRICATION METHODOLOGIES. 45

FIGURE 4.3: BASIC PROCESS FLOW FOR OUT-OF-PLANE MICRONEEDLE FABRICATION 49

FIGURE 4.4: FIRST FABRICATION RESULTS USING THE BASIC PROCESS DESIGN. TO BE NOTED ARE THE WEAK BASES OF THE HOLLOW CYLINDERS (OF VARIOUS GEOMETRICAL CROSS-SECTIONS AND DIMENSIONS) LEADING TO BENDING AND COLLAPSE OF THE FINAL STRUCTURES AFTER DEVELOPMENT. 50

FIGURE 4.5: DE-GASSING OF SU-8 INSIDE VACUUM OVEN. TO BE NOTED ARE THE COPIOUS NUMBER OF AIR BUBBLES WHICH DEFLATE AS SOON AS THE PRESSURE DROPS TO THE MINIMUM..... 52

FIGURE 4.6: SPECIALLY DESIGNED STAINLESS STEEL WAFER HOLDER WITH PERFORATED HOLES AND RAISED EDGES. 53

FIGURE 4.7: *CYLINDER BASES QUITE STRONG AND NO BENDING OBSERVED. HOWEVER, REGIONS OF UNDEVELOPED SU-8 OBSERVED.* 55

FIGURE 4.8: FABRICATED SU-8 HOLLOW CYLINDERS OF VARYING GEOMETRICAL CROSS-SECTIONS: CIRCULAR WITH CIRCULAR BORE (INNER DIAMETER: 50 μM, WALL THICKNESS: 15 μM), TRIANGULAR WITH TRIANGULAR BORE (WALL THICKNESS: 35 μM, BASE: 125 μM), AND TRIANGULAR WITH CIRCULAR BORE (INNER DIAMETER: 50 μM, BASE: 70 μM). AVERAGE HEIGHT: 400 μM. TO BE NOTED THAT THE MICRONEEDLES ARE ENTIRELY COMPOSED OF SU-8 AND STANDING OUT-OF-PLANE ON SI WAFER, THUS, THEIR LUMENS ARE BLOCKED AT THE LOWER END BY THE WAFER SUBSTRATE CORRESPONDING TO ARCHITECTURE 1 IN FIGURE 4.1. 55

FIGURE 4.9: LUMEN OF MICRONEEDLES (400 μM IN HEIGHT) OPEN RIGHT THROUGH THE LENGTH. OPEN SLIT THROUGH THE ENTIRE HEIGHT OF THE NEEDLES ILLUSTRATES THE FINE

DEVELOPMENT OF THE EDGES. THIS IS A POTENTIAL EXAMPLE OF A SOLID MICRONEEDLE COATED WITH A DRUG.....	56
FIGURE 4.10: SU-8 HOLLOW CIRCULAR CROSS-SECTION MICRONEEDLES. HEIGHT: 1540 MM, WALL THICKNESS: 15 MM, INNER DIAMETER: 100 MM. THUS, ASPECT RATIO > 100. (TOP LEFT): TALL SLENDER MICRONEEDLES STANDING ERECT WITHOUT ANY SIGNS OF BENDING. (TOP RIGHT, BOTTOM LEFT): WELL-DEFINED SHARP EDGES OF THE RIMS OF THE NEEDLES CAN BE EASILY OBSERVED INDICATING FINE PROCESSING. (BOTTOM RIGHT): TOP VIEW OF THE MICRONEEDLES APPARENTLY INDICATING THE LUMENS ARE HOLLOW AND A CLEAN DEVELOPMENT OF THE SU-8 HAS TAKEN PLACE. THESE MICRONEEDLES INDEED LOOK DENSELY PACKED BUT ARE NOT MEANT FOR SKIN PENETRATION.....	58
FIGURE 4.11: TRIANGULAR CROSS-SECTION MICRONEEDLES WITH CIRCULAR HOLLOW BORE. (DIMENSIONS – BASE: 70 MM, CIRCULAR LUMEN DIAMETER = 48 MM). THE SECOND TYPE OF STRUCTURE LOWER DOWN IN THE FIGURE IS ONE IN WHICH THE HOLLOW OF THE NEEDLE HAS BEEN INTENTIONALLY KEPT OPEN BY MASK DESIGN, TO ALLOW FOR A CLEAR VIEW OF THE LONGITUDINAL AXIS. THE SUBSTRATE SURFACE IS CLEAR INDICATING A SUCCESSFUL SU-8 DEVELOPMENT STEP.	59
FIGURE 4.12: CROSS-SECTIONAL VIEW OF FABRICATED SU-8 MICRONEEDLES MOULDED IN EPOXY, INDICATING THE NEEDLES ARE HOLLOW TILL THE BOTTOM.	60
FIGURE 4.13: PRINCIPLE BEHIND MOULDING THE MICRONEEDLES ON THE KOH-ETCHED PYRAMIDAL PITS TO FORM A SHARP ENDED TIP.....	62
FIGURE 4.14: TIP SHARPENING PROCESS FLOW – PART 1.	63
FIGURE 4.15: TIP SHARPENING PROCESS FLOW – PART 2.	65
FIGURE 4.16: DIFFERENCE BETWEEN PYRAMIDAL PITS AND TRENCHES.	65
FIGURE 4.17: EXCELLENT MOULDABILITY OF SU-8 ON SI. THE PYRAMIDS HAVE BEEN MOULDED IN THE KOH-ETCHED TRENCHES FOLLOWED BY A BLANK UV EXPOSURE. TO BE NOTED THAT THIS HAS BEEN CLEANLY RELEASED FROM THE SI WAFER SUBSTRATE, AND IS ENTIRELY COMPOSED OF SU-8.	66
FIGURE 4.18: CLOSE-UP SEM IMAGES OF MOULDED SU-8 ON SI AFTER RELEASE. SHARP EDGES AND SMOOTH SURFACES OBSERVED. SHARPNESS OF EDGE ROUNDNESS MEASURED TO BE UNDER 1µM.	67
FIGURE 4.19: INITIAL RESULTS OF THE INTERMEDIATE PROCESS DESIGN: MISALIGNMENT OF MICRONEEDLE TIPS WITH THE PYRAMIDAL PITS IS A MAJOR CAUSE OF CONCERN. ALSO, NON-UNIFORM CR-BLACK DEPOSITION HAS LED TO A DIRTY SUBSTRATE SURFACE.	68
FIGURE 4.20: STEP-BY-STEP PROGRESS IN CR-BLACK ELECTRODEPOSITION PROCESS. (A) UNSATISFACTORY GREENISH-BLACK (AND NOT GRAY-BLACK) COATING OF CR-BLACK FORMED. (B) CLOSE-UP OF ETCHED PYRAMIDAL PIT IN SI SUBSTRATE INDICATING NO CR-BLACK HAS BEEN DEPOSITED ON THE INNER WALLS OF THE PIT. (C) UNIFORM DARK GRAY CR-BLACK ELECTRODEPOSITION OBTAINED BY TUNING CURRENT (18 A), TIME (4 MINS) AND SEED LAYER CU THICKNESS (400 NM). (D) CLOSE-UP OF INNER WALLS OF PIT DISPLAYING UNIFORM CR-BLACK COATING AND THAT THE TERMINATING POINT OF THE PIT IS STILL VISIBLE.	70
FIGURE 4.21: AN ARRAY OF TRIANGULAR CROSS-SECTION MICRONEEDLES STANDING OUT-OF-PLANE ON THE KOH-ETCHED PITS. MARKED IMPROVEMENT IN ALIGNMENT AS WELL AS SURFACE TEXTURE OVER PREVIOUS RESULTS. IT IS TO BE NOTED THAT THE MICRONEEDLE TIPS ARE LYING	

INSIDE THE PYRAMIDAL PITS AS INTENDED, AND SOME OF THE MICRONEEDLES HAVE FALLEN OFF DUE TO POOR ADHESION. THE ENTIRE WAFER SUBSTRATE SURFACE IS COVERED WITH CR-BLACK. THE ALIGNMENT HAS BEEN IMPROVED BY MAKING USE OF THE SMALLEST SIZE ALIGNMENT MARKS IN THE SET OF ALIGNMENT MARKERS. PREVIOUSLY, THE LARGER SIZED ALIGNMENT MARKS WERE EMPLOYED AND THIS CAUSED A SIGNIFICANT MISALIGNMENT. 70

FIGURE 4.22: (LEFT) SHARP-TIPPED, TRIANGULAR CROSS-SECTIONED MICRONEEDLES WITH A TRIANGULAR CROSS-SECTIONED BORE: A – KOH-ETCHED PYRAMIDAL PIT ENDING AT A SHARP POINT, B – A MICRONEEDLE STANDING ON THE PIT, C – A FALLEN MICRONEEDLE DENOTING THE SHARPENED TIP FORMED BY MOULDING ON THE PYRAMIDAL PIT; (RIGHT) CLOSE-UP OF A SHARP TIP OF A MICRONEEDLE SHOWING THE TIP DIAMETER OF ABOUT 10 μm 71

FIGURE 4.23: (LEFT) THE BEVEL-SHAPED SHARP TIP OF A LOOSENED MICRONEEDLE IS PROMINENT HERE. (RIGHT) THE LUMEN OPENING AT POSTERIOR END (BOTTOM) AS WELL AS AT THE ANTERIOR END (SHARP TIP) IS ALSO CLEAR INDICATING THE ENDS ARE NOT CLOGGED, AND THAT MOST PROBABLY A HOLLOW LUMEN SHOULD EXIST. 71

FIGURE 4.24: SIDE VIEW OF A FABRICATED MICRONEEDLE RESULTING FROM THE INTERMEDIATE PROCESS FLOW. MEASURED NEEDLE LENGTH OF 334 μm AND BASE OF 128 μm , VIEWED AT A TILT OF 52°. NEEDLE WALL THICKNESS IS 10 μm 72

FIGURE 4.25: (LEFT): TRANSMISSION SPECTRUM OF 1 MM THICK UNEXPOSED SU-8100(126); (RIGHT) TRANSMITTED INTENSITY OF AN SU-8 FILM AT DIFFERENT WAVELENGTHS AFTER INCREASING EXPOSURE TIMES (127). 75

FIGURE 4.26: THICKNESS OF SU-8 VARYING WITH DIFFERENT EXPOSURE TIMES FOR GIVEN UV LAMP. 75

FIGURE 4.27: PLATFORM LAYER AFTER UNDEREXPOSURE. SHARP EDGES OF THE MICRONEEDLE TIPS CAN BE MADE OUT ONLY VAGUELY AS MARKED. THE TIPS ARE VISIBLE AFTER THE RELEASE OF THE SU-8 LAYER FROM THE SI SUBSTRATE. IT IS TO BE NOTED THAT SINCE THE MICRONEEDLE TIPS ARE FABRICATED TOP-DOWN WITH THE TIPS LYING IN CONTACT WITH THE SI MOULD, IT IS ONLY AFTER THE ENTIRE PLATFORM LAYER IS RELEASED THAT THESE TIPS CAN BE SEEN ON THE FRONT SIDE OF THE LAYER. FURTHERMORE, SINCE THE MICRONEEDLES HERE ARE EXTREMELY SHORT, IT IS ONLY THE MOULDED TIPS WHICH ARE VISIBLE. 76

FIGURE 4.28: FIRST PROMISING RESULTS OF PLATFORM LAYER STEP UNDER SEM. ENTIRE NEEDLE ARRAYS AS WELL AS PLATFORMS ARE MADE OF THE SAME MATERIAL, SU-8. THOUGH FAR FROM PERFECT, THIS DEMONSTRATES THAT THE PRINCIPLE OF MAKING THE PLATFORM, WORKS. HIGH INTERNAL STRESS NOT EVIDENT IN THE SEM IMAGE BUT PRESENT MORE AT A MACRO-SCALE PROVEN BY THE CURLING UP OF THE ENTIRE PLATFORM. (A) SU-8 MICRONEEDLES STANDING OUT-OF-PLANE ON AN SU-8 PLATFORM – THE MISALIGNMENT OF THE BASES WITH THE HOLES OF THE PLATFORM CAN BE CLEARLY OBSERVED. (B) SIDE-VIEW OF THE PLATFORM EXPLICITLY DEPICTING THE THICKNESS OF THE PLATFORM AND THE MONOLITHIC NATURE OF THE FABRICATED DEVICE. (C) CLOSE-UP VIEW OF SOME OF THE MICRONEEDLES SHOWING VERY STRAIGHT AND SMOOTH SIDEWALLS WITH WELL-DEFINED EDGES. (D) TOP-VIEW SHOWING MISALIGNMENT OF THE MICRONEEDLE BORES WITH THE HOLES IN THE PLATFORM. 77

FIGURE 4.29: SU-8 BLUNT-TIPPED MICRONEEDLES FABRICATED ON AN SU-8 PLATFORM. A – MOULDED SHARP-TIPS OF THE TRIANGULAR CROSS-SECTIONED MICRONEEDLE, B – A BORE OF THE PLATFORM MISALIGNED WITH THE BORE OF THE MICRONEEDLE. 78

FIGURE 4.30: WHY ALIGNMENT IS CRUCIAL AND HOW WHEN MISALIGNMENT OCCURS, THE ENTIRE BORE OF MICRONEEDLE CAN GET CROSS-LINKED INADVERTENTLY.	79
FIGURE 4.31: HOW MISALIGNMENT CAN BE CIRCUMVENTED BY A MASK DESIGN TOLERANCE.	80
FIGURE 4.32: INTERNAL STRESSES IN THE PLATFORM LAYER CAUSING IT TO CURL UP. THE WAVY FEATURES ON THE SURFACE OF THE PLATFORM ARE EVIDENT OF THE HIGH STRESSES THAT HAVE CREPT IN AFTER THE FINAL DEVELOPMENT STAGE OF THE SU-8. THE LARGE SOLID CYLINDERS IN THE LEFT FIGURE WERE CREATED JUST AS A TEST STRUCTURE AND HAVE NO SPECIAL SIGNIFICANCE.	82
FIGURE 4.33: THE SURFACE TEXTURE OF THE SU-8 PLATFORM CLEARLY DENOTES AMPLE INTERNAL STRESS. (LEFT) THE SMALL HEIGHT (174 μm) OF THE MICRONEEDLE IS NOTED. (RIGHT) A CLOSE-UP VIEW OF THE FABRICATED MICRONEEDLE ON PLATFORM BEFORE OPTIMIZATION...	83
FIGURE 4.34: BLANKET SU-8 MOULDING ON THE Si MASTER MOULD IN ORDER TO INSPECT THE BOTTOM SHARPNESS OF THE ANISOTROPICALLY ETCHED PYRAMIDAL PITS. (LEFT): AS EXPECTED, THE PITS HAVE NOT BEEN ETCHED TILL THEIR VERY LIMITS AND THE TOPS OF THE RELEASED SU-8 LAYER SHOWS THAT THEY ARE NOT SHARP. (RIGHT): A CLOSE-UP VIEW OF A SINGLE SU-8 SOLID PILLAR INDICATING A TOP SIDE LENGTH OF ABOUT 50 μm , BOTTOM LATERAL SIDE OF AROUND 285 μm , AND A HEIGHT OF 150 μm	84
FIGURE 4.35:(LEFT) SEM PICTURE OF THE FABRICATED MICRONEEDLE ARRAY ON PLATFORM ALBEIT WITH SHORT MICRONEEDLES (HEIGHT = 170 MICRONS), THAT RESEMBLE "STUBS" RATHER THAN NEEDLES. TO BE NOTED IS THE PLATFORM WHICH IS QUITE EASILY DISCERNIBLE, WITHOUT STRESSES, AND FLAT. (RIGHT): A CLOSE-UP VIEW OF A SINGLE SHORT MICRONEEDLE.	84
FIGURE 4.36: FINAL PROCESS FLOW INCORPORATING ALL CHANGES: A SUM TOTAL OF THE BASIC, INTERMEDIATE AND ADVANCED PROCESS DESIGN.	87
FIGURE 4.37: SHARP BEVEL-SHAPED TIPPED, HOLLOW (HB), OUT-OF-PLANE SU-8 MICRONEEDLES ON AN SU-8 PLATFORM. ENTIRE STRUCTURE IS COMPOSED OF ONE MATERIAL, THEREFORE, MONOLITHIC. (CONT'D..)	88
FIGURE 4.38: ANOTHER SEM PICTURE OF THE SAME BEVEL-SHAPED (HB) MICRONEEDLES FROM A SIDE-VIEW, CLEARLY INDICATING THE SLOPE OF THE TIP CONFORMS TO THE SLOPE OF THE 54.74° Si $\langle 111 \rangle$ CRYSTALLOGRAPHIC PLANE.	89
FIGURE 4.39: A VIEW OF A SINGLE BEVEL-SHAPED TIP MICRONEEDLE (HB). (LEFT): TO BE NOTED IS THE VERY PRONOUNCED HOLLOW OF THE LUMEN AS IS VISIBLE FROM THE TOP. ALSO VERY NOTICEABLE IS A PECULIAR BULGE IN THE "WAIST" REGION OF THE MICRONEEDLE SHAFT. CAREFUL PROCESS ANALYSIS SHOWS THAT THIS COULD BE THE RESULT OF AN INCOMPLETE PRE-BAKE TREATMENT TO AN INTERMEDIATE (CONT'D...) SPIN-COATED LAYER. (RIGHT): CLOSE-UP SIDE VIEW OF A MICRONEEDLE TIP. END TIP DIAMETER MEASURED TO BE AROUND 4 μm .	89
FIGURE 4.40: AN ARRAY OF MICRONEEDLES WITH BEVEL-SHAPED TIPS WITH A SLIT THROUGH THEIR ENTIRE HEIGHTS (HSB) STANDING OUT-OF-PLANE ON A SOLID PLATFORM WITHOUT ANY HOLES. DIMENSIONS - (MICRONEEDLE) HEIGHT = 600 μm , INNER DIAMETER = 66 μm , WALL THICKNESS = 25 μm ; PLATFORM THICKNESS = 200 μm . (LEFT): AN ARRAY OF BEVEL-SLIT MICRONEEDLES ON PLATFORM; (RIGHT): THE SHARP BEVEL-SHAPED TIP OF A SINGLE MICRONEEDLE IS OBSERVED. THE SLIT IS WELL-PRONOUNCED THROUGH THE ENTIRE HEIGHT. THIS CAN BE USED AS A SOLID OR SEMI-HOLLOW MICRONEEDLE.	90

FIGURE 4.41: TRIANGULAR CROSS-SECTION POLYMER MICRONEEDLES WITH VERY WELL-DEFINED WALL EDGES, AND A VERY CLEAR HOLLOW LUMEN, ALSO STANDING ON A POLYMER PLATFORM, ALL COMPOSED OF A SINGLE MATERIAL – SU-8; CROSS-SECTIONAL SHAPE: RIGHT-ANGLED ISOSCELES; DIMENSIONS – MICRONEEDLE HEIGHT = 1000 μM; OUTER HEIGHT = OUTER BASE = 175 μM; INNER HEIGHT = INNER BASE = 100 μM; PLATFORM THICKNESS = 200 μM..... 91

FIGURE 4.42: SEM PICTURE OF A CLOSE-UP VIEW OF TRIANGULAR CROSS-SECTIONAL MICRONEEDLE TIP. TIP DIAMETER < 4 μM. THE ROUGH EDGE OF THE TIP SURFACE MAY HAVE RESULTED FROM A HASTENED RELEASE STEP AT THE TIME OF DEVELOPMENT..... 91

FIGURE 4.43: PICTURE OF THE ENTIRE MICRONEEDLE ARRAY ON A PLATFORM VIEWED UNDER AN OPTICAL MICROSCOPE. SINCE THE MICROSCOPE CAN ONLY FOCUS AT A CERTAIN DEPTH AT A GIVEN TIME, SOME OF THE MICRONEEDLES APPEAR TO BE BLURRED. WHAT IS CLEARLY OBSERVABLE IS THE THICKNESS OF THE PLATFORM, AND THE FACT THAT BOTH THE NEEDLES AND THE PLATFORM ARE MADE OF A SINGULAR MATERIAL..... 92

FIGURE 4.44: OPENINGS AT THE REAR END OF THE PLATFORM CORRESPONDING TO THE MICRONEEDLE LUMEN BORES, AND ARE CONTINUOUS THROUGH THE THICKNESS OF THE PLATFORM. 92

FIGURE 4.45: ALREADY ILLUSTRATED PREVIOUSLY IN THE TEXT INDIVIDUALLY, THEY ARE DISPLAYED HERE ONCE AGAIN TO BRING OUT THE COMPARISON OF THE FABRICATED SU-8 BEVEL-SHAPED MICRONEEDLE TIP WITH THE REAL MOSQUITO FASCICLE. THE BIOMIMETIC ASPECT IS QUITE PRONOUNCED HERE. (A) CLOSE-UP SIDE VIEW OF THE FABRICATED TIP INDICATING ITS SHARPNESS; (B) SIDE VIEW SHOWING THE 54.74° SLOPED ANGLE OF THE SHARP TIP; (C) FRONT VIEW OF THE BEVEL-SHAPED TIP; (D) THE ACTUAL MOSQUITO FASCICLE TIP. THE BEVEL-SHAPED OPENING OF THE TIP BEARS A STRIKING SIMILARITY WITH THE FABRICATED TIPS. 93

FIGURE 5.1: CYCLIC LOADING-UNLOADING OF HOLLOW SU-8 CYLINDERS BY A NANOINDENTER OF 220 MICRONS IN DIAMETER. A SCHEMATIC OF THE TESTED MICRONEEDLE DIMENSIONS ARE ALSO GIVEN ALONGSIDE – INNER DIAMETER = 150 μM; OUTER DIAMETER = 250 μM. 100

FIGURE 5.2: SCHEMATIC OF FAILURE FORCE CHARACTERIZATION ON MICRONEEDLE ARRAY 101

FIGURE 5.3: DTS DELAMINATOR EXPERIMENTAL SET-UP FOR MEASURING FAILURE FORCE OF THE MICRONEEDLES. 101

FIGURE 5.4: LOAD-DISPLACEMENT GRAPH TO DETERMINE THE CRITICAL LOAD BEARING FORCE OF FABRICATED HOLLOW MICRONEEDLES. LOAD APPLIED IS MEASURED IN "NEWTONS" AND DISPLACEMENT IN "MICROMETERS". THIS TEST WAS PERFORMED ON AN ARRAY OF 45 MICRONEEDLES IN NUMBER, HOLLOW LUMEN, TRIANGULAR CROSS-SECTION, 1000 μM IN HEIGHT AS FABRICATED PREVIOUSLY (SEE FIGURE 4.41) . THE MAXIMUM LOAD APPLIED IS 10.35 N. 102

FIGURE 5.5: BEFORE AND AFTER VIEW OF THE COMPRESSIVE CRITICAL LOAD BEARING FORCE TEST ON THE MICRONEEDLE ARRAY. (RIGHT): THE ENTIRE NEEDLE ARRAY COMPRISING ALL INDIVIDUAL NEEDLES HAS UNDERGONE FAILURE. (LEFT): THE SAME NEEDLE ARRAY INTACT PRIOR TO TESTING..... 104

FIGURE 5.6: ALTERNATIVE SOLID MICRONEEDLE CROSS-SECTION - A BEVEL-SHAPED TIP COMBINED WITH A SLIT RUNNING THROUGH ITS ENTIRE LENGTH OF THE SHAFT. 105

FIGURE 5.7: LOAD-DISPLACEMENT GRAPH TO DETERMINE THE CRITICAL LOAD BEARING FORCE OF FABRICATED SOLID (WITH SLIT) MICRONEEDLES. THIS TEST WAS PERFORMED ON AN ARRAY OF

45 MICRONEEDLES IN NUMBER, OF AVERAGE HEIGHT 650 μm , BEVEL-SHAPED CROSS-SECTION WITH SLIT THROUGH ENTIRE SHAFT. THE MAXIMUM APPLIED LOAD IS 19.09 N.....	105
FIGURE 5.8: (LEFT) TOP VIEW OF THE INTACT SOLID BEVEL-SHAPED MICRONEEDLES WITH SLIT BEFORE COMPRESSIVE TEST; (RIGHT) TOP VIEW OF THE SAME AFTER TEST, DEPICTING BREAKAGE OF ALL THE MICRONEEDLES IN THE ARRAY INDICATING COMPLETE FAILURE.	106
FIGURE 5.9: LOAD-DISPLACEMENT GRAPH FOR SINGLE MICRONEEDLE WITH HOLLOW LUMEN, TRIANGULAR CROSS-SECTION, 1000 μm IN HEIGHT. THE MEASURED FAILURE FORCE IS 0.277 N.....	107
FIGURE 5.10: FAILURE LOAD MEASURED FOR 15 SINGLE MICRONEEDLES OF THE SAME DIMENSIONS (1000 MICRONS IN HEIGHT), HOLLOW LUMEN AND TRIANGULAR CROSS-SECTION TAKEN FROM 15 DIFFERENT ARRAYS; AND THE MEAN FAILURE LOAD OF 235 mN IS DEPICTED WITH THE HELP OF A STRAIGHT LINE.	108
FIGURE 5.11: SHAPE OF THE NANO-INDENTER USED FOR THIS SHEAR TEST – FRUSTUM OF A CONE. THE FORCE IS APPLIED ON THE SAMPLE BY THE SMALLER DISC OF RADIUS 10 μm	109
FIGURE 5.12: PRINCIPLE OF MEASURING SHEAR FORCE BY NANO-INDENTER.	110
FIGURE 5.13: STIFFNESS OF MICRONEEDLE MEASURED BY A NANO-INDENTER. MICRONEEDLE DIMENSIONS WERE 800 MICRONS IN HEIGHT, TRIANGULAR CROSS-SECTION WITH HOLLOW LUMEN. AS THE DISTANCE FROM THE BASE OF THE NEEDLE INCREASES THE STIFFNESS REDUCES RENDERING THE MICRONEEDLE MUCH MORE FLEXIBLE AT ITS BASE THAN AT ITS TIP.	111
FIGURE 5.14: NANO-INDENTER EXPERIMENTAL SET-UP, PARTS, WORKING PRINCIPLE AND EXAMPLE OF A REAL INDENTER TIP.	112
FIGURE 5.15: SCHEMATIC OF PENETRATION TEST CHARACTERIZATION ON FABRICATED MICRONEEDLE ARRAY.....	113
FIGURE 5.16: PENETRATION OF MICRONEEDLES INTO AGAR GEL. THE SQUARE OUTLINE INDICATES THE AREA COMPRISING AN ARRAY OF [3x3] HOLLOW MICRONEEDLES PENETRATED INSIDE THE AGAR GEL BY APPLYING A FORCE OF 63 mN. THUS, INSERTION FORCE OF EACH MICRONEEDLE IS 7mN. THE LIGHT GRAY COLOURED REGION SHOWS THAT THE MICRONEEDLES HAVE PENETRATED INSIDE THE AGAR GEL IN THIS REGION WHILE THE REST OF THE DARK GRAY AREA SIGNIFIES THE AGAR GEL LYING IN CONTACT WITH THE MICRONEEDLE TIPS AND NOT PENETRATED.	114
FIGURE 5.17: DESIGNED APPLICATOR FOR MICROFLUIDIC TESTING.	116
FIGURE 5.18: SYRINGE PUMPING FORCE FOR FLUID FLOW.....	116
FIGURE 5.19: (LEFT) ARRAY OF MICRONEEDLES MOUNTED ON A PLATFORM. (RIGHT) COLOURED WATER BEING EJECTED THROUGH THE HOLLOW MICRONEEDLES.	117
FIGURE 5.20: SU-8 SUBSTRATE STAINED WITH PLL TO PROMOTE CELL ADHESION ON FRONTSIDE. BULK OF THE SURFACE IS PREDOMINANTLY GREEN INDICATING CALCEIN-AM STAINED LIVE CELLS. [...]	120
FIGURE 5.21: FINGER TIP INSERTION TEST WITH FABRICATED MICRONEEDLE ARRAY. (TOP-LEFT): FINGER INSERTION INTO NEEDLE TIPS. (TOP-RIGHT, BOTTOM-RIGHT): SIDE VIEW OF PLATINUM COATED MICRONEEDLES, CLOSE-UP PERSPECTIVE VIEW OF THE SAME MICRONEEDLE ARRAY, RESPECTIVELY. (BOTTOM-LEFT): MARKINGS OF THE MICRONEEDLE INSERTIONS INTO THE SKIN. THE DARK PATCH SIGNIFIES A SLIGHT BLEEDING CAUSED BY ONE MICRONEEDLE.	123

FIGURE 6.1: A FUTURE VISION FOR THE FINAL DEVICE CULMINATING FROM THIS WORK: A CLOSED-LOOP COMPREHENSIVE TRANSDERMAL DRUG DELIVERY AND BLOOD EXTRACTION (USING MICRONEEDLES) SYSTEM. THE LFS AND IONTOPHORESIS MODULES COMPLEMENT THE MICRONEEDLES IN DRUG DELIVERY AND SIMPLY ENHANCE THE EFFICIENCY OF THE DEVICE. . 133

List of Tables

TABLE 2.1: COMPARISON OF DIFFERENT MICRONEEDLE ARCHITECTURES (15)..... 12

TABLE 3.1: COMPARISON OF THE VARIOUS PLANNED DESIGNS FOR THIS WORK: CROSS-SECTIONAL GEOMETRY, DIMENSIONS, MOMENT OF INERTIA AND CRITICAL FAILURE FORCES FOR HEIGHTS OF 600 μ M AND 1000 μ M. 36

TABLE 5.1: COMPARISON OF FABRICATED MICRONEEDLES IN TERMS OF MECHANICAL FAILURE FORCE. THE THREE CATEGORIES HIGHLIGHTED IN **BOLD** SIGNIFY THE TYPES SELECTED FOR FURTHER WORK. UNDERLINED VALUES INDICATE WHICH ONE OF THE TWO HEIGHTS (600 μ M OR 1000 μ M) WERE TESTED..... 122

1

Introduction

Abstract

This chapter briefly introduces the motivation behind the present work and then dives into the topic of transdermal drug delivery, why it is required, historical examples and occurrences in nature, methods of drug delivery, the structure of the human skin and how it influences the method of drug delivery. Further, why microneedles itself was chosen as the primary method in this work and what formed the inspiration to do so, is also discussed.

1.1 Transdermal drug delivery

1.1.1 A brief introduction

Oral administration of drugs is one of the oldest methods of drug delivery prevalent even till date. When ingested orally, the drug is absorbed from the gastro-intestinal (GI) tract and is transported via the portal vein to the liver which metabolizes some of the drug. This phenomenon is called the first-pass metabolism effect (see Figure 1.1) and is the main reason why the drug entering the systemic circulation after this process, is of much reduced concentration (1) and therefore has a low bioavailability. Bioavailability is defined as the fraction of a drug that enters the systemic circulation after being administered via a certain route (2). This is the primary disadvantage of the oral route of drug delivery, namely, the incomplete metabolism and first-pass metabolism reduce the bioavailability of the drug. The easier it is for a particular drug to be metabolized by the liver, lower will be its bioavailability. By definition only when a drug is administered intravenously, is its bioavailability 100% (2). This factor is kept in mind when designing the dosages for drug via non-intravenous administration. However, though for conventional drugs this may still be an acceptable norm, for hormonal and peptide-based drugs or “protein” drugs, this is no longer feasible as considerable amounts of the drug is lost via the first pass mechanism (3). Thus, transdermal drug delivery is one of the alternative methods of administering these types of drugs. Transdermal drug delivery is the delivery of drug molecules across the skin barrier layers and into the body.

Broadly speaking, the routes of drug delivery are (2):

- Parenteral: Intravenous (IV), Intramuscular (IM), Subcutaneous (SC)
- Inhaled: Eg. Nasal sprays
- Oral: Eg. conventional tablets and capsules
- Topical: Eg. eye drops, ear drops
- Rectal: Eg. Glycerin suppositories as laxative
- Transdermal: Eg. nicotine patches, hormonal patches

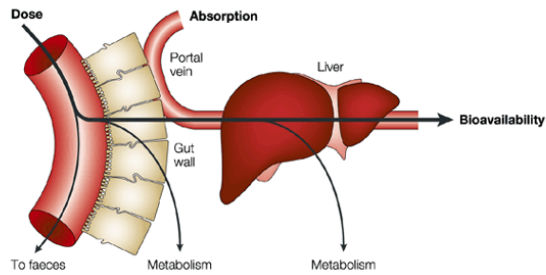


Figure 1.1: First pass metabolism affecting a drug. [Courtesy: Nature Reviews]

Of the many methods to by-pass the first pass metabolism, “transdermal” is one such of chief importance in the scope of this work. Not only does it circumvent the first pass effect, but is also more attractive due to its relatively painless mechanism compared with hypodermic syringe-based injections (4). Also, it does away with the medical wastes and needle-stick injuries associated with the latter. Furthermore, injections also pose the additional risk of re-transmission of diseases by re-use of the needles in developing countries and transdermal drug delivery can eliminate this. Being patient-friendly systems, it also helps to improve patient compliance. Before delving further into the types of transdermal drug delivery it is imperative to first understand the structure of the human skin, as illustrated in Figure 1.2.

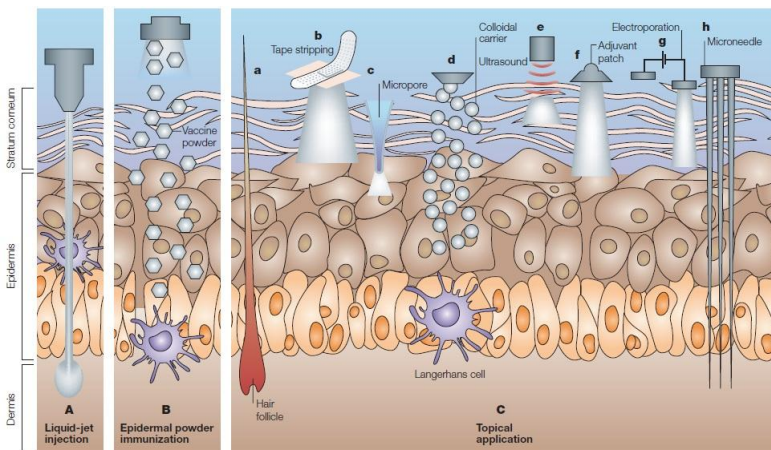


Figure 1.2: Cross-section of the human skin structure comparing the different methods of transdermal drug delivery. [Image Courtesy: Nature Reviews Immunology (5)]

As can be viewed in Figure 1.2, the uppermost layer of the skin called the stratum corneum has a thickness ranging from approximately tens of microns to a few hundred microns depending on the region of the body (6). Average thickness of the human stratum corneum is about 20 μm (7). The stratum corneum is made up of a dense network of dead cells called keratinocytes that provides the toughest diffusion barrier to all kinds of pathogens as well as drugs. Underneath the stratum corneum lies the viable epidermis which is usually about 10 times as thick as the stratum corneum, composed of stratified squamous epithelium and serves as the main functional barrier layer to the external environment, protecting the body from infections (8). Average thickness of the epidermis ranges from 100 μm to 500 μm . Below the epidermis, lies the dermis which comprise subcutaneous tissue, collagen matrix, mechano-pain-receptors, adipose tissue, blood vessels and lymph vessels (9). Mechano-receptors serve to detect specific properties of the stimulus such as its position, intensity, duration, velocity or acceleration. Egs. of such receptors are Merkel receptors and Ruffini endings which are involved in the sensing of pressure on the skin (10). Also of notable significance in the dermal layer is the presence of a rich concentration of immunogenic cells called Langerhans cells, which serves as the body's next line of defence after the skin barrier has been breached and are designed to initiate an immune response on detection of foreign antigens (11). This very property of the dermal layer has attracted considerable interest towards it as a target delivery destination for vaccines such as monoclonal antibodies

1.1.2 Types of transdermal drug delivery

Figure 1.2 gives a clear snapshot of the main methods of transdermal drug delivery.

- *Liquid jet injection* technique in section A of the Figure 1.2, is depicted. As is apparent from the image, this is a brute-force method for injection of high velocity fluids (typically around 100 m/s) into the skin with the fluid diameter varying between 76 μm and 360 μm (5). Due to the brute force nature of this method, it is not a painless mechanism.
- *Epidermal powder immunization* is illustrated in section B of the figure whereby a vaccine powder applied superficially to the stratum corneum diffuses into the dermis via the epidermis to reach the Langerhans cells.

- Topical administration has been showcased in section C.
 - *Hair follicles* aid in DNA immunization.
 - *Tape stripping* method is utilized to strip off the layer of stratum corneum in order to facilitate diffusion through the epidermis.
 - *Radio ablation* is applied to the stratum corneum to open up micropores in the epidermis and to thus, provide a diffusion path for the vaccine. (See Figure 1.3)
 - *Ultrasound or low frequency sonophoresis (LFS)* has been shown to result in cavitation inside the epidermis and dermis which further aids in a improving the diffusion of the drug.
 - *Topically applied adjuvants* such as cholera toxin can initiate the required immune response.
 - *Electroporation* is the application of a very high electric pulse in order to open up channels inside the skin to allow easy diffusion of drugs. Again it is another brute force method.
 - *Iontophoresis* is a technique of employing an electric charge to deliver a drug or chemical inside the skin using the principle of repulsion of like charged particles by electromotive force. (See Figure 1.3).
 - *Microneedles* are hollow tubes penetrated into the skin and serve as a conduit for the drug from outside the skin into the dermis, bypassing the epidermis.

In fact, broadly speaking, transdermal drug delivery is a systemic effect while topical drug delivery is a local effect.

1.1.3 Brief design considerations w.r.t. skin structure

From the above illustrated skin structure, it is evident that for an intra-dermal delivery of vaccines, the microneedle shaft length should be around 1000 μm in order to reach the dermis layer of the skin. If 60% of the length of the microneedle gets penetrated into the skin, then a shaft length of around 100 μm approximately should still lie within the dermis layer of the skin.

1.1.4 Why microneedles?

Of the aforementioned techniques, the most noteworthy contenders of transdermal drug delivery are: liquid jet injection, ultrasound and radio ablation, electroporation and iontophoresis. As already discussed, liquid jet injection suffers from the disadvantage of causing pain and occasional bleeding, in addition to the high cost of the device (5). Ultrasound and radio ablation are supplementary techniques to aid in topical application of drugs. Electroporation as well as iontophoresis suffer from the downsides of being complex to use by patients and expensive. Further, electroporation is also not completely devoid of pain. Iontophoresis, because of its technical complexities is still not well-controlled, resulting in inappropriate and uncontrolled drug delivery. Additionally, all these methods are limited by the size of the drug molecule which they can deliver, typically molecular masses of the order of a few hundred Daltons. But protein molecules which are generally greater than 10000 Da in size are still a far cry when it comes to these current transdermal drug delivery methods.

It is here that microneedles can circumvent most of the above limitations and at the same time provide for a relatively painless, cheap, robust and patient-friendly system. Furthermore, since microneedles can provide a hollow conduit, molecular size restrictions also do not apply in this case. In fact, the hollow conduit of the microneedle, once in place, can transport the drug molecule through the tough barrier resistance of the epidermis to reach the dermis directly for delivery to the site of Langerhans cells or even to blood vessels. Thus, it is clear why “microneedles” forms the selected method to be explored in this research.

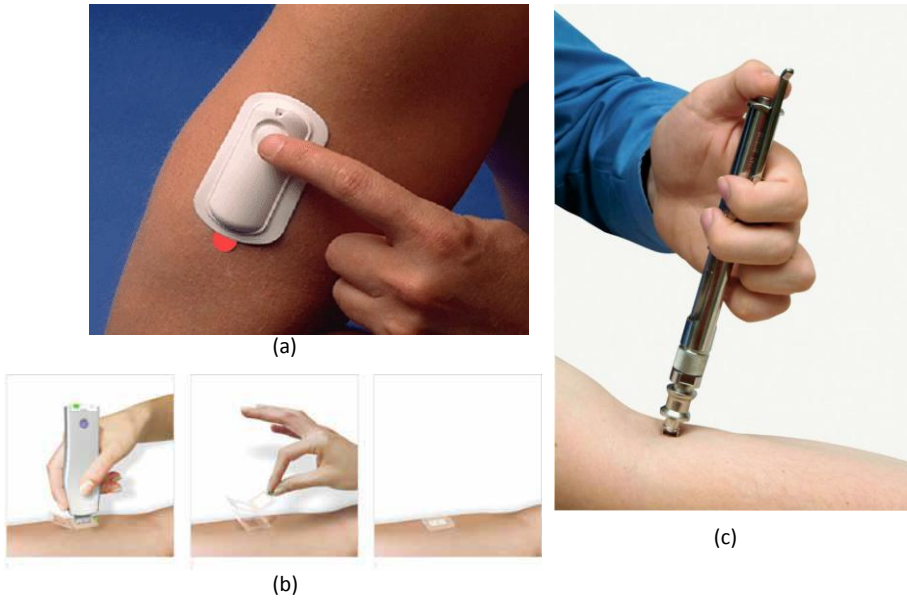


Figure 1.3: (a) ALZA's Fentanyl Iontophoresis patch, tradename Ionsys; (b) Application of TransPharma RF-MicroChannel technology-based Viaderm system to skin; (c) Polymedical DermoJet Injector using liquid jet injection.

1.2 Research Goal

The research goal is to design, fabricate and test a microneedle array device for painless transdermal drug delivery applications. The design should be flexible and versatile wherein the said microneedle's parameter can be changed easily without affecting the defined process flow. Hollow and solid microneedles should be made with a possibility for backside integration with a drug reservoir device. The final device should be flexible and polymeric in nature that can be disposed off safely. Furthermore, the fabricated microneedle device array should find itself more than one application with the same design or by a minor tweaking of the same design. Also, the process for fabrication must be as low-cost as possible, repeatable and scalable to large-scale production.

2

Microneedle Theory, Prior Art & Applications

Abstract

This chapter gives an insight into the principle of working of a microneedle, the different architectures possible and the pros and cons of each. Next, an overview of the state-of-the-art research in microneedles worldwide is presented for each kind of architecture. Some of the key features of each design are discussed and analyzed giving an insight into some of the design parameters to be borne in mind while embarking on a new design. Different possible applications of microneedles are also discussed extensively. Further, the global trend in microneedle research is evaluated and studied, and conclusions drawn on which are the areas to be improved upon and how this work is superior from similar work in the prior art.

2.1 Working principle – different architectures

The objective of employing a microneedle here, as is already stated in the previous chapter, is transdermal drug delivery. In this connection, the working principle of a microneedle or an array of microneedles (as they are more commonly used), depends on the type of architecture of the microneedle used. *Prima facie*, there are two broad categories: Solid and hollow. But the solid microneedles can be used in a variety of ways as is elucidated in the following diagram of Figure 2.1 (12).

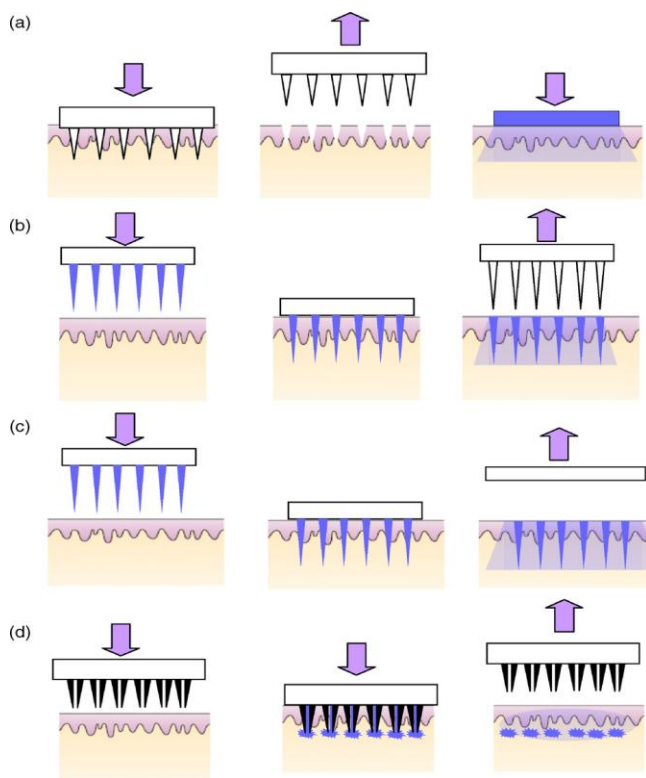


Figure 2.1: Different mechanisms of transdermal drug delivery using microneedle arrays. (a) Solid microneedles used for only pre-treatment of skin, after which drug is applied. (b) Solid microneedles, drug-coated – drug remains inside skin after needle withdrawal. (c) Resorbable microneedles encapsulated with drug remains inside skin even after withdrawal. (d) Hollow microneedles through which drug is injected, drug remains inside skin after needle withdrawal. [Source: *Int. J. Pharma*(12)]

As illustrated above in Figure 2.1, specifically there are four different mechanisms of utilizing microneedles to administer drugs transdermally. As already explained in Chapter I, the stratum corneum and the viable epidermis form the toughest barrier for drugs to diffuse through. Thus, puncturing the skin with solid needles in order to create through microchannels inside the epidermis, has been found to facilitate the diffusion of drugs through the layers (13). This is called the method of “pre-treatment” wherein typically an array of solid microneedles is punctured into the skin and then withdrawn immediately (Figure 2.1(a)). This is followed by the drug being applied to the stratum corneum so that it can diffuse inside through the epidermal layers with ease.

The next mechanism is that of a solid microneedle coated with a drug. When an array of such microneedles is inserted into the skin and then withdrawn after some time, the drug coating on the microneedles would dissolve inside the skin and remain there even after the microneedle array is withdrawn. This is as illustrated in Figure 2.1(b).

The third mechanism also employs a solid microneedle but unlike in the previous case, here the entire microneedle remains and dissolves inside the skin. There are two possible mechanisms in this case: one, the microneedle matrix itself is made up of the drug (or in combination with a biodegradable polymer) to be delivered, or two, a biodegradable polymer forms the outer shell encapsulating the desired drug. Of course, in both the cases, the entire microneedle is resorbed into the skin over a period of time – the dissolving time depends on the kind of biodegradable polymer used and the drug properties. This is depicted in Figure 2.1(c).

The fourth mechanism which is of most interest to us, uses the hollow microneedle topography. Here, an array of hollow microneedles is inserted into the skin to by-pass the epidermal layers and directly reach the dermis. A drug is injected through the hollow lumen of the microneedles to be delivered to the dermis directly without having to diffuse through the intermediate epidermal layers. Finally, the hollow microneedle array is withdrawn from the skin, as indicated in Figure 2.1(d).

These four architectures can be compared approximately (14) based on design simplicity and manufacturability, ease of use by patient, maximum possible drug dosage, control over drug delivery profile. A greater number of “+” signifies a better rating. This is illustrated in the following Table 2.1:

Microneedle Architecture	Simplicity of design and manufacturing	Ease of use by patient	Maximum amount of deliverable drug	Control over drug delivery profile
Microneedle pretreatment	+++	++	++	++
Microneedle patch (solid-coated & solid dissolving)	++	+++	+	++
Hollow microneedles	+	+	+++	+++

Table 2.1: Comparison of different microneedle architectures (15).

Delving deeper into the above table, gives us some quick insights. It is clear that solid microneedles for pre-treatment are the simplest to design and manufacture though its patient-friendly usage, amount of drug that can be delivered as well as control over the drug delivery profile are just of medium rating. It is to be noted here that since pre-treatment requires the patient to follow up the microneedle puncturing with administering of the actual drug dose, it ranks lower on the patient-friendliness. Though the solid microneedles on patch would be applied by the patient in exactly the same manner (both being array of solid microneedles), still it ranks higher on patient usage primarily because the needle patch can be applied on the skin and left there for a few hours by the patient without having to bother about the drug administration separately (unlike in pre-treatment). Thus, ease of use is highest in the case of the microneedle patch. However, the maximum amount of drug that can be delivered is a tad bit lower than pre-treatment and in fact lowest of the three types because on solid coated needles, the maximum amount of the drug to be delivered is a function of the total surface area available for coating the drug on to the microneedle. In case of the dissolvable needles too, though a greater number of needles could translate into a higher amount of the drug to be delivered, in practice the number of microneedles is a trade-off with the total insertion force required (*fakir-bed* effect, explained later), and is thus limited. Coming to hollow microneedles, it is a mix of extremes as can be observed from the table. On one hand, the ease of design and manufacture, along with ease of patient-usage is minimum whereas the drug deliverability and control over dosage profile are highest. Since this is a hollow conduit mechanism through which

drugs can be injected, it is clear why there the limit on maximum amount of drugs to be delivered is much higher than the other methods. If a time-controlled injection mechanism is adopted, then the dosage profile of the drug can also be controlled. However, the downsides of this architecture is also very obvious – it is undoubtedly very challenging to design and manufacture tall, thin, hollow though strong microstructures (as shall be expounded later on). At the same time, using such a system with an applicator for the patient may not be very straightforward. Thus, the challenge clearly is to bridge these gaps in the hollow microneedle design.

2.2 Prior art research in microneedles

As enlisted above, microneedles can be classified into four categories:

- Solid (uncoated) microneedles for skin pre-treatment
- Solid microneedles coated with a drug
- Solid dissolvable microneedles
- Hollow microneedles

Thus, this is how the prior art research here shall also be classified discussing each type in the above order.

2.2.1 Solid microneedles

Solid microneedles are broadly made of one of the three different materials, namely, silicon, metal or polymer. Additionally, other inorganic materials such as glass (16) and quartz (17) have also been used (see Figure 2.2). The glass microneedles were fabricated using conventional micropipette pulling techniques, achieving a length of 900 μm with a sharp bevel-shaped tip. The quartz microneedles were made using conventional MEMS processing utilizing isotropic wet etching resulting in the very sharp tips of tip diameter 10 μm , and microneedle height of 400 – 700 μm . These transparent quartz microneedles are being used for precise real-time allergy skin tests in patients.

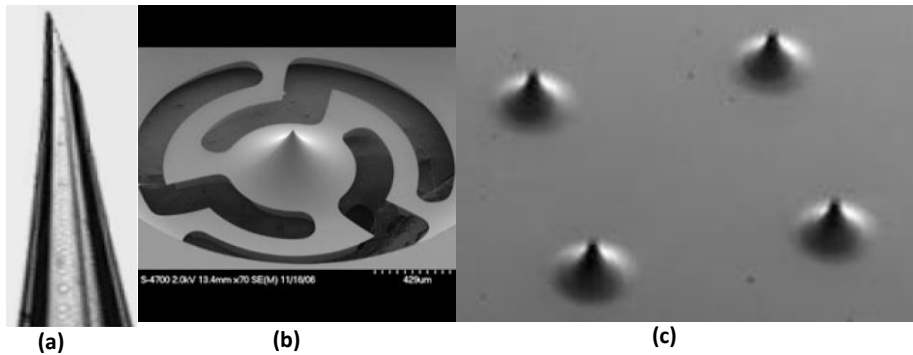


Figure 2.2: (a) Solid glass microneedle with bevel-shaped tip, 900 μm tall (16); (b) Quartz microneedle "lancet"(17); (c) An array of quartz microneedles for skin allergy test (17).

2.2.1.1 Silicon microneedles

By far, these constitute the most common type of solid microneedles, being fashioned out of the Si wafer substrate itself. A wide variety of fabrication techniques have been employed for making Si microneedles ranging from wet etching to dry etching, isotropic to anisotropic. A few popular ones are illustrated here. Since wet etching is a much cheaper process than dry etching, it can have a bearing on the economical feasibility of the process. Solid microneedles have been fabricated by anisotropic wet etching, that is, by KOH, along the crystal planes of Si (18), or also by isotropic wet etch in alkaline solvents (19). However, wet etch may be more time consuming and dry etching could also be more accurate. Thus, solid microneedles were also made from deep reactive ion etching (DRIE), a kind of anisotropic dry etch (20), as well as from inductively coupled plasma (ICP) etching, a kind of isotropic dry etch (21). Sometimes to circumvent the downsides of each method, several techniques such as isotropic dry etching using ICP have been combined with anisotropic wet etching to fabricate a sharp solid microneedle (22)(23). It is however to be borne in mind that with Si microneedles the length of the fabricated microneedle is typically dependent on the thickness of the Si wafer, and based on the size of the Si wafer used these thicknesses could vary from 350 μm (for 3" wafers) to 540 μm (for 6" wafers) to 700 μm (for 8" wafers). Therefore, it should be noted that if even taller microneedles are required then two Si wafers must be bonded to produce the desired height.

2.2.1.2 Metal microneedles

It is to be understood that Si being brittle always runs the risk of breakage inside the skin. This is undesirable. Thus, metals can provide the necessary mechanical strength. A variety of metals have been used in making microneedles: gold, platinum, stainless steel, titanium, tantalum or even nickel. A common metal deposition technique in microfabrication is sputtering – titanium microneedles have been made by this process (24) for blood extraction from the skin. Metal electroplating or electroless plating techniques have also been employed for deposition of metal on positive or negative microneedle moulds and finally releasing the microneedles from the moulds (25)(26). Laser ablation and laser cutting methods have also been used to fashion out in-plane microneedles from titanium or stainless steel two-dimensional sheets and then bent 90° to form out-of-plane three-dimensional structures (15)(27). Wet etching has also been employed to fabricate metal microneedles(28).

2.2.1.3 Polymer microneedles

Due to the inherent risks of Si and metal microneedles of breaking inside the skin and entering the blood circulation, polymer microneedle research is the latest global trend. A host of fabrication techniques have been utilized to make solid polymer microneedles – the most common being moulding techniques wherein the polymer is cast into a negative mould of a microneedle and then cured and released. Typically the master moulds are made of Si or metal, an intermediate negative polymer mould made of PDMS is made from the master. Finally, the actual structural polymer which could be UV-curable such as SU-8 or non-UV curable such as polycarbonate (29) or polymethylmethacrylate (PMMA) (30) is cast on the negative polymer mould to create the positive microneedle structure after cooling and solidification.

Lithography, electroplating and moulding (LIGA) is a technique used to generate high-aspect ratio structures, typically of the order of greater than 100:1, with very vertical sidewalls. LIGA employing deep inclined X-ray exposure and vertical exposure has been utilized to fabricate high aspect ratio structures with PMMA which exhibits photosensitivity towards X-rays (29). However, it is to be noted that though X-ray LIGA can produce highly desirable structures, it is however, prohibitively expensive. Other photosensitive materials such as the UV-curable epoxy, SU-8, has also been

used widely for fabrication of solid polymer microneedles (31). Gray-scale lithography is commonly employed to create a UV-path diminishing in intensity in order to create tapering structures, and thus, to give shape to a sharp tip. Also, a combined technique of microlenses on transparent glass substrates together with a backside photolithographic exposure produces a conical microneedle structure due to the converging optical effect accruing from the microlens (31).

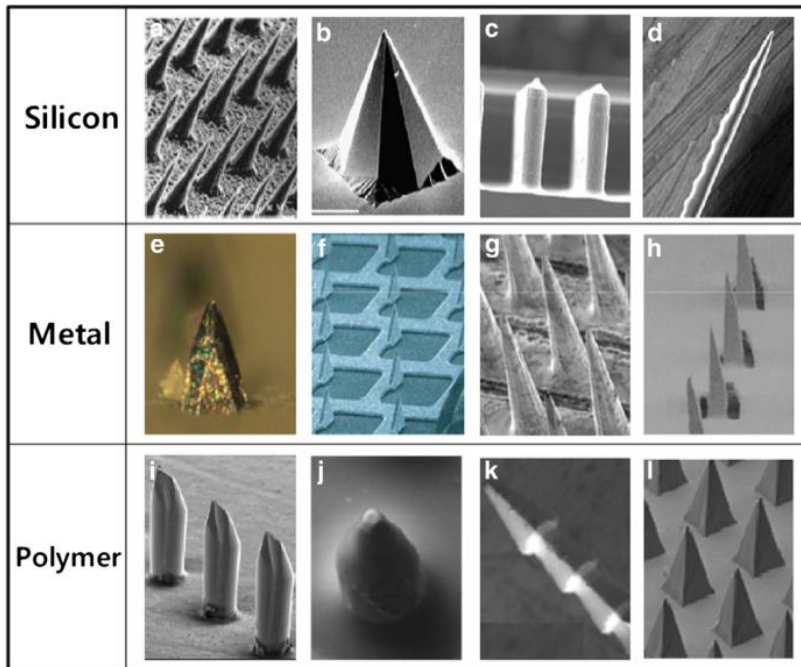


Figure 2.3: Examples of fabricated solid microneedles. (a)(32); (b)(33); (c) (34); (d) (35); (e) (36); (f) (20); (g) (37); (h) (38); (i) (39); (j) (29); (k) (40); (l) (41)

2.2.1.4 Ceramic microneedles

Ceramics such as alumina have also been used for making microneedles primarily for low cost processes and also for achieving a high degree of porosity within the solid microneedle structure inside which drugs may be loaded for delivery (42). Typically, micromoulding techniques were employed here to make a PDMS mould which was then filled with the ceramic slurry and sintered to produce the desired microneedles.

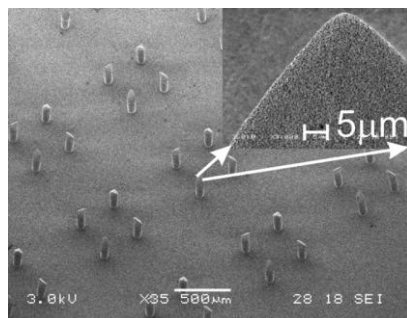


Figure 2.4: SEM image of fabricated ceramic microneedle arrays - individual microneedle length of 300 μm and width of 100 μm , and a tip diameter of about 5 μm (42).

2.2.2 Solid coated microneedles

What was described above is mainly microneedles solid in nature which can be used for skin pre-treatment before a manual topical application of the drug on the skin surface. However, solid microneedles can also be coated with a drug formulation and thereby used directly as a drug delivery vehicle. Upon insertion into the skin, the drug payload dissolves gradually or quickly inside the tissue, and finally the microneedle is withdrawn. Several techniques are in vogue for coating the solid microneedle surface. Dip-coating is, by far, the simplest method wherein the entire microneedle array is dipped in a large reservoir containing the drug formulation solution (43) once or multiple times, or into individual microwells for each corresponding microneedle(44). Spray-coating is yet another widely used technique wherein an aqueous solution of the drug comprising the active drug substance: a vaccine, drug molecule or another active ingredient; a surfactant to increase wettability of the microneedle surface; combined sometimes with a stabilizing agent to prevent the drug from being affected adversely by the drying and storage steps (44)(45)(46). One such spraying approach used an atomizer for breaking the coating solution into miniscule droplets for coating (33). A notable downside of the solid coated microneedles is that the amount of drug to be delivered is limited by the surface area available for coating and is typically less than 1 mg for small microneedle arrays (47).

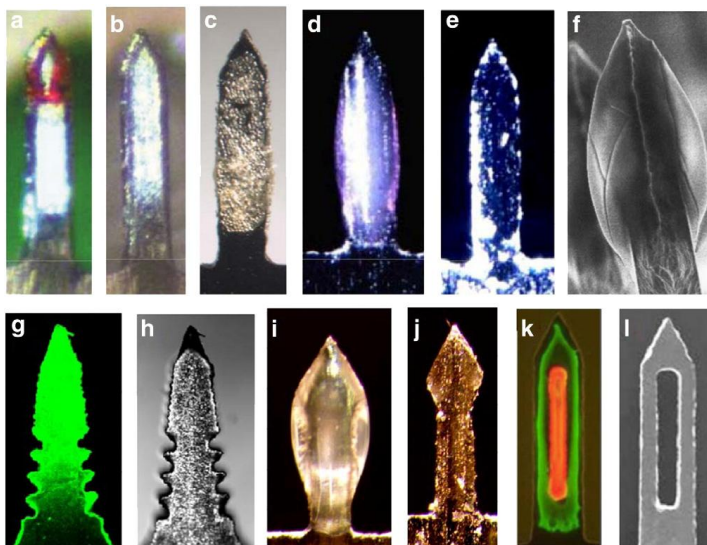


Figure 2.5: Examples of coated solid microneedles. a & b: (48); c (42); d & e: (46); f: (33); g & h:(49); i & j: (50); k & l: (51)

2.2.3 Solid dissolvable microneedles

As described in Figure 2.1, dissolvable microneedles once inserted inside the skin, remains inside and dissolves gradually over time, releasing its drug payload inside the skin. The advantage with this type of microneedles is that no needle sharps are generated and once applied, the patient need not bother about removing the microneedle patch. This helps in making this system the most patient-friendly and convenient to use. Typically, a biodegradable polymer is used for making the bulk matrix of the microneedle structure encapsulating the active drug ingredient. Very often, due to the method of making this in combination with a biodegradable polymer and a drug, the latter has to be re-formulated. This polymer-drug mix is water-soluble so that it can dissolve inside the skin tissues at a pre-determined rate. Most commonly, micromoulding techniques are used here as well. Some of the biodegradable polymers which have been used in the fabrication of dissolvable microneedles are carboxymethyl cellulose (CMC) (52), chondroitin sulfate(53), dextran (54), dextrin (54), polyvinylpyrrolidone (PVP) (55), polyvinyl alcohol (PVA) (56), polylactoglycolic acid (PLGA) (57), fibroin (58) and sugars (59). Care must be taken to ensure that the polymer melt solutions are cured at temperatures not detrimental to the

encapsulated drug or protein. Some of the active ingredients that have been tested thus, are the human growth hormone encapsulated in sodium chondroitin sulfate microneedles (60), erythropoietin (EPO) encapsulated in dextrin, and insulin encapsulated in chondroitin – both hydrophilic water soluble polymers, at room temperatures (61)(62).

A subtle distinction herein needs to be made between water-soluble polymers and the biodegradable polymers. The former dissolves rapidly inside the skin in a matter of minutes, typically ranging between 5 minutes to under an hour depending on the kind of polymer used (63), whereas classic biodegradable polymers usually take several days to months to dissolve completely inside the skin, and is used for a controlled drug delivery as may be required for a particular dosage profile (64).

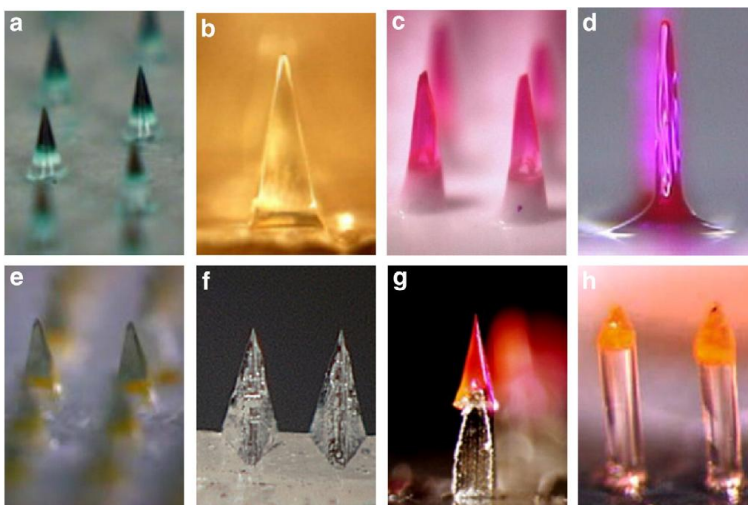


Figure 2.6: Examples of dissolvable microneedles composed of water soluble polymers and biodegradable polymers. a: (52); b:(65); c (55); d: (62); e: (66); f: (67); g: (68); h: (69)

2.2.4 Hollow microneedles

Hollow microneedles, as described in Figure 2.1, serve as a conduit for the drug solution from outside to inside the skin where it can be deposited. Therefore, unlike in the case of solid coated or solid dissolving microneedles, here the drug payload cannot be in a solid state. On one hand, while this could be a disadvantage, since in the aqueous state, the drug formulations are much more sensitive to temperature changes than in the

solid form (depending, of course, on the type of drug), on the other hand, this provides more flexibility in terms of maximum amount of drug to be delivered, as well as utilizing existing range of drugs without undertaking reformulation as they are, to combine with this for drug delivery. Since they are hollow microneedles through which the drug must be made to flow and be injected inside the skin, this necessitates a pressure-driven flow mechanism alike to the conventional hypodermic syringe-based system (70). Thus, pressure and the flow-rate can also be modulated for achieving a desired drug dosage profile. Since this kind of a system cannot be administered readily as a patch without certain other additions, it also translates into more patient complexity in usage as it requires the use of trained personnel or pre-trained patients. Due to their nature, hollow microneedles are mostly combined with an injection-based system, called an applicator. The applicator controls the force with which the microneedle array firstly is inserted into the skin, and next controls the pressure and flow rate of the injecting fluid (71). In some cases, a built-in drug reservoir on the back-side of the microneedle array can also be provided and piezoelectric actuation based-pressure could be used for pushing the drug through the hollow needles (72). Another approach could be the use of an on-chip heater which causes a membrane to expand, thereby driving up pressure to push out the drug solution (73). In essence, to drive out the fluid through the microneedle, an external pumping mechanism must be provided for – either on-chip or as an external ancillary unit.

Typically, hollow microneedles have been fabricated using classic MEMS fabrication techniques – ranging from deep reactive ion etching (DRIE) (74)(75), laser micromachining (76), wet etching(77) to deep X-ray lithography (78). Most commonly used material for making hollow microneedles has been Si due to its easy compatibility with the conventional semiconductor processing techniques. The simplest and one of the earliest approaches has been to etch through holes in Si wafer substrates using DRIE and then to etch out tall pillars around the holes (79). The resultant structures look like tall hollow cylinders with flat or unsharpened tips. Further additions were made to this process to combine them with a host of other techniques, for instance, selective wet anisotropic etch to fashion out sharp tips or even dry isotropic etch for making sharp tips(75). Various such combinations to wet and dry etching have been used in conjunction or in alternation or successively to create sharp tipped hollow microneedles. Some approaches have also relied on layer-by-layer fabrication techniques to make in-plane hollow microneedles with hollows which have subsequently been assembled out-of-plane to form a desired microneedle array for drug

delivery (80). Laser techniques have been used too for making holes in a solid pillar though this could be very tedious since the holes are only made by the laser one microneedle at a time (76)(81).

Si apart, also glass, metal and polymer have been used extensively for fabrication of hollow microneedles. Glass hollow microneedles were fabricated using conventional molten micropipette drawing techniques (82). The standard 30-gauge hypodermic needles have also been surprisingly used as “hollow microneedles” precisely by allowing only the tip of the needle totalling 1.5 mm to be protruding outside while the remaining length of the needle remains hidden behind view and is attached to a pre-filled syringe (83). Besides this, other metal microneedle fabrication approaches have used sputtering and electroplating with a sputtered-seed layer as metal deposition techniques on a polymer mould followed by dissolving the polymer to release the metal needle (76). Or, another approach used wet etching of copper combined with sequential electroless plating of copper and nickel layers to produce hollow metal microneedles (67). Polymers such as PMMA and the epoxy-based resin, SU-8 have also been used widely for making hollow microneedles (30). More often than not, a combination of techniques have been used – micromoulding together with photolithography for making the needle body (84) and laser drilling for making the hollow lumen (76) and mechanical polishing at angles for making the sharp tip (85). Photosensitive polymers have the advantage that using an appropriate mask, select areas of the photoresist mass can be cross-linked when exposed to the UV radiation, and the rest of the un-crosslinked areas may be removed upon development. This is a unique property of photosensitive polymers which allows circumvention of the more expensive and time-consuming steps such as DRIE or laser drilling. Hollow polymer microneedles with side-openings were also made using excimer laser techniques combined with hot embossing (86).

Wang et al at Georgia Tech (84) fabricated a hollow microneedle array by moulding SU-8 on a PDMS mould. The PDMS mould was made by casting PDMS on an SU-8 master mould, which in turn was made by casting SU-8 on a $<100>$ Si wafer fashioned with hollow pyramidal pits obtained by anisotropic etching of Si. Thus, the tip diameters of the microneedles obtained ranged between 15 to 25 μm . The cross-sectional shape of the microneedle was a square. The heights of the microneedle measured 825 μm and 400 μm in width, with the lumen diameter 120 μm and an average smallest wall thickness of about 100 μm , translating into an aspect ratio of between 8 to 16. This approach was very similar to the approach used here in this work but with a few noteworthy differences:

- 1) Si wafer was used as the mould and not SU-8 or PDMS – this resulted in much sharper tips with tip diameters ranging around 5 μm .
- 2) A much higher aspect ratio of greater than 40 was achieved with our process.
- 3) Higher shaft lengths of greater than 1000 μm were achieved with a hollow lumen throughout.
- 4) An anti-reflection layer of Cr-black was used to prevent undesired cross-linking by way of internal reflection of the UV radiation.
- 5) The cross-sectional area of the microneedle in this research were triangular, C-shaped and bevel-shaped – which are unique w.r.t. the prior art.

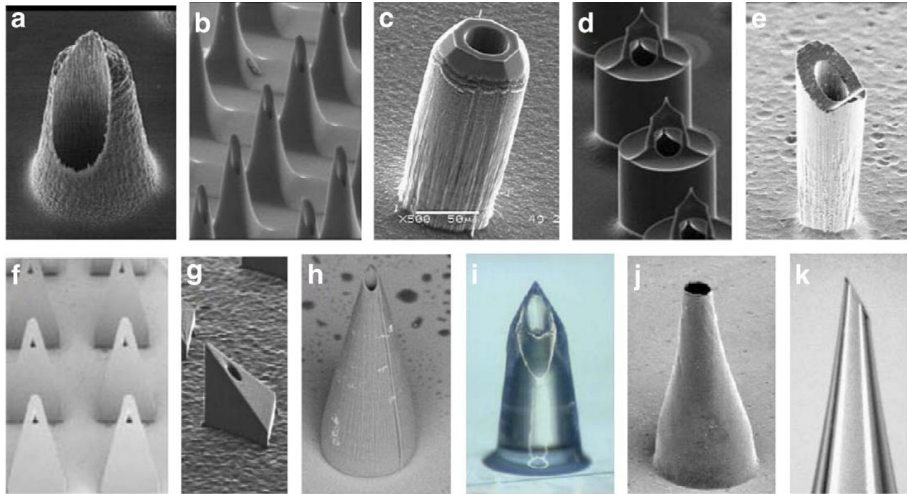


Figure 2.7: Examples of fabricated hollow microneedles of Si, metal and polymer materials. a: (87); b: (88); c: (77); d: (89); e: (90); f:(91); g: (75) h: (92); i:(93); j:(76); k: (94)

2.2.4.1 Ideal hollow microneedle

Since this work draws its inspiration from a mosquito fascicle as expounded in Section 3.1, the ideal dimensions for the biomimetic microneedle are that of a mosquito “needle” with a needle shaft length of about 2 mm, wall thickness of 5 μm and an inner diameter of 20 μm . The prior art has numerous examples of hollow microneedles but it is the mosquito needle only which is truly painless and is capable of both delivering a drug (anti-coagulant to prevent blood clotting) as well as blood extraction.

2.2.4.2 Problem to solve

Tall, hollow, high-aspect ratio polymeric microneedles with sharp tips that could be used both for transdermal drug delivery as well as blood sampling do not yet exist in the prior art. So this is the first problem to solve. Secondly, a robust, elegant and scalable process is required that should be comprise minimal steps and ensure maximum repeatability as well as versatility. Thirdly, such a process would have to be flexible w.r.t. variability in design height of the microneedle, variability in the cross-sectional area and geometric shape as well as basic architecture of the microneedle – solid or hollow, in addition to variability in the thickness of the base plate. Since such a microneedle in its entirety with all the aforementioned components or the complete process of making it such, does not yet exist – this presents the set of problems to solve.

2.3 Applications

It has been touted here so far that the main application of microneedles lies in drug delivery, and rightly so. But even within the ambit of drug delivery there are several sub-classes which may be worthwhile to be studied slightly more in detail to give a clearer insight into the required features of a microneedle based on its application.

In concise, following are the broad applications of microneedles:

- Delivery to skin
- Delivery to eye
- Delivery to cells
- Other applications

Arguably, delivery to the skin has been the most sought after application of microneedles more so because of its low-risk, and high attraction associated with the advantages. However other exciting applications are also emerging such as intraocular drug delivery and treatment for restenosis.

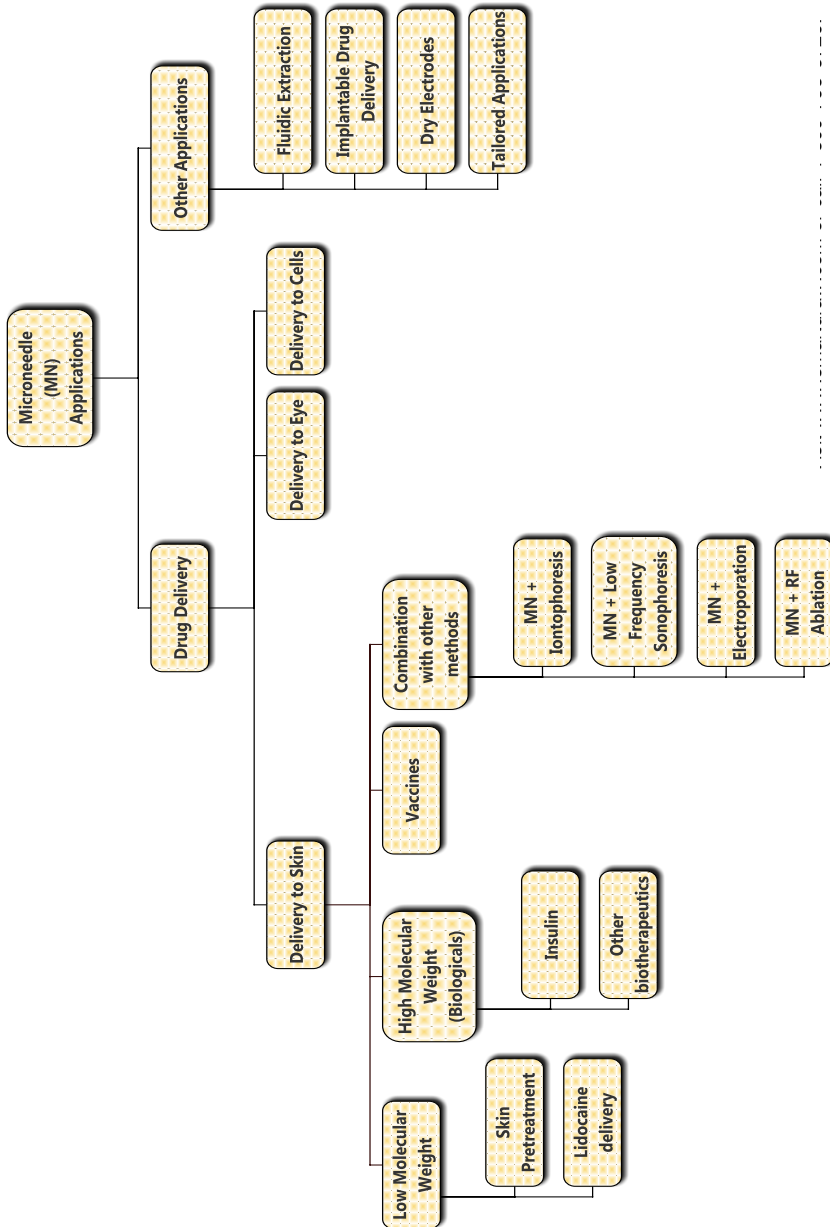


Figure 2.8: An extensive flowchart of the wide range of applications of microneedles.

As described above in Figure 2.8, delivery to the skin can be further divided into three sub-categories: 1) Low molecular weight drugs 2) High molecular weight drugs 3) Vaccines.

Low molecular weight drugs are relatively easier to deliver through the skin layers as they find lesser resistance to their diffusion than large molecular size drugs due to their large diffusion coefficients. Thus, simple skin pretreatment with microneedles is also sufficient to deliver these drugs. Small marker molecules such as calcein (molecular weight 623 Da) were studied for diffusion through human cadaver skin. When microneedles were inserted into skin and left in place thereby plugging the holes, the permeability was observed to increase by 1000-fold. When the microneedles were inserted and removed immediately, the permeability was observed to have increased by 10,000-fold (95).

Coated and hollow microneedles have been used for delivery of lidocaine, as a local anaesthesia. Hollow polymer microneedles were used to inject lidocaine intradermally into live patients and this was compared to a normal hypodermic injection. While the local anaesthesia effect produced by both the methods was same, patients experienced much less pain with the microneedle injection.

Large molecules (typically greater than 10,000 Da) such as peptides, proteins, DNA, RNA etc. have a much smaller diffusion coefficient than smaller molecules and hence, find it very difficult to diffuse through the skin layers. As previously discussed, these kinds of drugs are not administered orally due to the first-pass metabolism and are thus, delivered with a hypodermic injection. Given that typically only small doses, less than 1 mg, of these drugs are required, these form suitable candidates for delivery via microneedles. Insulin has been shown to be delivered effectively by microneedle pretreatment, solid dissolvable needles as well as hollow Si microneedles. Several other biologicals such as EPO, heparin, leuprolide acetate, desmopressin, human growth hormone desmopressin, salmon calcitonin and PTH have been shown to be delivered successfully by microneedles.

Vaccines, as already stated, have been found to be the most attractive candidates in the near-term future to be administered with microneedles (96) *vis-a-vis* the conventional hypodermic injections. This is due to several reasons: low pain compared to hypodermic injections, elimination of medical personnel to enable patient to administer himself and most importantly, the rich presence of the dendritic cells in the intradermal region of the skin facilitates a good immune response with even a small quantity of the vaccine drug. This is important towards overall cost-

reduction of individual doses as it leads to dose-sparing. Further, in developing countries, this could also lead to elimination of needle sharps and prevent needle re-use which has been a cause of major health hazard. Further, a dried form of the vaccine coated on a microneedle helps lower its sensitivity towards temperature thereby helping to reduce the high logistical cost associated with maintaining the cold chain across the entire supply chain.

A combination of microneedles with other techniques such as iontophoresis and low frequency sonophoresis has been shown to increase drug permeability by several fold (97). For example, skin pretreatment with microneedles followed by iontophoresis was used to administer oligonucleotides (98) and human growth hormone (99).

Intra-ocular delivery of drugs is another recent application of microneedles and it was shown that microneedles could be used effectively to deliver drugs to the sclera and corneal stroma (100), and that the bioavailability of the drug was raised by two orders of magnitude compared with topical delivery (101).

Of the other applications, the ones worth mentioning is one, use of microneedles as microelectrodes as dry electrodes, or even implantable neural electrodes combined with neural drug delivery. Two, microneedles recently was used for treatment of restenosis, by delivery of drugs to the inner walls of the cardiac artery from outside the artery with microneedles inserted inside the wall (102). Three, other applications such a implantable drug delivery may also be demonstrated with microneedles of the appropriate topography and design.

3

Design

Abstract

The main inspiration for the design is briefly highlighted at the beginning of the chapter. This is followed by the design objectives of the work and based on this the dimensions of the microneedles are decided. Next, the structural material for the microneedle is also chosen here, and the reasons outlined for such a choice. Based on the material properties as well as the structural dimensions the mechanical stability of the resulting microneedle is determined. Further, the final architecture of the end-device as envisaged is discussed highlighting the cause for a trade-off in the number of microneedles per array and the maximum drug delivered into the skin.

3.1 Design inspiration

Nature has always provided us with great inspiration and trying to mimic nature has been the goal of science in various different fields of life. Here too, the inspiration for the microneedle design was drawn from the humble or as some might say, the “annoying” mosquito. Though other blood suctioning insects have been discussed earlier here, the mosquito has truly a very remarkable engineering mechanism. Firstly, it possesses a ‘microneedle’ called the fascicle which is about 1.8 mm in length, about 4.5 μm in wall thickness and 22 μm inner diameter (103), giving it an aspect ratio of 400! Secondly, it is only a mechanical engineering marvel that a structure as long, thin and hollow as that does not undergo mechanical failure on penetration inside the skin. The main reason for this is that the mosquito employs a host of stabilizing manoeuvres to prevent buckling of its fascicle – the most prominent one of them being application of a non-conservative follower force in the form of axial vibration of its head and fascicle at about 15 Hz during penetration till complete penetration has taken place when vibration reduces to 7 Hz (104)(105). Secondly, the enclosing pair of protective sheaths around the fascicle (called the labium), spreads open during penetration, anchoring themselves on the skin surface causing the

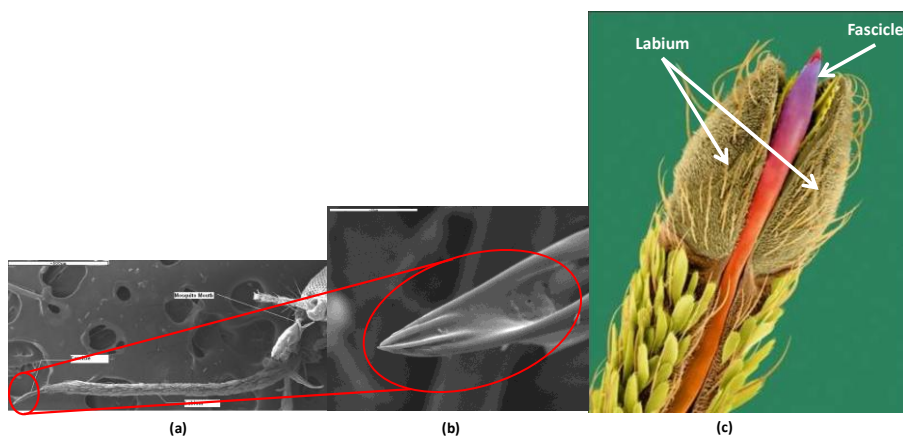


Figure 3.1: (a) The mosquito mouth, labium (sheath) and fascicle (needle); (b) Close-up view of mosquito fascicle tip; (c) Digitally enhanced image of fascicle enclosed in labia. [Source: (104)]

skin to be stretched outwards, thereby lowering the penetration force for the fascicle significantly (104). Third most remarkable feature is the tip of the fascicle itself – the reinforced tip to provide mechanical strength can be noted from Figure 3.1.

The structural material of the fascicle is chitin possessing a Young's modulus of elasticity ranging from 10 to 200 GPa (106). Tensile strength of chitin is about 65 MPa. After the fascicle is well penetrated and finds itself a blood vessel to contact for blood supply, it first injects an anti-coagulant into the skin to prevent the blood from clotting. Finally, it uses its pneumatic pumping mechanism to suction out the blood.

What can we learn from above is that the mosquito displays very elegant engineering mechanism at three stages of the blood withdrawal process: 1) The entire process of penetration of its fascicle into the skin involving skin stretching and axial vibration for reduction of insertion force and mechanical stability; 2) Delivery of anti-coagulant to prevent blood-clotting; 3) Use of a pneumatic pump to suction blood. Furthermore, on the structural side, the very shape of the fascicle tip itself inspires awe. Figure 3.1 (b) above illustrates the SEM image of the tip of the mosquito fascicle. It is clear that the tip is reinforced to give it additional mechanical strength during insertion into skin. Also the bevel-shaped geometry of the tip of the fascicle complements its sharpness. In fact, the bevel-shaped tip can be roughly compared to a triangular geometry as well.

With the above biomimetic inspiration in mind the design objectives may be set forth.

3.2 Design objectives

To first decide upon a set of design objectives it is first imperative to decide the target application and thus, the target dimensions. In our case, the target applications are as follows:

- Intradermal drug delivery
- Blood plasma and interstitial fluid withdrawal

Height: For intradermal drug delivery, the microneedle target height to be achieved is 1000 – 1200 μm . Blood plasma withdrawal necessitates a height of at least 1200 μm . Thus, the microneedle target height is 1200 μm to be used for both applications.

Inner diameter, Wall thickness: Based on mechanical stability design considerations (discussed in a later section), the wall thickness should be kept at a minimum of 25 μm and the inner diameter should be designed for at least 60 μm .

Geometry: In a bid to mimic the mosquito fascicle design or even the hypodermic needle design, two target geometrical cross-section designs have been frozen: bevel-shaped and triangular. The reason for choosing these two particular geometries is that they have an innate sharpened feature accruing due to their very geometries. It is to be noted here that neither the hypodermic needle nor the mosquito needle has a “bevel-shaped” *cross-section*. They both have a bevel-shaped *tip* and a *circular cross-section* only.

Sharpness: The sharpness of the needle tip translates into lesser insertion force into the skin and therefore, lesser pain for the patient. In this case, keeping in mind the values in literature, the target sharpness is a tip diameter of less than 15 μm . Due to the fabrication process utilized; this tip shall be angled at 54.74° to the horizontal.

Further, the desired single, triangular cross-sectioned, hollow, sharp microneedle may be envisaged as in Figure 3.2.

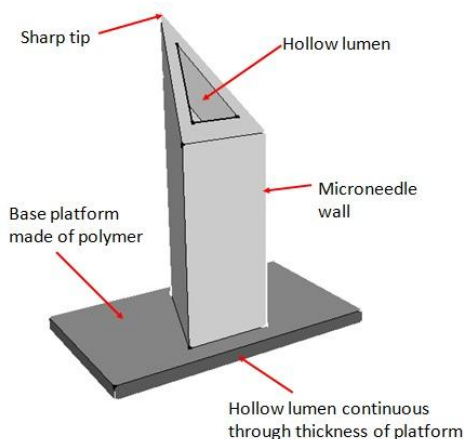


Figure 3.2: A 3-D representation of the envisaged fabricated single, hollow, triangular cross-section microneedle on a platform. Note the similarity of the angled triangular tip to the bevel-shaped tip of the actual mosquito. Also to be noted is the sharp tip arising from the vertex of the triangle itself and is a natural benefit of the chosen geometry.

3.3 Choice of structural material

3.3.1 Material considerations

The exploration of structural material began first with the process of elimination. Since the target device was meant to be a low-cost one, it straightaway necessitated the use of low cost raw materials. Biocompatibility is almost not an issue with the most commonly used materials like Si and metals because these maybe coated with parylene (USP Class VI polymer) to make them biocompatible. However, biocompatibility, in itself, is a widely debated topic since no material can be pronounced “biocompatible” in a blanket sense. Biocompatibility varies with the target application and device, it may vary widely from one application to another though the same materials may be employed. However, given that re-use of needles and needle-stick injuries are a cause of concern, especially in developing countries, it was decided to zero in on polymers as the structural material. So the given advantage of polymers over Si and metals is clearly elimination of needle-sharps and a full disposal by incineration, preventing needle-reuse. Given the plethora of options available within the set of polymers, the next consideration was given to ease of fabrication using conventional MEMS processing. For the design specifications (Section 3.2) aiming for a target aspect ratio of at least 48 meant the chosen material should be capable of high-aspect ratio fabrication, deposition of thick layers about 1.5 μm , and be of sufficient mechanical strength. Photopatternability was also another desired characteristic. Of photopatternable polymers, the following were considered: a) Poly(methyl methacrylate) (PMMA) b) Poly(methyl glutarimide) (PMGI) c) SU-8

3.3.2 Final choice of material - SU-8

Of the above, PMMA is more well-known for its use as an X-ray or electron-beam lithography resist. PMGI can produce very high contrast, very high resolution structures of the order of 20 nm (107) but with e-beam lithography. On the other hand, SU-8 has been used quite widely for fabrication of 3-dimensional structures by lithography as a negative tone photoresist. Further, its excellent properties of coating, planarization, highly vertical walls and ease of processing together with its mechanical and chemical stability, makes it a favourite candidate of choice for this work.

SU-8 2000 from MicroChem Inc., (Newton, MA, US) was selected as the final structural material for this work.

3.3.3 Properties of SU-8

In a nutshell, some of the more pertinent properties of SU-8 are listed as follows (108):

- Negative tone photoresist composed of Bisphenol A Novolak epoxy – cross-links on exposure to UV radiation.
- Contains photoacid generator which on irradiation produces a low concentration of acid which in turn acts as a catalyst for cross-linking.
- SU-8 allows deeper penetration of longer wavelengths (>365 nm), shallow penetration of shorter wavelengths (< 365 nm).
- High aspect ratio (HAR), well-defined structures can be achieved.
- Polymer shrinkage on cross-linking = 7.5%
- Mouldable with PDMS and other moulds.
- Layer thicknesses between 2 μm in a single-coat process and 3 mm in multi-coat process can be achieved.
- Young's Modulus = 4.02 GPa; Tensile strength = 34 MPa (109)(110).
- Glass Temperature (T_g) (fully cross-linked) $> 200^\circ\text{C}$
- Degradation Temperature (fully cross-linked) $\sim 380^\circ\text{C}$
- Cross-linked SU-8 is chemically very inert
- Propylene glycol methyl ether acetate (PGMEA) is the most common developer solution for SU-8.
- Percentage of polymerization of SU-8 depends on several factors such as baking time and temperature, exposure dosage, post-exposure bake as well as the hard bake. Longer baking times, higher exposure dosage and a subsequent hard bake ensures almost 100% polymerization (111), though exact numbers are not available with the manufacturer. However, in the context of this work, it was found that after the high exposure dosage, the subsequent post-exposure bake and the final hard-bake, the SU-8 fails to reflow on further heating as it has already been cross-linked completely.

A quick comparison of SU-8 with chitin shows that the latter has a much higher Young's modulus of elasticity between 10 to 200 GPa with a fracture toughness ranging from 0.2 to 2 kJ/m^2 (106) while SU-8, being an epoxy,

has a much lower Young's modulus between 2 GPa and 4 GPa with a fracture toughness of about 0.04 kJ/m² (112) (113). From these values, it is quite evident that chitin is a more superior material in terms of toughness as well as less brittle compared to SU-8. However, from a fabrication point of view, SU-8 scores above chitin especially with respect to HAR fabrication and photopatternability property.

A simple example of SU-8 fabrication scheme is demonstrated below in Figure 3.3(a) and (b).

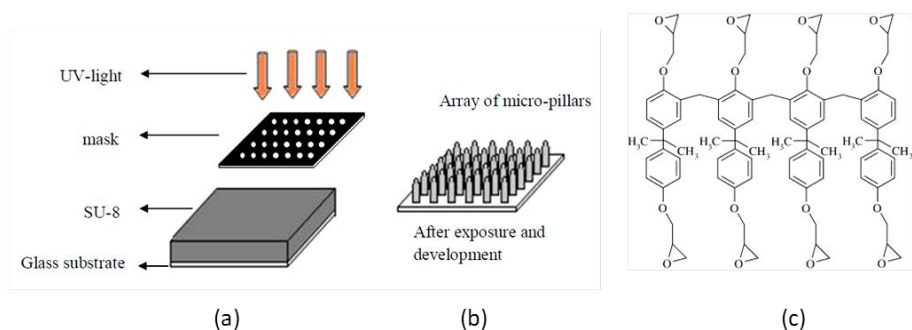


Figure 3.3: (a) SU-8 coated on a glass substrate exposed via a mask to UV radiation; (b) Array of HAR micro-pillars formed after cross-linking by UV exposure and subsequent development [Source:(114)] (c) Molecular structure of Bisphenol A Novolak epoxy contained in SU-8.[Source: (114)(115)].

3.4 Mechanical design

3.4.1 Individual Microneedle

From Euler's Column theory (116), we know that the critical failure force, P , due to bending, for a fixed-free column of length l is given as:

$$P = \frac{\pi^2 EI}{4l^2} \quad 3-1$$

where E is the Young's modulus of elasticity of the material of the microneedle and I is the moment of inertia of the microneedle cross-section.

According to mechanical engineering principles, the buckling will take place about that axis through the centre of gravity (C.G.) which has a lower moment of inertia(117). Since, all the cross-sections used here have a lower I_{xx} (I about $X-X^1$) than I_{yy} (I about $Y-Y^1$), only the I_{xx} for the different geometries have been tabulated in Table 3.1. As an example, for the triangular cross-section this is given by:

$$I_{tr} = \frac{BH^3}{36} - \frac{bh^3}{36} \tag{3-2}$$

From, Figure 3.2, a cross-section of the microneedle can be illustrated as in the following figure:

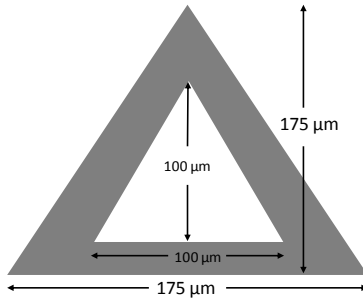


Figure 3.4: A cross-section of the designed microneedle. Both the triangles are isosceles with each having the height and base as indicated.

With $E = 4.02$ GPa for the SU-8 used, and the length l being $1000 \mu\text{m}$, substituting in Equation $P = \frac{\pi^2 EI}{4l^2}$ 3-1 and

$$I_{tr} = \frac{BH^3}{36} - \frac{bh^3}{36} \tag{3-2}, \text{ we get:}$$

Critical Failure Force, $P = 0.231$ N or, 231 mN

According to values in literature (118), the skin insertion force of a microneedle of tip diameter less than $15 \mu\text{m}$, ranges from 5 mN to 100 mN. Assuming the maximum insertion force of 100 mN, we get:

$$\frac{\text{Failure force}}{\text{Insertion force}} > 1 \quad 3-3$$

Thus, the microneedle was designed to be mechanically stable during the skin insertion process.

The triangular cross-section microneedles were the most desired ones due to their similarity in shape with the mosquito fascicle structure. However, other geometrical cross-sections were also designed: solid circular (SC), hollow circular (HC), C-shaped (CS), hollow triangular with triangular cross-section (HTTC), hollow triangular with circular cross-section (HTCC), hollow bevel-shaped (HB) and hollow-slit bevel-shaped (HSB). These cross-sections are illustrated as follows in Figure 3.5.

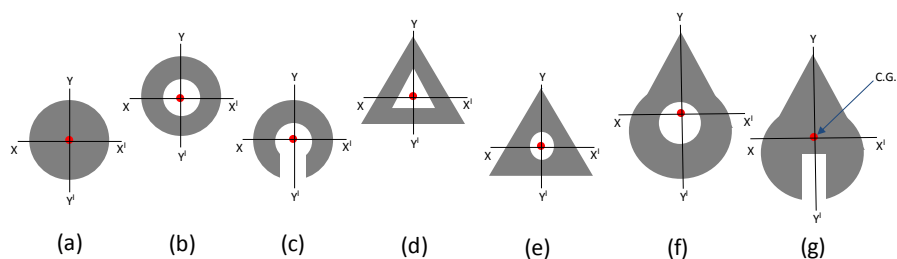


Figure 3.5: Various microneedle cross-sections that were designed. The red dot in the centre of each shape indicates its centre of gravity (C.G.) while the $X-X'$ and $Y-Y'$ axes are also denoted. (a) Solid circular (SC) (b) Hollow circular (HC) (c) C-shaped (CS) (d) Hollow triangular with triangular cross-section (HTTC) (e) Hollow triangular with circular cross-section (HTCC) (f) Hollow bevel-shaped (HB) (g) Hollow-slit bevel-shaped (HSB). [Note: figures not drawn to scale]

A comparison of the calculated critical failure forces of microneedles designed with the above cross-sections and of the same height, 1000 μm , is listed in the following Table 3.1:

Cross-section geometry	Dimensions (in μm)	Moment of Inertia I_{xx} ($\times 10^{-18} \text{m}^4$)	Critical Failure Force (in mN for $l=600 \mu\text{m}$)	Critical Failure Force (in mN for $l=1000 \mu\text{m}$)
SC	r = 40	2.01	55	20
HC	Outer dia = 80, inner dia = 50	1.70	47	17
CS	Outer dia = 80, inner dia = 50, rect.opening = 15x30	1.14	31	11
HTTC	Outer base = 175 Outer ht = 175 Inner base = 100 Inner height = 100	23.3	641	231
HTCC	Outer base & ht = same as HTTC, Inner circ. dia = 75	24.5	676	243
HB	Inner circ. dia = 66 wall th = 25 Tri. ht&base = 116 semicirc dia = 116	13.4	370	133
HSB	Wall th = 25 Tri. Ht & base = 116 semicirc dia = 116 Rect = 25x333	18.4	505	182

Table 3.1: Comparison of the various planned designs for this work: cross-sectional geometry, dimensions, moment of inertia and critical failure forces for heights of 600 μm and 1000 μm .

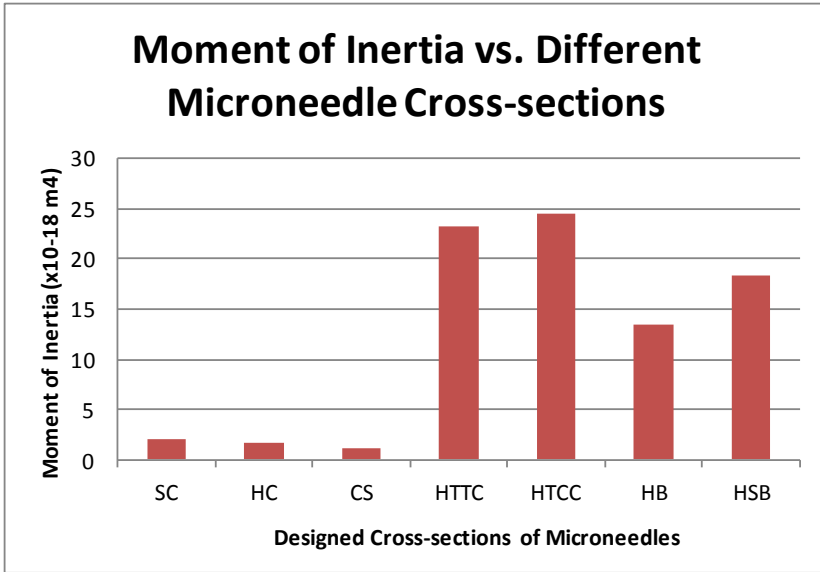


Figure 3.6: Comparison of the different moments of inertias of the designed microneedles in this work.

From Table 3.1 it is clearly observed that the critical failure force is highest for the HTCC followed by the HTTC type of microneedles. This, in turn, follows from the fact that the failure force is directly proportional to moment of inertia (I) as can be observed from Equation $P = \frac{\pi^2 EI}{4l^2}$

3-1.

Figure 3.6 compares the moment of inertias of the different cross-sections of the microneedles thereby, comparing also their relative failure forces. In the light of this, we can summarize that the HTCC is the strongest microneedle designed followed by HTTC, then HSB and finally HB. The CS variety is the weakest, and even intuitively this can be analyzed thus, resulting due to its small moment of inertia. Therefore, an identical trend across the different cross-sections are also observed in comparison with critical failure forces.

3.4.2 Microneedle Array (MNA)

Since the volume of single hollow microneedle is very small, several such microneedles are needed in order to achieve the desired flow rate as well as to deliver the required volume of drug. For instance, if we consider the bevel-shaped (BS) microneedle from the above table, the volume capacity of that needle inside its hollow lumen for a 1000 μm height, is merely $3.4 \times 10^{-3} \mu\text{l}$. A small volume capacity limits the volume flow rate. To overcome this, a larger number of microneedles are arranged in an array.

However, it is quite a well-known fact from fundamental physics that pressure is the ratio of applied force to a given area on which it is applied. For a given force, as the area is increased, the pressure is reduced. A classic example given is the famed “fakir-bed effect” wherein a fakir or a saint lies down on a bed of sharp pointed end nails (see Figure 3.7)), and yet appears to be unhurt. The secret lies in the fact that due to his entire weight being distributed over the bed of nails, the net pressure experienced by his body is much lesser than compared to when he would be lying down on only nail. It is the same with microneedle arrays. Indiscriminate increase in the number of microneedles for increasing the total drug payload, would not work since the total insertion force required to penetrate so many more needles would be correspondingly higher. To put it in perspective, say microneedles with tip diameters less than 10 μm require a maximum insertion force of 100 mN each, considering uniform steady-state velocity of motion of microneedle before impact. (For a high velocity or high impulse type of impact, the insertion force shall be lower). If 500 mN is the total application force spread over a 100 number of microneedles, then, the pressure exerted on skin by each microneedle tip shall be 63.66 MPa. However, if the same application force of 500 mN is employed to insert only 5 number of microneedles, then the corresponding pressure exerted on skin shall be raised by several orders of magnitude to 1.27 GPa. A higher pressure exerted by the same given force, necessarily means that the process of penetration would be smoother and relatively less painful than in the previous case. To summarize, if N is the number of needles or nails in this case, and if F_{tot} is the sum total of the load applied on N needles, then the load applied per needle, F_n

$$F_n = \frac{F_{\text{tot}}}{N} \quad 3-4$$

Thus, to avoid this effect, a trade-off is required between the number of microneedles on the array and the maximum drug payload to be delivered inside the skin. Thus, four number of microneedles arranged in a 2x2 matrix was selected as the ideal microneedle array for this work. Also, for the purpose of maintaining geometrical symmetry as well as to aid in insertion, a 5th microneedle may be placed at the centre of the 4 microneedles.

Inter-needle spacing between adjacent microneedles plays a crucial role in this too. If the microneedles are very closely packed, then not only is the applied force re-distributed but also, all the needle tips seem to form one continuous invisible flat surface thereby raising the insertion force for the entire array by orders of magnitude. As shown by Haider et al (119), an increase in the inter-needle spacing reduces the insertion force and thus, 1.5 mm was their designed spacing for a transdermal drug delivery application. In this work inter-needle spacing was designed at 1 mm end-to-end.



Figure 3.7: An Indian saint of a high monastic order, performing penance on a bed of nails in Varanasi in 1907. This is the "fakir-bed effect" wherein the fakir is not hurt by the bed of nails.

4

Process Design & Fabrication

Abstract

In this chapter which forms the core of the work done during the research, the process goals are defined at the outset keeping in mind the defined device parameters as well as constraints of resources and process limitations. Various process ideas have been briefly discussed before narrowing down and freezing the final process design. The process is described step by step from scratch, basic pitfalls, their causes and rectifications, and how the device is fabricated gradually while it grows functionally at the same time. The entire process has been developed hands-on and built-up step by step adding on to the previous process step, and finally optimized to give shape to the desired fabricated microneedles.

4.1 Introduction to the Process

As detailed in the previous Chapter 3 on design, the objective of the process is to fabricate tall, sharp, hollow microneedles on a platform with the hollow lumens of the microneedles continuous through the corresponding holes of the base platform as illustrated in Figure 4.1. Broadly breaking it down into two steps, Figure 4.1 (1) shows the first process goal, namely, to fabricate tall, hollow microneedles on a solid platform, and then the final goal as pictured in Figure 4.1 (2) showing a cross-section of the tall, sharp, hollow microneedles on a platform with coinciding holes. Keeping this in mind, this chapter is divided into the following parts:

- 4.2 Goals & Challenges of the Process
- 4.3 A fundamental principle
- 4.4 Process Conceptualization – various proposals
- 4.5 Basic Process Design
- 4.6 Intermediate Process Design
- 4.7 Advanced Process Design
- 4.8 Final Optimization of the Process
- 4.9 Salient features of the process

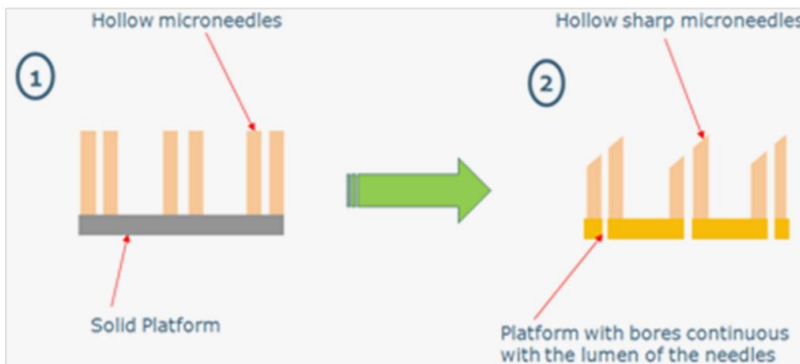


Figure 4.1: Cross-section of two basic architectures realised in this work: 1) Hollow microneedles standing on solid platform, 2) Hollow needles on a platform with open bores coinciding with hollow lumens of microneedles.

4.2 Goals & Challenges of the Process

As illustrated in Figure 4.1, these are the two basic architectures setting forth the step-by-step development to achieve the target goal of fabrication. Delving deeper, looking at Figure 4.1 (1), these are mostly hollow cylinders standing on a solid platform. These cylinders should have geometrical cross-sections consistent with design requirements set down in the Chapter 3 - Design. Thus, triangular cross-sections of microneedles with a triangular cross-section bore should be made possible. Normal circular cross-section microneedles should also be achievable. In fact, cross-sectional geometry should not be a constraint irrespective of the process chosen. Next, since not just transdermal drug delivery is desired but also, blood sampling could be a potential application, tall microneedles with their heights in the order of about 1000 μm should be achievable. Given inner diameters of around 60 μm and wall thicknesses in the range of about 25 μm , target aspect ratios should be 40 or greater. This high-aspect ratio target for hollow microneedles with such narrow lumens provides one of the most challenging requirements to be met especially because the long lumen of the needle needs to be hollow right through.

Another question which arises immediately when such tall slender pillar-like structures are discussed is obviously, their mechanical strength and stability and their resistance to undergo buckling on application of load. This characteristic feature is imperative without which the entire effort of making them would be defeated. Next on examining Figure 4.1 (2), the next set of features become prominent additionally to the previous features namely, sharp tips and a platform with holes. Thus, tip sharpening is a step which should be ideally compatible *in-situ* with the process. Of course, the needles could be sharpened as a post-processing step, if required, but that is not ideal.

The platform with its holes is the next most challenging goal to be met. The hollow of the microneedles must be continuous through the holes to provide for fluid conduit through the needles to the external environment. This is crucial for transport of fluids from say, a drug reservoir at the posterior end (end attached to the platform) of the microneedle through the hollow lumen to the anterior end (sharpened tip end inserted into skin). Of course, again as in the case with tip sharpening, the platform could be fabricated separately and then integrated with the microneedle in a post-processing step but as simple as that may appear, it could be extremely tedious and thus, ideally, it is desired to make the platform and the holes and

the bonding with the needles *in-situ*. What is also of prime importance here is the strength of bonding between the needle and the platform, exact coinciding of the hole of the platform with the lumen of the needle and this is a formidable challenge which has been discussed in great detail later on. Essentially, the process target goals can be summed up as follows:

1. Flexibility of design parameters – height, geometry, dimensions
2. High aspect ratio structures
3. Hollow lumens inside microneedle
4. Tall, strong structures
5. Tip sharpening (*in-situ*, if possible)
6. Platform with holes (*in-situ*, if possible)
7. Bonding microneedles with platform (*in-situ*, if possible)

Thus, given the target goals of the process, we can now proceed to conceptualize and design the optimal process to meet the above goals.

4.3 A Fundamental Principle of Fabrication

Having frozen upon the basic architecture, material to be used and the basic fabrication principle, there is still another important issue to be considered before commencing with the actual process design – and that is, to choose between in-plane fabrication and out-of-plane fabrication. As illustrated in Figure 4.2 below, in-plane fabrication, as the name itself suggests, means fabrication of the structure in the plane of the substrate, or the longest axis of the structure lies parallel to the plane of the substrate. Out-of-plane fabrication, on the other hand means the longest axis of the fabricated structure lies orthogonal to the plane of the substrate.

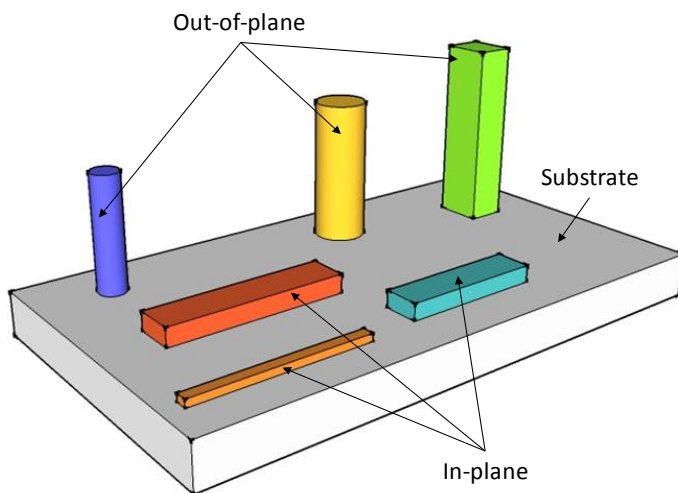


Figure 4.2: Graphical 3-D representation distinguishing between in-plane and out-of-plane fabrication methodologies.

Now, in this case of microneedles, a great deal would depend on whether an in-plane or out-of-plane fabrication method is chosen. Let us consider both the cases. Harking back to the chapter on design, it may be recalled that a 3-D array of microneedles is the final goal to be achieved. Or, in other words, a matrix-like architecture is desired such as [2x2] or [3x3] or [nxn] where n is the number of microneedles in each row and column, thus, giving rise to an n^2 number of needles. For eg., a [3x3] architecture would comprise 3 numbers of needles in rows and another 3 in column in the appearance of a [3x3] matrix, totalling 9 needles in number in that array. Now, if an in-plane

fabrication technique is used for this kind of architecture, it can be imagined that only single rows of needles can be fabricated in-plane (2-D fabrication), which have to be then assembled in a 3-D fashion in an array after the fabrication is over in order to produce a [3x3] matrix arrangement. This assembling the microneedles on a platform could be very tedious, though, not impossible (85). However, another critical feature of this process would then be the platform of the microneedles itself bearing the open bores which would correspond to the hollow lumens of the needles (see Figure 4.1 – (2)). This would entail another fabrication process only for making the platforms itself. Finally, assembling the hollow microneedles onto the platform would require a great deal of expertise not only in ensuring proper bonding between the microneedle bottom rim and the platform but also an accurate alignment between the hollow of the microneedle lumen and the bore of the platform which must coincide exactly to allow an open channel for the conduit of fluids. This entire complexity can be avoided if out-of-plane method of fabrication is chosen. However, the upside of the in-plane fabrication method is that there is verily no limitation on the length of the microneedles that can be achieved. Since it is an in-plane method, the hollowness of the lumen as well as the exact length of the microneedle can be very well controlled by tuning the mask design. This is the primary singular advantage the in-plane fabrication method has over the out-of-plane method. Coming to the out-of-plane method, the process in itself is much more elegant and simple. Not only can the microneedles be fabricated in a 3-D array straightaway thereby circumventing an arduous assembly step later on (85), but also the platform itself containing the hollow bores can be fabricated *in-situ* facilitating a good bonding between the platform and the needles. And the whole process can be termed simplistically as “monolithic” producing the complete 3-D array of microneedles as a final end product of the process. From a mass production point of view, this is an attractive option too as it minimizes post-processing requirements significantly in terms of final usage. However, the downside of the out-of-plane fabrication method, is rooted in the very physics of the fabrication principle in this case. Since UV light is the chief agent for giving the final shape to the needles and more so, for defining the hollow lumen, it is essential that the UV radiation reaches the bottom of the microneedle walls in order to crosslink them to provide sufficient structural strength to the microneedle. This becomes increasingly difficult with the tall heights of the microneedles ($> 1000 \mu\text{m}$), as the UV light must penetrate into this depth and that too via a small opening, effectively leading to diminishing intensity till it finally reaches the bottom of the microneedles. This is one of the potential downsides of the out-of-

plane process. Another issue is the possible dispersion of the UV radiation at greater depths of the SU-8 leading to undesired cross-linking which could in turn lead to blocking of the hollow lumen of the microneedle.

However, after having weighed the aforementioned pros and cons it was finally decided to select the out-of-plane fabrication method over the in-plane one, simply for the elegance and relative simplicity of the former over the latter.

4.4 Basic process design

Before proceeding with the basic process design, a fundamental feature about the structural material in question, namely, SU-8 needs to be understood and its implications in the fabrication. This is discussed in the following section.

4.4.1 A basic principle of SU-8

With the basic architecture of the microneedles was already frozen upon, it was necessary to next consider the various options for fabrication. The primary structural material for the microneedles, as already discussed in Chapter 3, is SU-8, a negative-tone photoresist. The ideal method to exploit the properties of this photoresist would be to utilize it by way of photolithography, namely, exposing certain areas of the photoresist to incident UV light and thereby cross-linking those portions while the rest of the uncrosslinked portions could be removed. Essentially SU-8 contains a photoacid generator which when exposed to UV radiation produces an acid which acts as a catalyst for cross-linking. Further, it ensues from the cross-linking process that UV light contact with the SU-8 photoresist hardens it. This could be a cause of potential concern should the UV radiation suffers undesired dispersion within the mass of the SU-8 thereby causing cross-linking within the hollow lumen of the needle. Or, another possibility is the reflection off the surface of the substrate itself and this could lead to a possible cross-linking at the bottom of the microneedle blocking the lumen completely or partially.

4.4.2 The basic process flow

As illustrated in Figure 4.3 the basic process design comprises manually coating a silicon wafer surface with a thick layer of SU-8 which is then subjected to a pre-baking step, followed by UV exposure, followed by a post-exposure bake. Finally, a development step is performed for removal of the uncrosslinked portion of the SU-8 giving form to hollow cylinder-like structures or unsharpened microneedles.

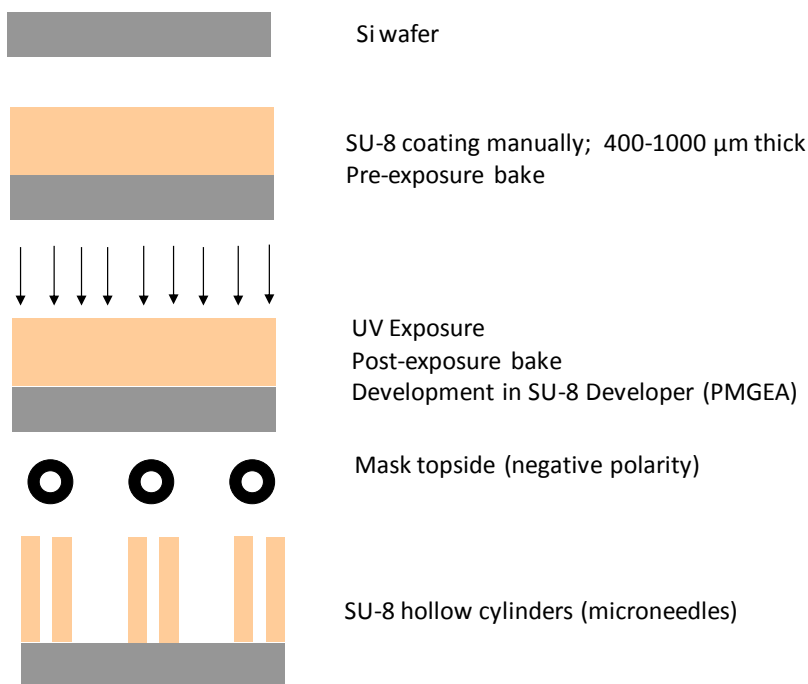


Figure 4.3: Basic process flow for out-of-plane microneedle fabrication

As is seen from the above process flow diagram, the microneedles fabricated here correspond to the architecture elucidated in Figure 4.1 (1), namely with a solid platform without any inlet channel for the microneedle lumens.

4.4.3 Basic process: discussion, issues and results

As simplistic as the basic process may appear, a discussion of it is far from complete without delving into the nitty gritty of it, and for this reason, it is essential to discuss it threadbare from the initial fabrication results point of view. The initial results of the above fabrication process are illustrated as follows in Figure 4.4.

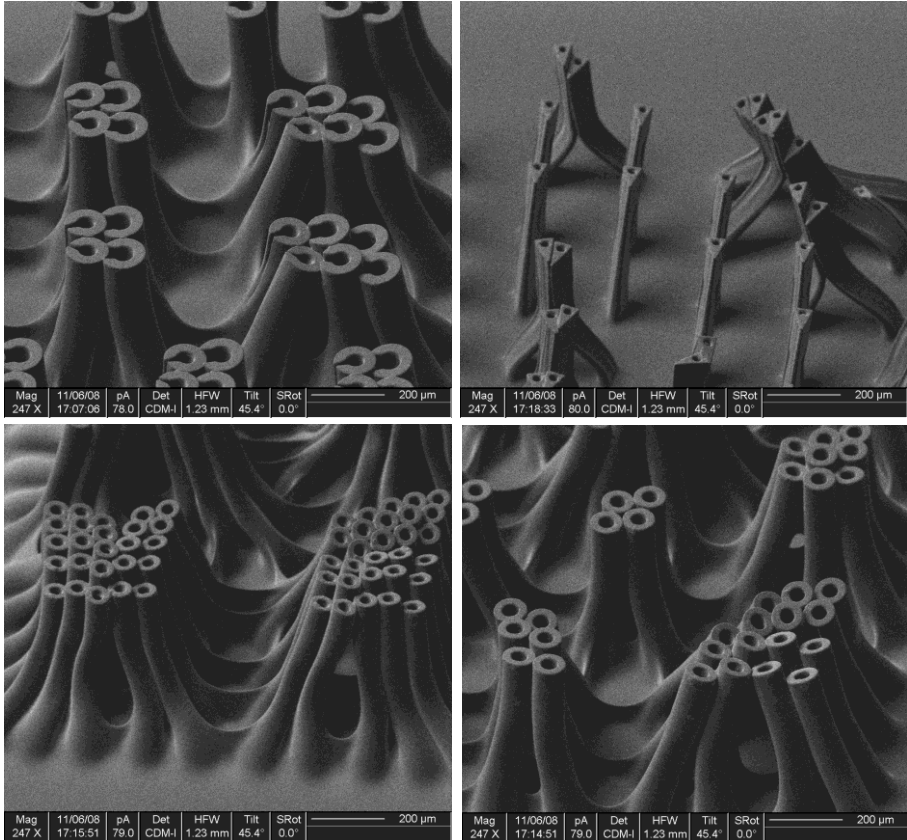


Figure 4.4: First fabrication results using the basic process design. To be noted are the weak bases of the hollow cylinders (of various geometrical cross-sections and dimensions) leading to bending and collapse of the final structures after development.

The process employed is fairly straight-forward. Since SU-8 is basically a negative photoresist material, this property has been exploited. This enables one to circumvent the entire arduous process of isotropic etch by deep reactive ion etching (DRIE) in order to create vertical out-of-plane structures. In order to fabricate thick structures, the SU-8 is simply poured out of its bottle directly onto the Si wafer substrate while it is lying on a precision weighing scale. SU-8 200 is used here for all fabrication. The thickness is controlled by measuring the weight of the SU-8 on the wafer.

The optimum weight of SU-8 to be placed on the wafer, corresponding to a specific thickness, is obtained by trial and error. A good

rule of thumb that is usually followed is to ensure that the solvent concentration of the SU-8 is less than 12% after pre-bake. It has been observed that the conventional process flow for fabricating SU-8 structures as reported in literature does not hold good in this case as the SU-8 structural layer here is much thicker than is usually the case. And thus, manual coating is resorted to in contrast to the conventional spin-coating method. But due to the high thickness of the layer a very typical problem is encountered, namely, the large concentration gradient of the solvent from the bulk of the SU-8 material to the surface after the soft-bake step. This leads to issues in the later stages in terms of base-pillar strength which becomes greatly weakened as the solvent material which is supposed to have been evaporated in the pre-exposure bake stage, did not evaporate completely from the lower layers, thus leading to this problem as clearly illustrated in Figure 4.4. Another severe problem that is encountered in such thick layers is the formation of a copious quantity of air bubbles. Obviously, the next step of UV exposure cannot be executed properly if these air bubbles are present.

To overcome these obstacles, the pre-exposure bake was divided into two parts. First, multi-layer SU-8 spin-coating along with pre-bakes were carried out (120), which was followed by a degassing step. However, in contrast to the work performed by (120), wherein every spun layer was not only pre-baked but also exposed and subjected to post-exposure bake and curing followed by a final development step, here in our case, only multiple spin-coats and multiple pre-bakes were performed while resorting to a single final exposure, post-exposure bake and development step. To elucidate further, a 150 μm thick layer of SU-8 is spun on the wafer and is subjected to a pre-bake at 90°C for 4 hours, and is allowed to cool down for another 4 hours. This step is repeated 7 times with 7 consecutive layers of SU-8 in order to obtain a thickness of greater than 1000 μm with a relatively much lower solvent concentration than in the previous process. However, due to this consecutive spin-coating of layers on top of each other, inevitably, air bubbles get trapped inside and these have to be eliminated finally before carrying out the UV exposure.

This elimination of the trapped air bubbles is done in a vacuum oven at 95°C. During the vacuum oven degassing step it should be noted that at first, only the heating is switched on, and not the vacuum pump. As the semi-solid soft SU-8 starts melting and reflowing, the uneven SU-8 surface is transformed and becomes more or less flat (flowing according to the slope of the wafer substrate and thus, it is critical to ensure that that wafer substrate is positioned absolutely horizontally flat without any slopes to

prevent flowing out of the SU-8 from any one side of the wafer). At this juncture, if the wafer is brought out of the oven and observed closely, it would be noticed that more bubbles have formed inside the bulk of the SU-8 layer. This is absolutely detrimental to the photolithography process which is next. Thus, when the SU-8 is observed to have fully melted and spread evenly over the full Si-wafer, the vacuum pump is turned on. As the pressure inside the oven falls, it is observed that the air bubbles are expanding in a dramatic manner, till a certain point when it appears as if the entire wafer surface is covered with one large bubble (See Figure 4.5). At the moment the air pressure reaches the lowest value of around 10^{-4} bar, suddenly the large air bubble collapses, followed by a sporadic and continuous bursting occurring all throughout the SU-8 surface till no more bubbles are to be seen.

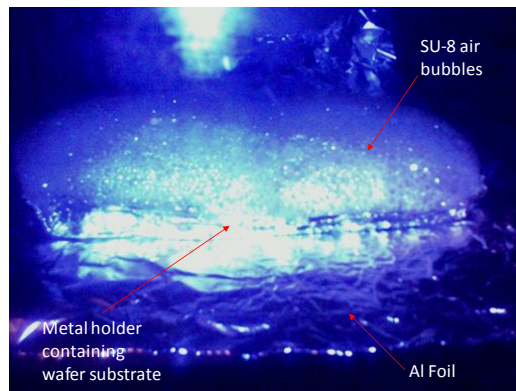


Figure 4.5: De-gassing of SU-8 inside vacuum oven. To be noted are the copious number of air bubbles which deflate as soon as the pressure drops to the minimum.

However, there is still another issue to be grappled with. During this entire process of SU-8 melting and reflowing, followed by the air bubbles' expansion and collapse, much of the SU-8 material is lost as it tends to flow out of the wafer boundary especially when the bubbles collapse. To overcome this problem, a special round stainless steel plate with a diameter slightly greater than the wafer diameter, with through holes and a raised boundary, (the height of which should be much greater than the desired height of the needles) was constructed in order to hold the reflowed SU-8 within the wafer boundary, as shown in Figure 4.6. So, once the bubbles have collapsed showing a clear SU-8 surface, the air pressure inside the oven is raised once again. It is to be noted that the oven temperature should still be

kept at 95°C for reasons that shall become clear later. When the air pressure reaches normal atmospheric levels, the oven chamber is opened and the wafer holder containing the wafer is brought out. It will not be observed that due to the reflow and the sporadic bursting of the air bubbles the SU-8 material has spread everywhere, and thus the wafer in all probability would now be stuck to the bottom of the stainless steel wafer holder. But since the temperature was maintained at 95°C, when the wafer is brought out, the SU-8 is still in a semi-molten state. Acetone is poured via the through-holes on the bottom of the wafer holder to dissolve the SU-8 sticking to the bottom of the wafer, and a pair of tweezers is used to gently take the wafer off the stainless steel surface. This step is a very critical one and must be done as quickly as possible, because more the time consumed to take the wafer off the stainless steel surface, the more difficult it becomes to do so as the SU-8 cools down very rapidly preventing further removal. The holes on the bottom of the stainless steel surface serve to allow acetone reach the bottom surface of the wafer to allow the detachment of the SU-8. This step would have been much simpler had the wafer been allowed to cool down substantially, but the fact that it is to be done immediately after taking out of the oven, makes this step the most challenging yet apparently very trivial. Normally, this step of removal of the wafer substrate holding the SU-8, from the wafer holder must be performed in less than one minute after taking it out of the vacuum oven.

Once this step has been completed, the SU-8 is allowed to cool down to room temperature. The surface texture is now smooth and non-sticky with no air bubbles. The SU-8 is then subjected to UV exposure through a patterned chromium mask. To ensure adequate exposure throughout the thick layer, an exposure dosage of 12 J/cm² is used.

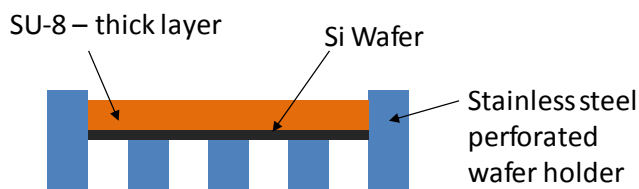


Figure 4.6: Specially designed stainless steel wafer holder with perforated holes and raised edges.

Next, a post-exposure baking step is carried out for the exposed SU-8, in an oven, at 80°C, for 1 hour. After baking, temperature is ramped down to room temperature over a period of 3 hours. This is followed by a development step for 10 minutes.

The approximate total time in performing one full run takes anywhere between 7 to 9 working days. It is to be noted that should the wafer substrate (mould) be in good order (no stress or cracks), it can be re-used for at least 6 to 7 runs. The Cr-black layer lasts just as long and can also be re-used along with the Si wafer substrate.

By performing the above arduous series of multi-layer spin-coating of SU-8, individually followed by pre-baking, and finally a single degassing step, exposure step and a development step, it can be safely inferred that the previous issue of non-uniform solvent removal leading to collapse of pillar bases, should be resolved. As proven by the ensuing fabrication results, this is indeed the case as illustrated in Figure 4.7 below.

As observed from Figure 4.4 and Figure 4.7, the previous defect of the weak bases had been resolved, but the appearance of undeveloped SU-8 didn't yet render the process perfect. This was then solved by changing the development from a normal development bath to an ultrasonic one and raising the development time to 20 minutes. It is to be again borne in mind that just an optimal amount of time inside the ultrasonic bath is permitted as prolonged periods therein would risk damaging the high-aspect ratio structures of the SU-8. After incorporating this change, the following results were achieved as depicted in Figure 4.8 below.

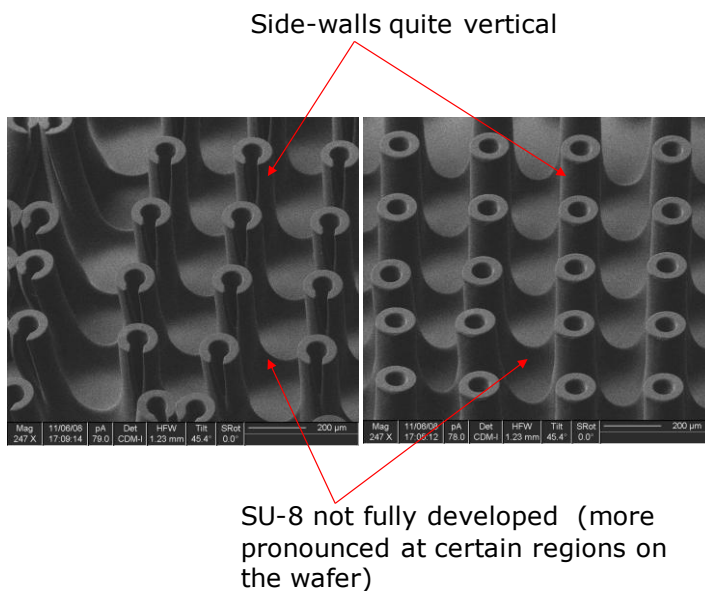


Figure 4.7: Cylinder bases quite strong and no bending observed. However, regions of undeveloped SU-8 observed.

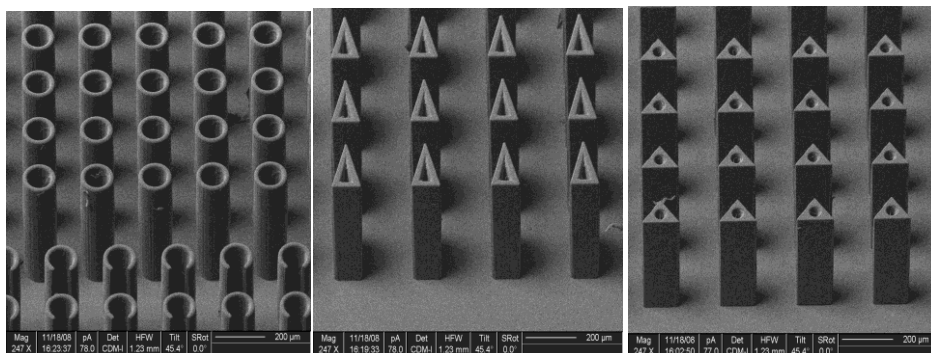
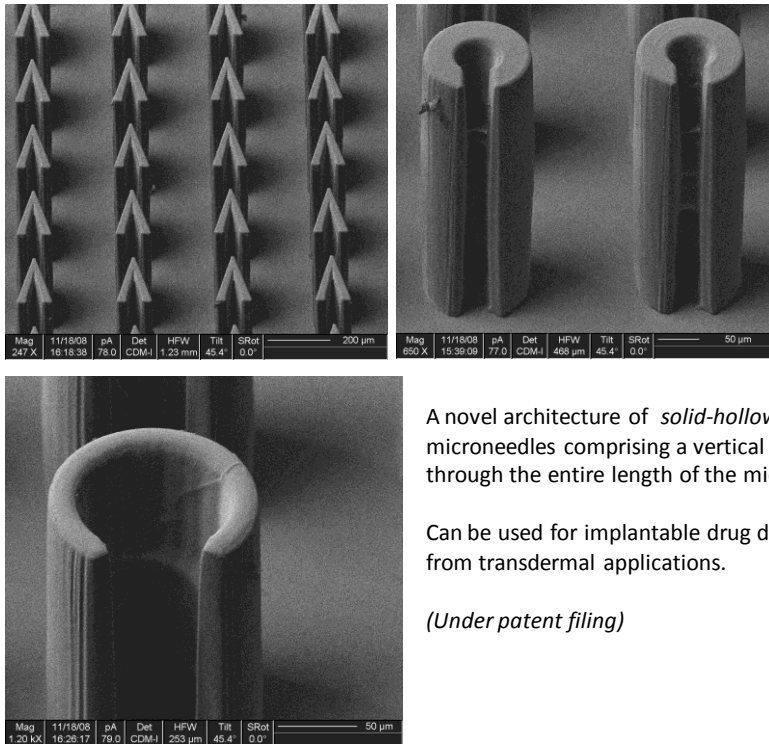


Figure 4.8: Fabricated SU-8 hollow cylinders of varying geometrical cross-sections: circular with circular bore (inner diameter: 50 μ m, wall thickness: 15 μ m), triangular with triangular bore (wall thickness: 35 μ m, base: 125 μ m), and triangular with circular bore (inner diameter: 50 μ m, base: 70 μ m). Average height: 400 μ m. To be noted that the microneedles are entirely composed of SU-8 and standing out-of-plane on Si wafer, thus, their lumens are blocked at the lower end by the wafer substrate corresponding to architecture 1 in Figure 4.1.

The images of Figure 4.8 and Figure 4.9, demonstrate the workability of the designed basic process. However, the fabricated pillars above possessed a height of only around 400 μm , translating into a maximum aspect ratio of just less than 30. In fact, for achieving this, as can be reasoned, only 3 multiple spin-coats sufficed for the given height. The true test of the process would be to fabricate the same structures but at much greater heights leading to higher aspect ratios. As described in detail previously, up to 7 multilayer spin-coating depositions of SU-8 were performed to achieve heights of the microneedle greater than 1000 μm . The fabricated results are illustrated in the following Figure 4.10.



A novel architecture of *solid-hollow* microneedles comprising a vertical slit through the entire length of the microneedle.

Can be used for implantable drug delivery apart from transdermal applications.

(Under patent filing)

Figure 4.9: Lumen of microneedles (400 μm in height) open right through the length. Open slit through the entire height of the needles illustrates the fine development of the edges. This is a potential example of a solid microneedle coated with a drug.

To elucidate further on the novelty of the structures depicted in Figure 4.9, these can neither be classified as solid nor as hollow. They are a bit of both and also in-between. The essential novelty lies in its unique cross-sectional geometry since it has a slit running through its entire shaft length providing it an adequate volume to serve as a chamber to store drugs. What ensues therefore is that since the exit area for the drug inside the skin is quite large compared to when there is no slit, the drug can diffuse out passively while the microneedle is entrenched inside the skin, eliminating the need for any active infusion pumps.

As can be seen from Figure 4.10, the measured dimensions of the fabricated microneedles were an inner diameter of 100 μm with a wall thickness of 15 μm . With a measured height of 1540 μm , an aspect-ratio of around 103 has been achieved. Further, the walls of the microneedles are quite straight and the edges are sharp and well-defined. Different cross-sectional shapes of microneedles were also fabricated as high-aspect ratio structures as shown in Figure 4.11, which shows triangular cross-sectioned ones with circular hollows as the lumen.

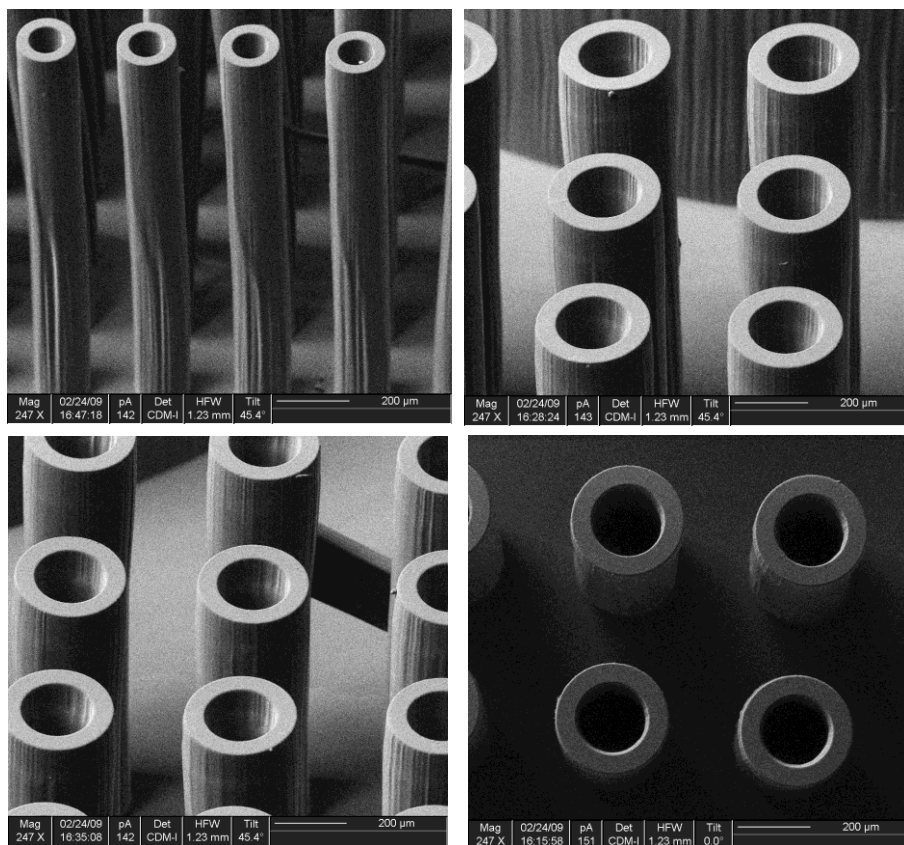


Figure 4.10: SU-8 hollow circular cross-section microneedles. Height: 1540 μm , Wall thickness: 15 μm , Inner diameter: 100 μm . Thus, aspect ratio > 100 . (Top Left): Tall slender microneedles standing erect without any signs of bending. (Top Right, Bottom Left): Well-defined sharp edges of the rims of the needles can be easily observed indicating fine processing. (Bottom Right): Top view of the microneedles apparently indicating the lumens are hollow and a clean development of the SU-8 has taken place. These microneedles indeed look densely packed but are not meant for skin penetration.

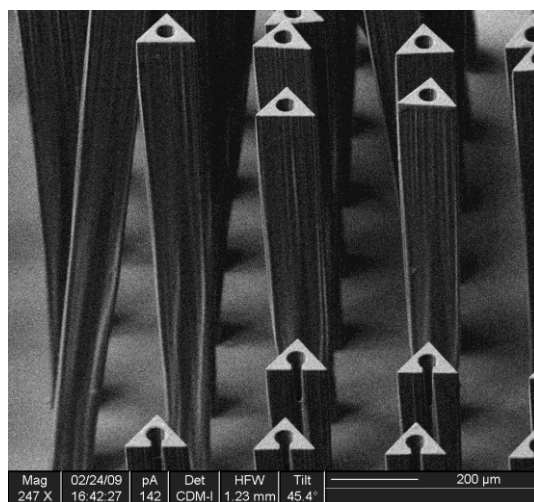


Figure 4.11: Triangular cross-section microneedles with circular hollow bore. (Dimensions – Base: $70\ \mu\text{m}$, circular lumen diameter = $48\ \mu\text{m}$). The second type of structure lower down in the figure is one in which the hollow of the needle has been intentionally kept open by mask design, to allow for a clear view of the longitudinal axis. The substrate surface is clear indicating a successful SU-8 development step.

From the above Figure 4.11, it may be observed that due to the smaller lateral dimensions of the triangular cross-section microneedles compared to the previous cylindrical one, the apparent pillar strength of the needle appears to be less than its cylindrical counterpart and this derives directly from Euler's pillar theory.

4.4.3.1 Preliminary testing of hollowness of fabricated microneedles

To investigate whether the fabricated microneedles are hollow right up to the bottom, a small section of the wafer substrate holding the needles was removed by dicing, and moulded in epoxy, keeping the orientation of the needles such that the longitudinal axis of the needles is parallel to the grinding plane. The epoxy mould was ground manually and checked intermittently under the microscope. It has been observed that the microneedles' bores were open right up to the bottom as can be seen from Figure 4.12. The presence of air bubbles in some of the needles, and epoxy in the rest, prove that they are hollow inside. This is indeed quite promising

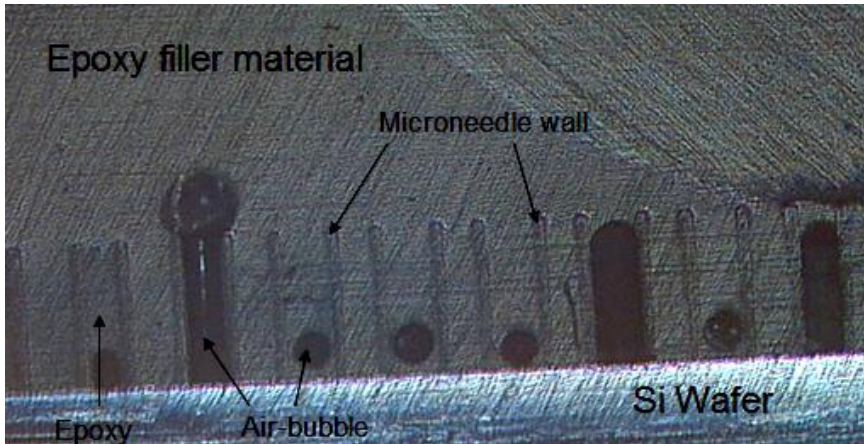


Figure 4.12: Cross-sectional view of fabricated SU-8 microneedles moulded in epoxy, indicating the needles are hollow till the bottom.

as it means though such high aspect ratios are involved, and there is always the risk of an incomplete development or undesired cross-linking of the SU-8 at the deeper regions due to dispersive and reflective effects of the UV radiation, none of it is predominant (or even if it is, it is a rare phenomenon). Thus, this is testimony to the fact that the basic process functions satisfactorily meeting the desired process goals.

4.5 Intermediate process design

4.5.1 Introduction to tip sharpening

Having discussed the basic process design at length, the next process target goal to be achieved is the sharpening of the microneedle tips. A sharp tip is imperative for minimizing the insertion force of the microneedle into the skin. Thus, sharper the tip, less is the insertion force required, consequently translating into lesser pain felt by the patient. One of the approaches to fabricating sharp tipped hollow polymer microneedles in the past has been using a process of laser drilling through bore of the solid polymer needle (121). This process is expensive and would have limited scalability. Another approach was by SU-8 molding on polydimethylsiloxane (PDMS) master templates (122). Here the average microneedle tip diameters obtained were between 15 to 25 μm .

As per the listed goals under section 4.2, tip sharpening step would be ideal should it be incorporated in-situ in the current process. Keeping this in mind, a combination of techniques of moulding and photolithography were decided upon. Thus, pyramidal shaped trenches were etched in a Si wafer using KOH anisotropic etching. SU-8 polymer was next cast on these trenches followed by lithography on SU-8. This was followed by development resulting in out-of-plane sharp-ended microneedles. Furthermore, a novel design feature here is the use of triangular cross-section of the microneedle structure in aiding the formation of the desired sharp bevel-tip. In contrast to values reported in literature, sharper tips with tip diameters averaging under 2 μm have been achieved with this process.

4.5.2 Tip sharpening design – principle of moulding

Anisotropic etching with KOH on Si $\langle 100 \rangle$ wafer results in a pyramidal pit, the walls of which are at an angle of 54.74° in accordance with properties of anisotropic etching of $\langle 100 \rangle$ Si wafer. For this, it is essential to ensure that the mask edges are aligned to the wafer $\langle 110 \rangle$ direction. The SU-8 microneedles were aligned such that their tips should coincide with the sharp tips of the pyramidal grooves on the wafer, in order for them to form a sharp tip, as shown in Figure 4.13.

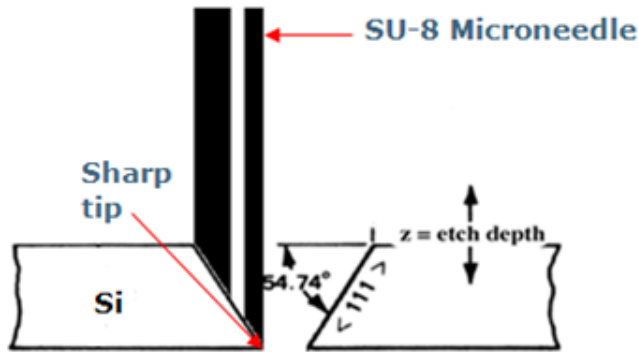


Figure 4.13: Principle behind moulding the microneedles on the KOH-etched pyramidal pits to form a sharp ended tip.

Furthermore, to facilitate an even more pronounced formation of the bevel-shaped sharp tips, triangular cross-sectional design of the microneedle with a triangular cross-sectional bore was adopted. The main reason behind this idea was that the triangular shaped geometry would aid naturally in the formation of bevel-shaped tips. The cross-section shape was designed as a right-angled isosceles triangle with base $92\ \mu\text{m}$ and sides $65\ \mu\text{m}$ each, with a wall thickness of $10\ \mu\text{m}$, such that one of the 45° vertices coincides with the pyramidal pit's sharp bottom point. The main reason why bevel-shaped tips were desired is because the microneedle is based on a biomimetic design inspired from that of that of a mosquito proboscis tip (123). The height of the microneedle was designed for $300\ \mu\text{m}$ mainly as an initial test to demonstrate primarily the concept of tip sharpening by molding.

4.5.3 Process flow incorporating tip sharpening

The basic fabrication principle as reported earlier for high-aspect ratio microneedles under section 4.4.2 still remained the same with a few additional steps. Here, first windows were patterned on an oxidized $\langle 100 \rangle$ Si wafer in order to create openings for the KOH-etch step as shown in Figure 4.14. Then KOH etching was carried out in a KOH solution of 30% by weight at a temperature of 60°C . These parameters were chosen in accordance with values from literature for silicon oxide masked KOH etching (124).

A Polymer-based Transdermal Drug Delivery System Using Microneedles

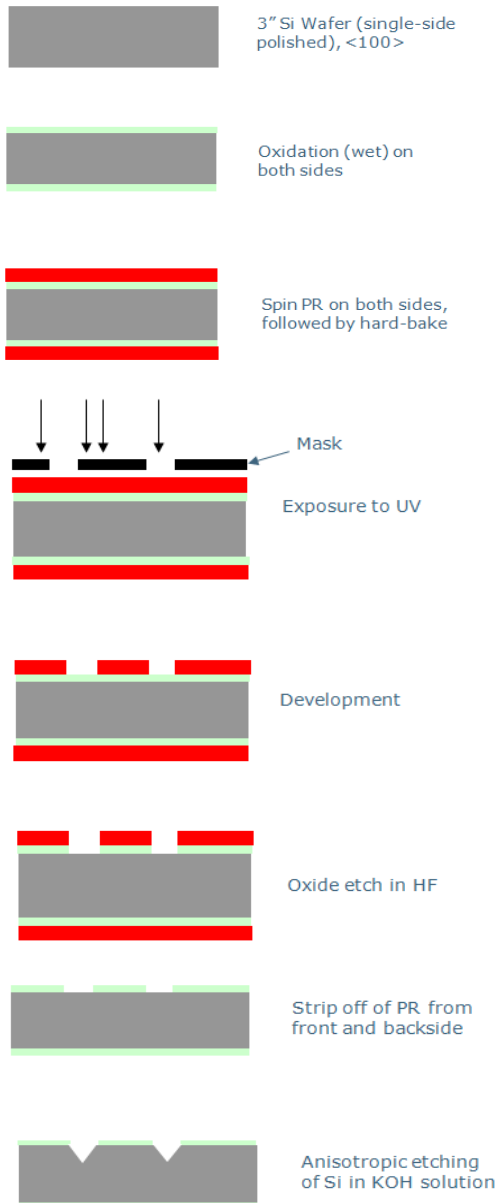
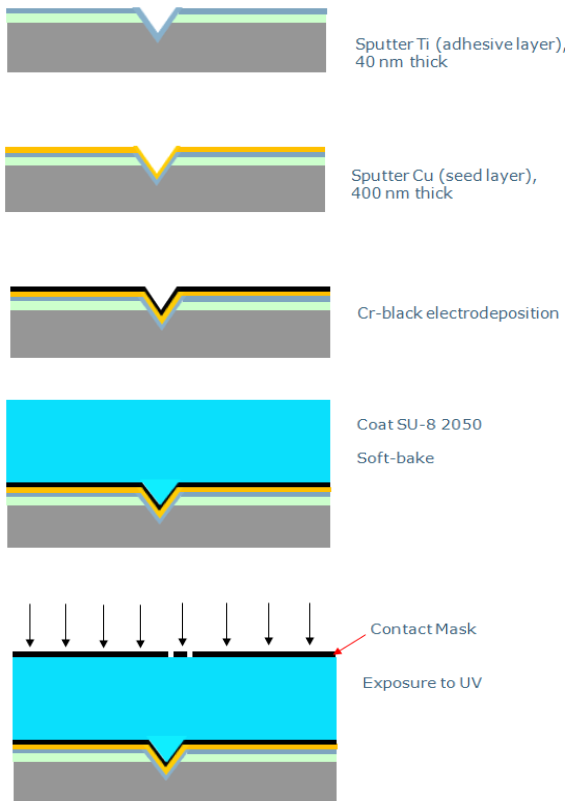


Figure 4.14: Tip sharpening process flow – Part 1.

It is to be noted from Figure 4.13 that at the step of UV-exposure on the SU-8, there is a very high risk of the UV light getting reflected off the inclined plane of the pyramidal pit wall and in turn cross-linking the entire microneedle bore. This is highly undesirable. To solve this problem, an anti-reflective coating of chromium-black (Cr-black) was used. This is another novelty in the process and has not yet been reported earlier. Cr-black has a very low reflectance less than 5% in the UV region and was very suitable for our purpose. This Cr-black coating was done by electrodeposition (125). Prior to this step, an adhesive layer of Ti followed by a seed layer of Cu was sputtered as shown in Figure 4.15.



(Cont'd)

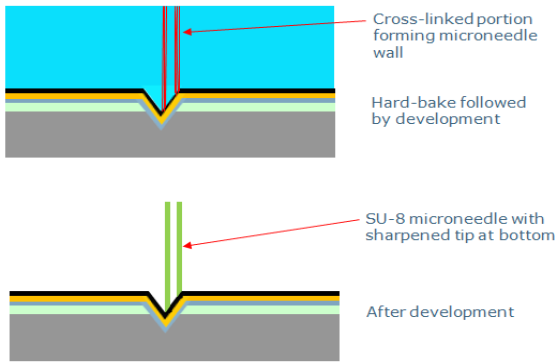


Figure 4.15: Tip sharpening process flow – Part 2.

So KOH etching results in pyramidal pits or trenches (from a top view, ‘pits’ are merely squares with their inclined tapering sidewalls terminating in a point whereas ‘trenches’ from a top view are only rectangles with their inclined sidewalls of the longer axis terminating in a line as illustrated in Figure 4.16).

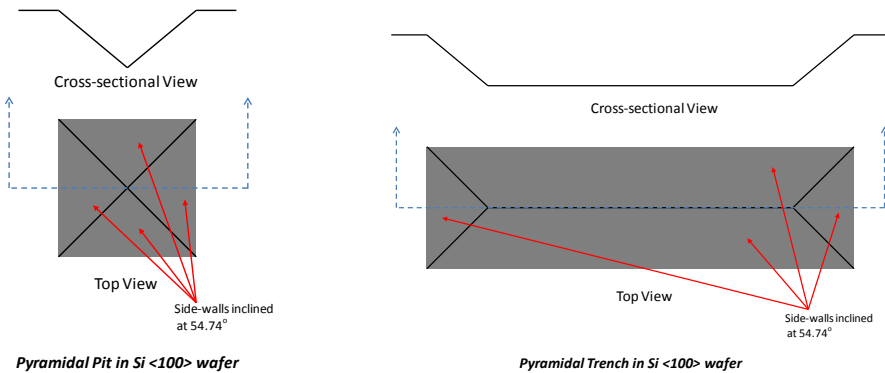


Figure 4.16: Difference between pyramidal pits and trenches.

As a side note, the primary difference in functionality in pits and trenches is that only one microneedle can be moulded and patterned in a pit whereas in a trench a row of microneedles can be moulded and patterned.

After KOH etching and chromium black electrodeposition, exactly the same process steps as enumerated in section 4.4.2 is followed. The only added step herein is that instead of a completely flat Si wafer substrate, a pre-moulded Si substrate is utilized so that the tips of the needles are moulded in the pyramidal pits or trenches thereby imparting them their sharpness. Also it is to be noted that now the microneedles are not fabricated with their top-up but rather with their tops-down, since the tips of the needles are in contact with the inclined side-walls of the pyramidal grooves on the wafer substrate in contrast with the initial fabrication results. It is to be noted further that no sacrificial layer has been used here for release as shall be elucidated later.

4.5.3.1 Mouldability of SU-8 on Si

Before proceeding to fabrication using the above process, it was essential to first ascertain the moulding capability of SU-8 on a test Si-wafer with prior-etched KOH-etched pyramidal grooves and release the same. A short-loop test was executed to examine this, and the excellent mouldability was proven by the illustrated results in Figure 4.17.

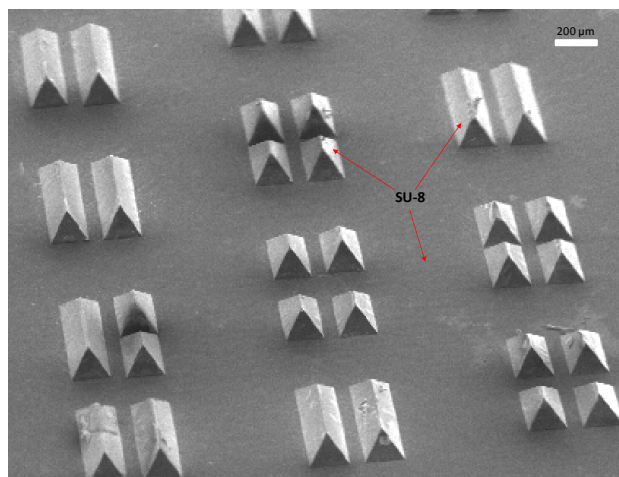


Figure 4.17: Excellent mouldability of SU-8 on Si. The pyramids have been moulded in the KOH-etched trenches followed by a blank UV exposure. To be noted that this has been cleanly released from the Si wafer substrate, and is entirely composed of SU-8.

To elucidate further about the short-loop test, simple KOH-etched trenches were made in $\langle 100 \rangle$ Si wafer and SU-8 was cast into it by the same multi-

layer spin-coating procedure interspersed by individual pre-bakes and finally followed by a vacuum oven step and a blank UV exposure without any mask. This was followed by a regular post-exposure bake (section 4.4). The only difference herein was the long development time needed, around 5 hours followed by immersion in HF buffer solution for 7 hours in order to dissolve the oxide layer lying immediately underneath the SU-8 layer, and acting as a sacrificial layer. It is only after the oxide is removed completely that the entire layer of SU-8 comprising the pyramids is cleanly released automatically from the wafer substrate, rinsed in water and dried to show the above result in Figure 4.17. More close-up images of the SU-8 moulding display sharp and well-defined edges in addition to a resulting smooth surface, as proven by Figure 4.18.

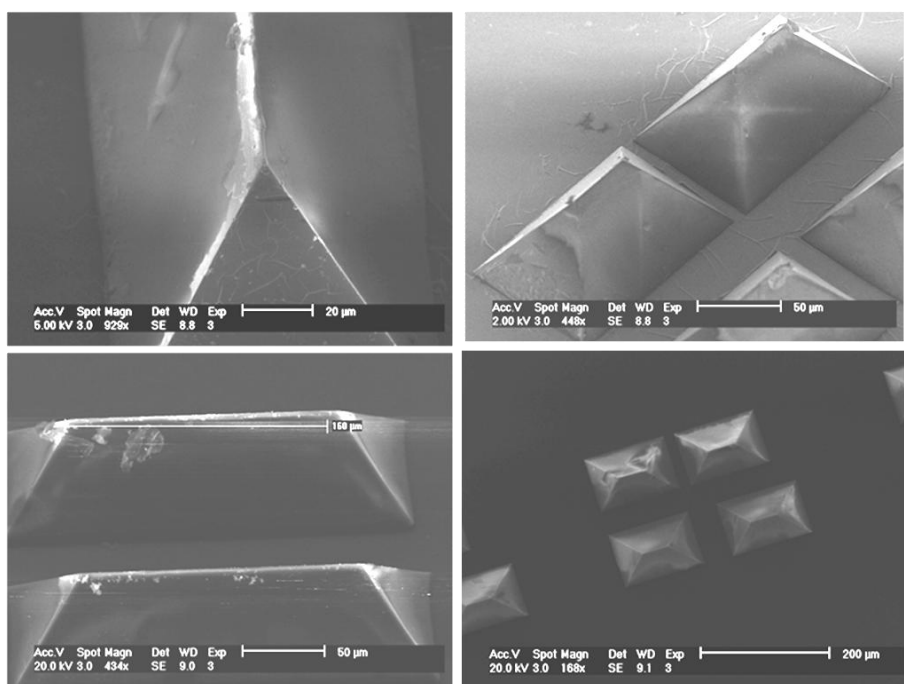


Figure 4.18: Close-up SEM images of moulded SU-8 on Si after release. Sharp edges and smooth surfaces observed. Sharpness of edge roundness measured to be under 1 μm.

4.5.4 Intermediate process: results, issues and discussion

The outcome of the intermediate process is that triangular-cross-sectional microneedles with bevel-shaped sharp tips have been fabricated. It is to be understood that since no platform exists at this stage, the individual microneedles can be observed standing on their sharp tips inside their respective pyramidal pits without having been released from the wafer substrate as depicted in Figure 4.19.

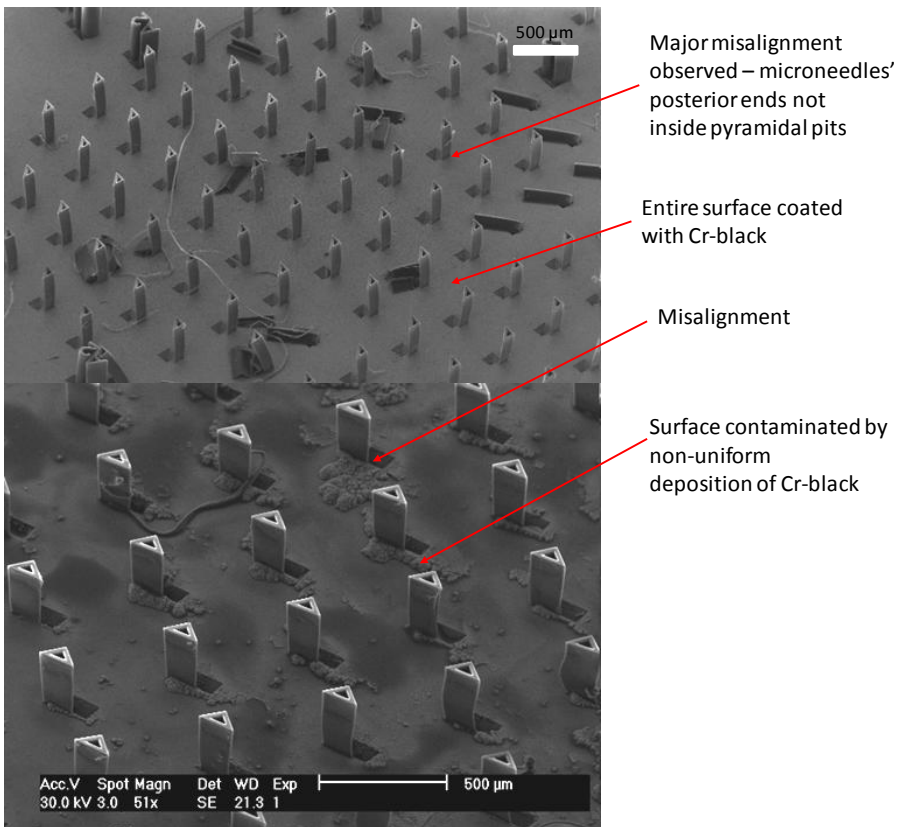


Figure 4.19: Initial results of the intermediate process design: Misalignment of microneedle tips with the pyramidal pits is a major cause of concern. Also, non-uniform Cr-black deposition has led to a dirty substrate surface.

Clearly, as can be observed from Figure 4.19, misalignment of the microneedle posterior ends with the pyramidal pits is a challenge because the

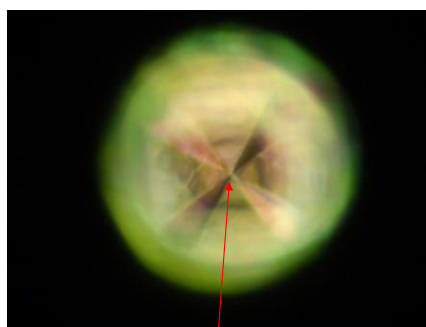
alignment needs to be performed through a thick layer of underlying SU-8 block. The second issue that can be observed is the apparent dirtying of the substrate surface by the non-uniform deposition of Cr-black. The latter issue is compounded by the fact that many a time it was noticed that Cr-black was not deposited on the sloped side-walls of the pyramidal pits or trenches. Thus, the Cr-black deposition step was examined in great detail by implementing a series of short loop tests (Figure 4.20) to optimize the Cr-black coating. Finally, a high current of 18 A for a long time duration of 4 minutes was found to be working perfectly for a well uniformed deposition. In addition, it had to be ensured that the seed layer of copper had sufficient coverage over the edges of the pits in order to provide the requisite electrical conductivity necessary for the ensuing electrochemical deposition of Cr-black.



Unsatisfactory greenish black coloured Cr-black coating

KOH-etched pit's sidewall not coated with Cr-black

(a)



Close-up of pyramidal pit clearly showing no presence of Cr-black. Sharp terminating point of pit is quite apparent.

(b)

(Cont'd)

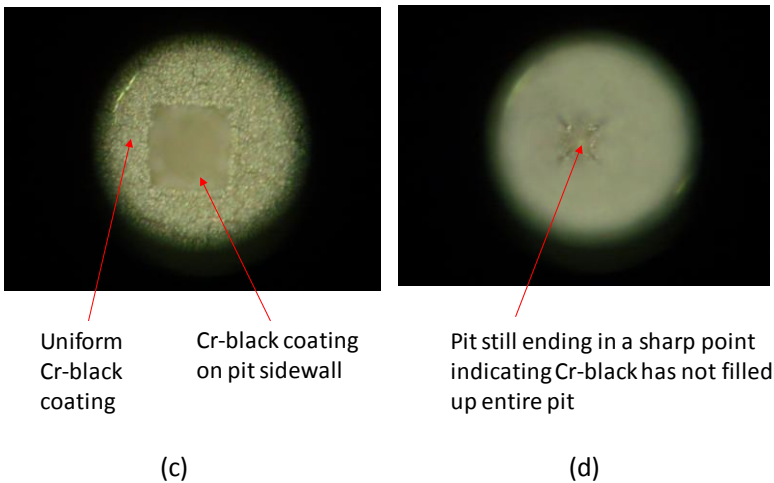


Figure 4.20: Step-by-step progress in Cr-black electrodeposition process. (a) Unsatisfactory greenish-black (and not gray-black) coating of Cr-black formed. (b) Close-up of etched pyramidal pit in Si substrate indicating no Cr-black has been deposited on the inner walls of the pit. (c) Uniform dark gray Cr-black electrodeposition obtained by tuning current (18 A), time (4 mins) and seed layer Cu thickness (400 nm). (d) Close-up of inner walls of pit displaying uniform Cr-black coating and that the terminating point of the pit is still visible.

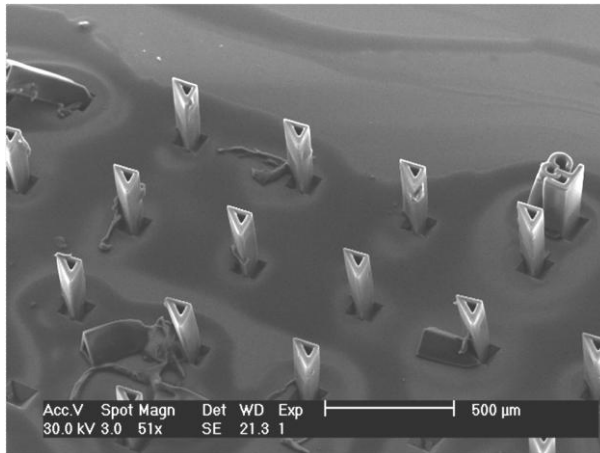


Figure 4.21: An array of triangular cross-section microneedles standing out-of-plane on the KOH-etched pits. Marked improvement in alignment as well as surface texture over previous results. It is to be noted that the microneedle tips are lying inside the pyramidal pits as intended, and some of the microneedles have fallen off due to poor adhesion. The entire wafer

substrate surface is covered with Cr-black. The alignment has been improved by making use of the smallest size alignment marks in the set of alignment markers. Previously, the larger sized alignment marks were employed and this caused a significant misalignment.

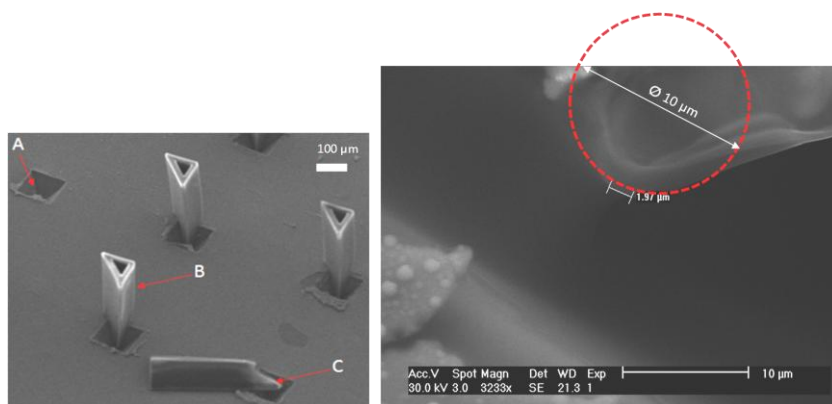


Figure 4.22: (Left) Sharp-tipped, triangular cross-sectioned microneedles with a triangular cross-sectioned bore: A – KOH-etched pyramidal pit ending at a sharp point, B – a microneedle standing on the pit, C – a fallen microneedle denoting the sharpened tip formed by moulding on the pyramidal pit; (Right) Close-up of a sharp tip of a microneedle showing the tip diameter of about 10 µm.

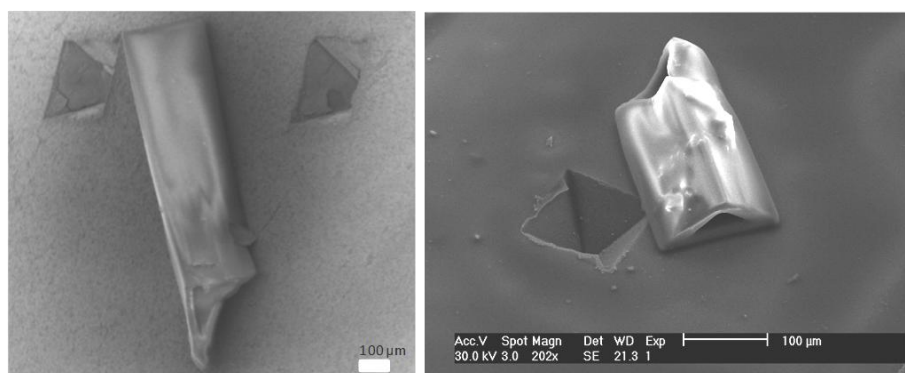


Figure 4.23: (Left) The bevel-shaped sharp tip of a loosened microneedle is prominent here. (Right) The lumen opening at posterior end (bottom) as well as at the anterior end (sharp tip) is also clear indicating the ends are not clogged, and that most probably a hollow lumen should exist.

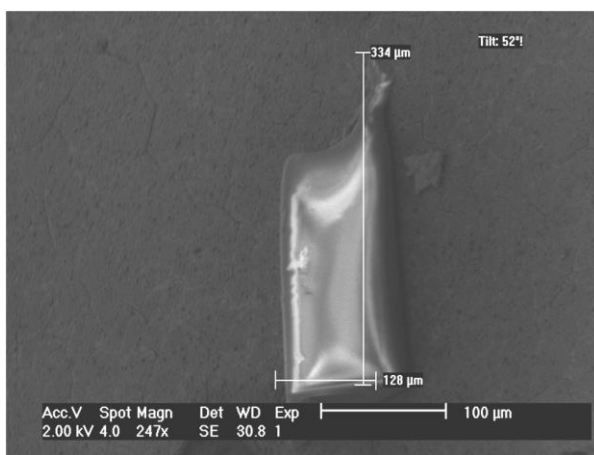


Figure 4.24: Side view of a fabricated microneedle resulting from the intermediate process flow. Measured needle length of 334 μm and base of 128 μm , viewed at a tilt of 52°. Needle wall thickness is 10 μm .

Thus, from the intermediate process design, the heights of the needle obtained were around 300 μm with a base-length of around 128 μm , as shown in Figure 4.24. Further, from Figure 4.22 and Figure 4.23, it is proven that the fabricated microneedles are quite sharp at 1.97 μm needle tip diameter and they have a clear hollow lumen open at both ends, respectively. Figure 4.21 indicates that the misalignment problem has been greatly overcome though it still requires further optimization. Also the surface texture from the resulting Cr-black deposition is much smoother and cleaner than before. For a moulding process such as this, this is a significant achievement. However, should it be desired to release the microneedles from the substrate here, perhaps a simple chemical etching of the immediate underlying layer of Cr-black would suffice.

Sharp-tipped bevel-shaped hollow microneedles have thus, been fabricated successfully with SU-8 polymer, using a combination of moulding and photolithography techniques. The molding step can easily be scaled up for mass production and together with a cheap polymer-based structural material like SU-8, serves as a low-cost means for producing these microneedles. As it is impractical to handle individual needles, it was refrained from releasing microneedles from the substrate at this stage. The next stage of the work involves creating a platform for the microneedle base which has holes continuous with the bore of the microneedle, so that the

system can be used further for integrating with microfluidics for transdermal drug delivery.

4.6 Advanced process design

This section takes the design of the microneedle up to the final step of integrating it with a platform as per our initial process target goals. Here, the concept of the platform is discussed thoroughly – its function, prerequisites and conceptualizing its design process, and integrating it with the primary process flow. Efforts are made to keep the process as simple and monolithic as possible, at the same time focussing on the “in-situ” part as elucidated in the initial process goals.

4.6.1 The platform – what? why?

The platform is simply a base plate perforated with through holes on which the array of microneedles stands orthogonally.

The platform is required to serve two purposes:

- 1) To serve as a base plate for handling the microneedle array, and
- 2) To ensure that the drug stored in the drug reservoir situated behind the platform, can flow into the microneedle lumen through the hollow channel located in the thickness of the platform corresponding to the microneedle lumen diameter.

The following criteria were to be met while designing the platform layer:

- 1) Good adhesion between end of the microneedle and the platform layer.
- 2) Hollow channel through the thickness of the platform layer connecting the lumen of the microneedle to the external environment.
- 3) Ease of fabrication by keeping use of additional materials at its minimum.

4.6.2 Fabrication options for platform layer

Following were the fabrication options considered for making the platform layer:

- 1) Pre-fabricate a platform layer of 200 μm thickness using a polymer material (say SU-8) and glue it onto the array of SU-8 microneedles

before developing the latter. For this, of course, alignment at this step with the bores of the microneedles and the hollows of the platform would be crucial. Also, extreme care needed to be taken to ensure that in the process of applying the glue that the glue did not clog up the platform openings, for that would then completely defeat the purpose.

- 2) Coat an additional layer of SU-8 onto the microneedle structural layer and carry out the pre-baking steps before aligning the mask to the microneedle bores and then performing exposure to cross-link the platform. Finally, development would be carried out in a single step, and since both the microneedle and the platform are made of the same material, the bonding between the two layers would be satisfactory, and the structure would be released as a single one after development.
- 3) Use the existing thick layer of SU-8 forming the microneedle structure itself, to make the platform layer by cross-linking only a thin uppermost layer by employing the photopatternable features of SU-8. Already accomplished by Wang et al (84), this is indeed the most feasible yet challenging process.

The third method, as can be seen, was the most elegant of the three methods evaluated. Furthermore, it did not necessitate the use of any additional material or additional bonding steps or additional heat processing on the existing SU-8 structure. Not just that, but the fact that the existing layer of SU-8 would be used for the platform also meant that the ends of the microneedle would remain embedded *inside* the new platform layer compared to lying *outside* just in contact with an adjacent new platform layer. Obviously, this implied better bonding of the microneedle ends with the platform.

4.6.3 Advanced Process Design: Results, Issues & Discussion

The main principle underlying the photolithography of the platform layer is the characteristic feature of SU-8 transmission response to different wavelengths of UV light (See Figure 4.25). Essentially, longer wavelengths (greater than 365 nm) penetrate deeper into the photoresist while shorter

wavelengths (less than 365 nm) penetrate only a shallow layer. This principle is exploited here to cross-link only the shallow uppermost portion of the SU-8.

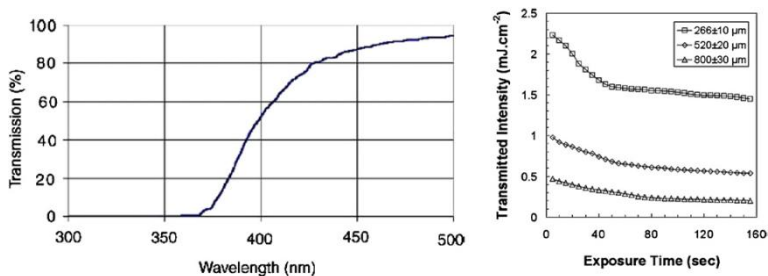


Figure 4.25: (Left): Transmission spectrum of 1 mm thick unexposed SU-8100(126); (Right) Transmitted intensity of an SU-8 film at different wavelengths after increasing exposure times (127).

To arrive at the correct parameters for the platform exposure dosage several short loop experiments were performed. Initial results were far from satisfactory but broadly speaking, data accumulated over several experiments pointed to the following trend as shown in Figure 4.26.

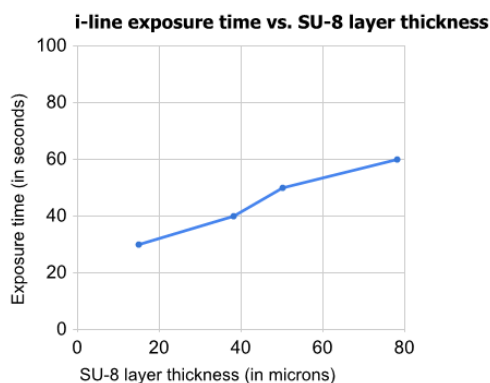


Figure 4.26: Thickness of SU-8 varying with different exposure times for given UV lamp.

In the process of optimization, the following results were obtained when the exposure was deemed to be too less for the platform, as illustrated in the following Figure 4.27.

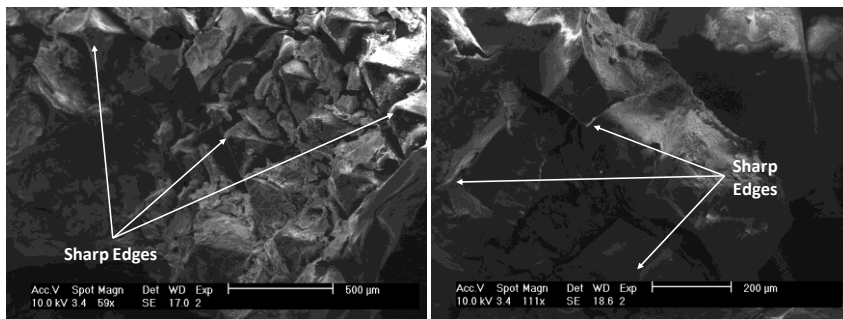


Figure 4.27: Platform layer after underexposure. Sharp edges of the microneedle tips can be made out only vaguely as marked. The tips are visible after the release of the SU-8 layer from the Si substrate. It is to be noted that since the microneedle tips are fabricated top-down with the tips lying in contact with the Si mould, it is only after the entire platform layer is released that these tips can be seen on the front side of the layer. Furthermore, since the microneedles here are extremely short, it is only the moulded tips which are visible.

As discouraging as the above results may look, on inspecting closely, vague shapes of the sharp tips of the microneedles can be observed by the keen eye. It is an indication that though apparently quite faraway from desired results, a slight tuning of the exposure parameters could be the right way to resolving this issue. And so, further optimization of this process step led to more promising results as shown below in Figure 4.28.

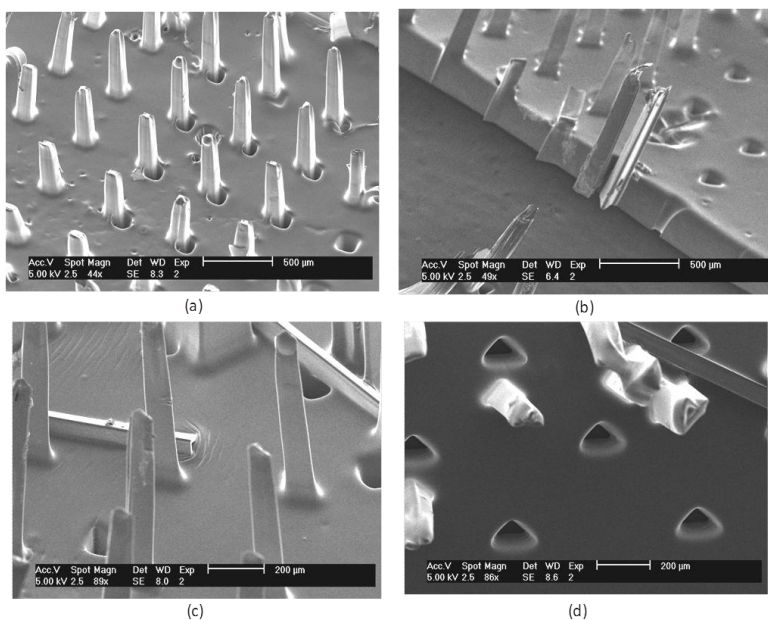


Figure 4.28: First promising results of platform layer step under SEM. Entire needle arrays as well as platforms are made of the same material, SU-8. Though far from perfect, this demonstrates that the principle of making the platform, works. High internal stress not evident in the SEM image but present more at a macro-scale proven by the curling up of the entire platform. (a) SU-8 microneedles standing out-of-plane on an SU-8 platform – the misalignment of the bases with the holes of the platform can be clearly observed. (b) Side-view of the platform explicitly depicting the thickness of the platform and the monolithic nature of the fabricated device. (c) Close-up view of some of the microneedles showing very straight and smooth sidewalls with well-defined edges. (d) Top-view showing misalignment of the microneedle bores with the holes in the platform.

From the above Figure 4.28 it is quite evident that several issues still remained to be solved:

1. Misalignment of the microneedles with the holes of the platform.
2. High internal stresses of the platform layer after development.
3. Unsharpened (blunt) tips of the microneedles.
4. Shortened heights of the microneedle shafts.
- 5.

What however, was satisfactory, was that the platform layer was sufficiently thick, about 250 μm (See Figure 4.29) and the resulting bonding between the

microneedle ends and the platform appeared to be good on close inspection. Of course, this needed to be proven further by mechanical tests.

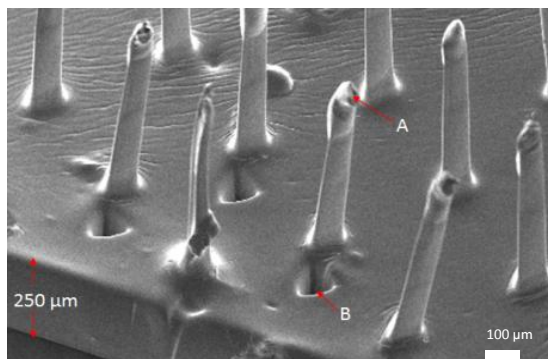


Figure 4.29: SU-8 blunt-tipped microneedles fabricated on an SU-8 platform. A – Moulded sharp-tips of the triangular cross-sectioned microneedle, B – a bore of the platform misaligned with the bore of the microneedle.

Each of the aforementioned issues had their roots in some other unique causes, and not necessarily the platform step. However, since the platform step was the last processing step after which the whole device was released, inevitably, all the final issues would be reflected herein.

We shall now proceed to discuss the first issues here only since it pertains directly to the platform step, the rest we shall dwell on under the next section on final optimization (Section 4.7).

- Misalignment of the microneedles with the holes of the platform

It is to be noted that prior to the platform exposure step, the wafer was already coated with a thick layer of SU-8 forming the structural layer of the microneedles and therefore its thickness corresponding to the length of the microneedle shaft, that is, around 1000 to 1500 μm . It should also be borne in mind that the alignment marks lie only on the wafer which is situated below this thick layer of SU-8. Thus, alignment is not so straightforward though SU-8 might be optically transparent as focussing on the correct depth by the microscope requires some practice. However, at the mask design level, the misalignment could be minimized to a certain extent by ensuring a design tolerance of 5 μm . Thus, if diameter of the inner bore of the microneedle was 100 μm , with a wall thickness of 15 μm , the diameter of

the mask design for platform to protect the inner bore was 110 μm . Since the wall of the microneedle was already cross-linked in the previous exposure step, even if a misalignment occurs by 5 μm , the inner bore of the microneedle still remains protected as the size of the protecting mask pattern is greater than the actual inner bore. This can be further elucidated in the following diagrams - Figure 4.30, Figure 4.31.

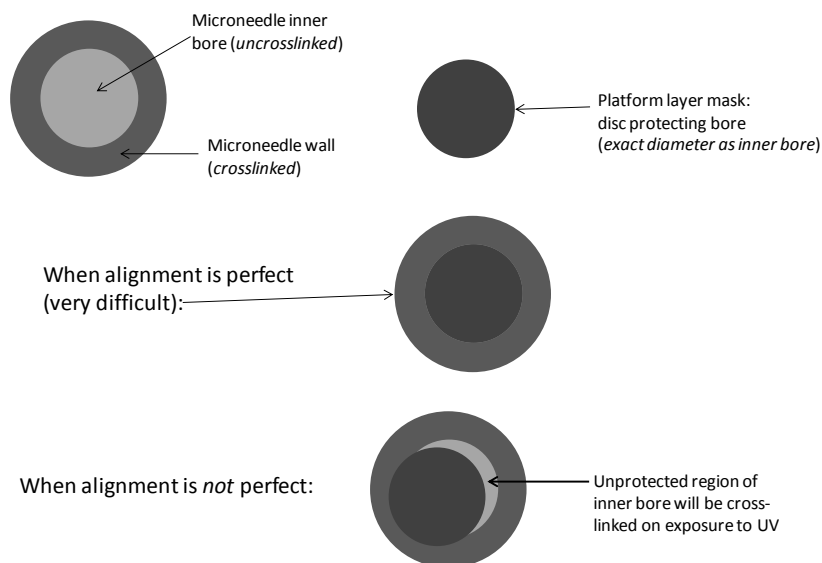


Figure 4.30: Why alignment is crucial and how when misalignment occurs, the entire bore of microneedle can get cross-linked inadvertently.

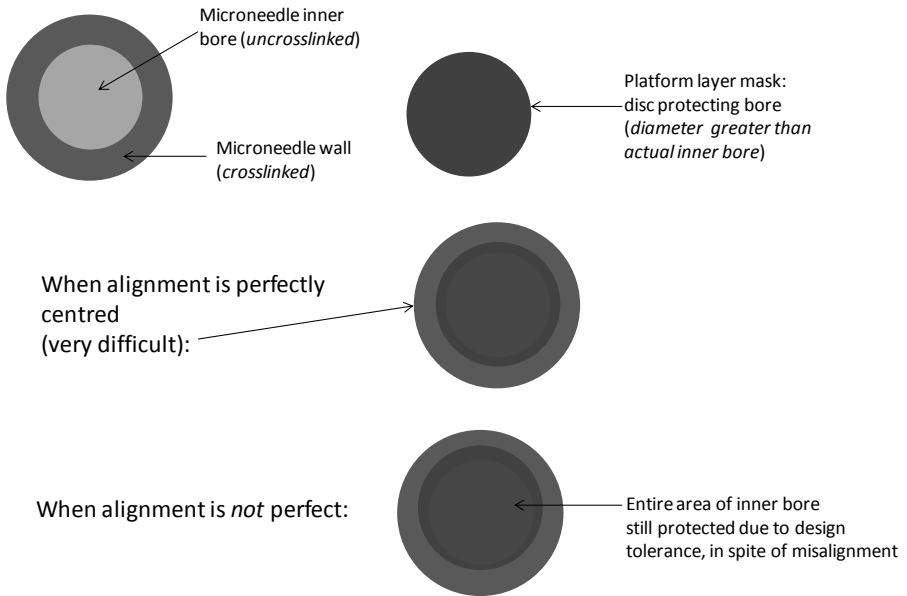


Figure 4.31: How misalignment can be circumvented by a mask design tolerance.

4.7 Final optimization of the process

As evident from Figure 4.28, the following issues still remained to be resolved:

- 1) Misalignment of the microneedles with the holes of the platform
- 2) High internal stresses of the platform layer after development
- 3) Unsharpened tips of the microneedles
- 4) Shortened heights of the microneedle shafts

Of these the first one was already dealt with in the previous section. We shall now discuss the causes and solutions for the remaining three other issues.

4.7.1 Resolving vital issues

- High internal stresses of the platform layer after development

Initial results demonstrated that there was a very high degree of internal stress inside the final microneedle-array-on-platform structure, due to which the platform curled up and was impossible to keep the platform bottom standing on a flat surface. One of the main reasons for this could be the difference in the energy exposure dosage of the microneedle structural layer (very high) vs. the platform layer (much lower). This could be a very valid reason for the curling up of the platform (Figure 4.32, Figure 4.33). Thus, one of the analyses is that difference in the exposure dosage could be a valid cause. However, it is also obvious that the actual optical energy is received by the microneedle shafts mainly and *not* the entire SU-8 layer *per se*. Hence, most of the SU-8 layer is un-crosslinked and ultimately removed. The difference in the energy dosage would be valid only for the microneedle shafts, but comparing the volume of the needle shafts (very small) to the volume of thick platform layer (much greater) per needle array, would only point to dismissal of this theory, as this small volume should not have such a pronounced effect on the whole platform as such.

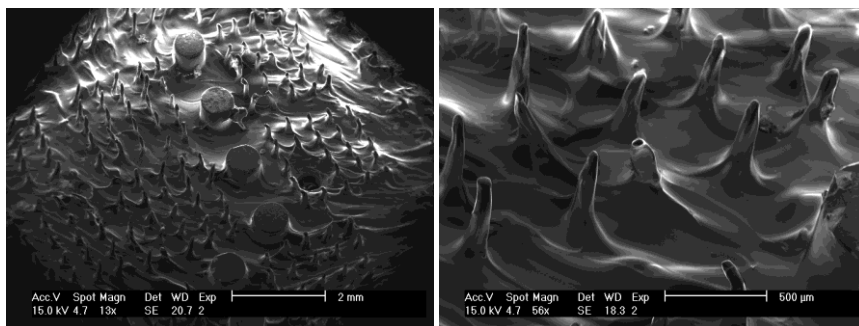


Figure 4.32: Internal stresses in the platform layer causing it to curl up. The wavy features on the surface of the platform are evident of the high stresses that have crept in after the final development stage of the SU-8. The large solid cylinders in the left figure were created just as a test structure and have no special significance.

However, a key point which has been missed all along was the development step itself. The above results were obtained after a development step of 4 hours. This time duration was determined by the time taken by all the microneedle arrays to be released automatically from the wafer. However, on closer observation it was found that during the first 3 hours of development, majority of the microneedle arrays were released from the substrate and began to float around in the SU-8 developer solution, propylene glycol monomethyl ether acetate (PMGEA). Only a few of the remaining arrays with a more complicated geometry of needle cross-sections or with a larger number of needles per array, that is, having a great contact area, were the ones to be still attached to the surface. In an attempt to wait for these remaining arrays also to be released from the surface, the development time was raised to 4 hours, and it was during this additional one hour time that the “good” arrays which had been already released, absorbed much of the developer solution and curled up even while in the solution. When development time was restricted to only 3 hours however, it was observed that the majority of the needle arrays were released and were just slightly in contact with the wafer surface. A very slight force was enough to dislodge them and pick them up with tweezers. After rinsing with IPA (isopropyl alcohol) and finally with water, the excess fluid was soaked in cleanroom wipes and the platform layer appeared to be quite flat with no signs of stress or curling.

After the development time was shortened to 3 hours, the fabricated platforms appeared devoid of internal stress as illustrated in section 4.7.3. Figure 4.37.

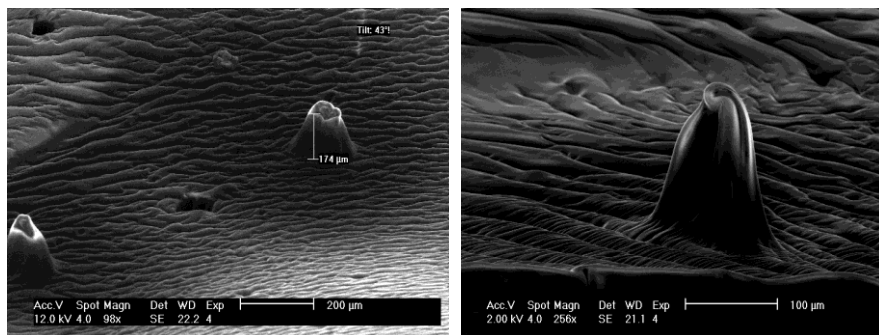


Figure 4.33: The surface texture of the SU-8 platform clearly denotes ample internal stress. (Left) The small height (174 μm) of the microneedle is noted. (Right) A close-up view of the fabricated microneedle on platform before optimization.

- Unsharpened tips of the microneedles

Though initially, the microneedle tips were designed to be moulded only atop the 54.74° inclined crystallographic $\langle 111 \rangle$ planes of Si wafer, however, at a later stage it was found that subsequently due to misalignment and swelling of SU-8 during processing, the tip of the microneedle landed inevitably at the bottom of the anisotropically etched pit or trench. In case, the bottom was not etched right till its natural etch stop, that is, at the vertex of the pyramidal groove, it was possible that the microneedle tip should take the form of the pit bottom. A closer look at Figure 4.28 shall confirm this observation. To verify this, a blanket coat of SU-8 was performed on the master mould to check if the wafer master had been anisotropically etched till its very limit, and the results were as observed in Figure 4.34.

As is quite evident, the master mould is required to be etched further till its natural etch stop limit is reached, that is, when the pyramidal pit or the groove terminates in a point or a line respectively. This shall fulfil an important step in the final optimization of the process.

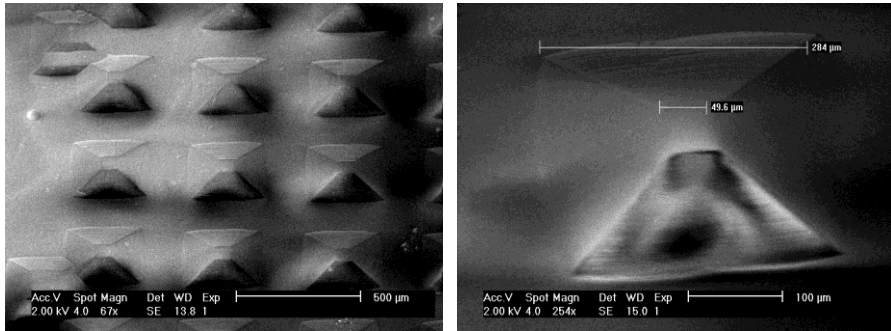


Figure 4.34: Blanket SU-8 moulding on the Si master mould in order to inspect the bottom sharpness of the anisotropically etched pyramidal pits. (Left): As expected, the pits have not been etched till their very limits and the tops of the released SU-8 layer shows that they are not sharp. (Right): A close-up view of a single SU-8 solid pillar indicating a top side length of about 50 µm, bottom lateral side of around 285 µm, and a height of 150 µm.

- Shortened heights of the microneedle shafts

As can be understood from the results of the ultimate release step by development, the fabricated microneedle heights were indeed much shorter than expected. Even after the internal stress problems were ironed out, the heights of the microneedles fabricated averaged around 170 - 200 µm only which was a far cry from what was the design objective of around 1300 - 1500 µm, as depicted in Figure 4.35.

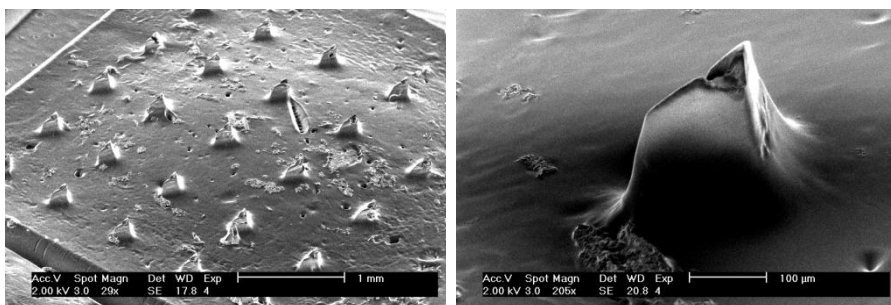


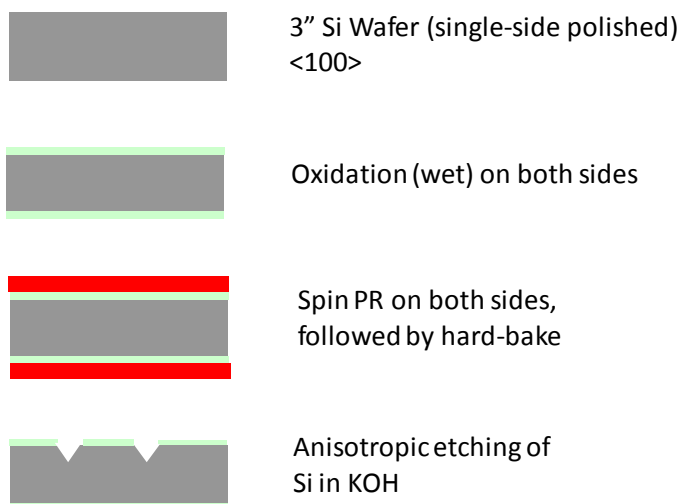
Figure 4.35: (Left) SEM picture of the fabricated microneedle array on platform albeit with short microneedles (height = 170 microns), that resemble "stubs" rather than needles. To be noted is the platform which is quite easily discernible, without stresses, and flat. (Right): A close-up view of a single short microneedle.

On a detailed step-by-step analysis, the main cause of this issue was found to be rooted in a step which has already been discussed in-depth earlier on,

namely, the “de-gassing step” in the vacuum oven (section 4.4.3). It is to be understood that during this step, more than 50% of the SU-8 tends to be lost by means of overflow from the wafer substrate. If this loss in SU-8 is not compensated, the resulting SU-8 thickness becomes a fraction of what it was originally deemed to be. Thus, in order to compensate for the loss of the SU-8 during this de-gassing process, this step is repeated again. In other words, once the de-gassed SU-8 layer was obtained, another 3 or 4 thin (150 μm thick) layers SU-8 were deposited by multilayer spin-coating interspersed with the regular pre-baking. This was again made to undergo the same de-gassing in a vacuum oven. The resulting SU-8 layer thickness was commensurate with the desired height of the microneedle.

4.7.2 Final process flow

Before proceeding to discuss the results from optimization, it could be worthwhile to once again recapitulate the entire process flow, as described in the following process flow diagram (See Figure 4.36)



(Cont'd..).



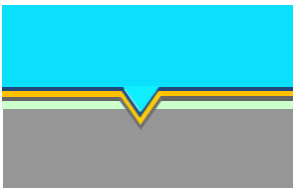
Sputter Ti (adhesive layer), 40 nm th.



Sputter Cu (seed layer), 400 nm th.

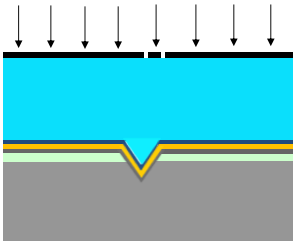


Cr-black electroplating



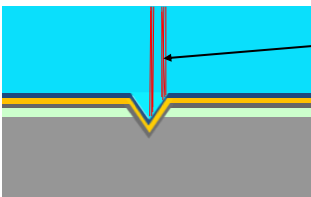
Coat SU-8
(multiple-spin coat)

Soft-bake, Degassing



Contact Mask

Exposure to UV
(for making needle-shafts)



Cross-linked portion
forming microneedle
wall

(Cont'd...)

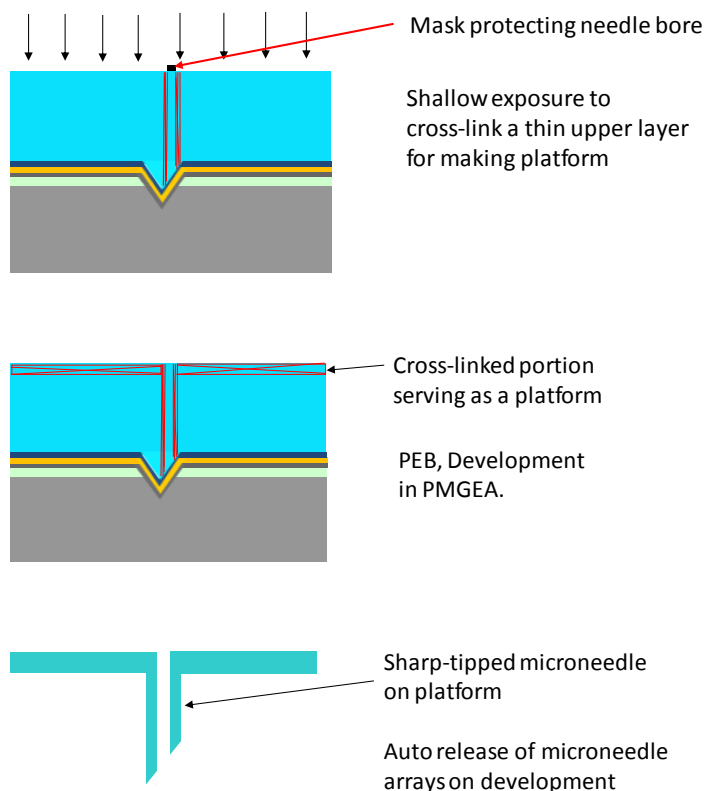


Figure 4.36: Final Process flow incorporating all changes: a sum total of the basic, intermediate and advanced process design.

To put it in a nutshell and to summarize the detailed process flow above, this is a moulding technique combined with photolithography. SU-8 is used as the structural material of the microneedles as well as the platform layer, thereby making this a very elegant and monolithic process. In fact, this is the very hallmark of the process. The KOH-etched grooves give the desired angular slope to the tip as well as impart it its sharpness derived from the sharp edges of the pyramidal pit. Next, the coated SU-8 (spincoated, pre-baked, vacuum oven degassed) on the mould master is patterned by deep UV lithography to cross-link and form the main body of the microneedle. This is followed by another shallow exposure to form the platform layer from the

same mass of SU-8 without addition of any new material or even additional SU-8. Doing thus, eliminates the chances of non-bonding or non-adhesion between the microneedle bottom rims and the adjoining platform layer. Being composed of the same material, the resulting bonding strength should be good, and as is found later on in the next chapter on tests, this is indeed the case. Next, the post-exposure bake is carried out at the regular 80°C in an oven. Finally, development was carried out in PMGEA solution for 3 hours with regular stirring. The platforms with the microneedle arrays were released automatically from the wafer substrate. It is to be noted that unlike usual SU-8 processing, this process eliminates the need for a sacrificial layer. This is facilitated by a very small contact area between the microneedle tip anchored on the sloped surface of the pyramidal pits. The force of adhesion between this small tip interfacial area and the Cr-black coated substrate is not great, which aids in the automatic release of the SU-8 microneedle arrays.

4.7.3 Final results from optimized process: *a discussion*

Thus, resolving the aforementioned issues, and after incorporating all the above solutions into the process, finally, the process was optimized, and following results were obtained. See the following Figure 4.37 to Figure 4.44.

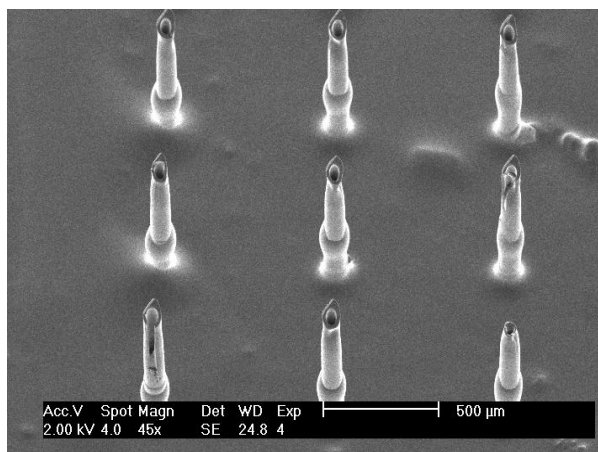


Figure 4.37: Sharp bevel-shaped tipped, hollow (HB), out-of-plane SU-8 microneedles on an SU-8 platform. Entire structure is composed of one material, therefore, monolithic. (Cont'd..)

Dimensions - (Microneedle) Height = 1000 μm , Inner diameter = 66 μm , wall thickness = 25 μm ; Platform thickness = 200 μm

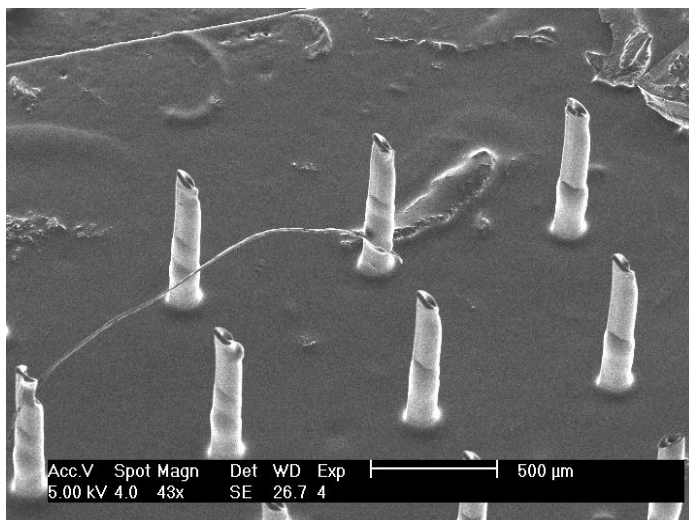


Figure 4.38: Another SEM picture of the same bevel-shaped (HB) microneedles from a side-view, clearly indicating the slope of the tip conforms to the slope of the 54.74° Si $\langle 111 \rangle$ crystallographic plane.

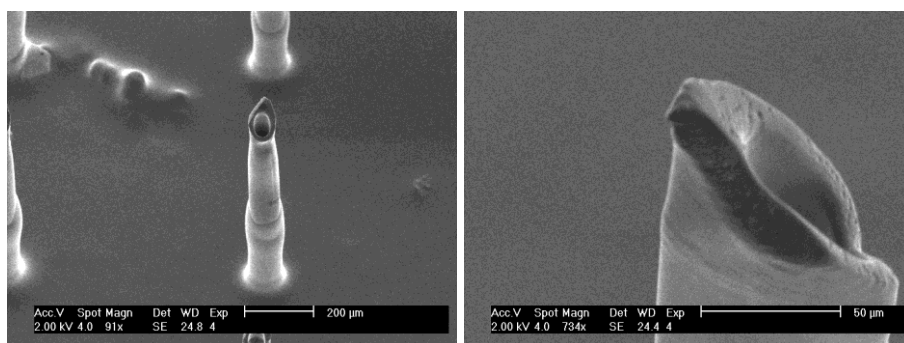


Figure 4.39: A view of a single bevel-shaped tip microneedle (HB). (Left): To be noted is the very pronounced hollow of the lumen as is visible from the top. Also very noticeable is a peculiar bulge in the "waist" region of the microneedle shaft. Careful process analysis shows that this could be the result of an incomplete pre-bake treatment to an intermediate (Cont'd...)

spin-coated layer. (Right): Close-up side view of a microneedle tip. End tip diameter measured to be around $4\ \mu\text{m}$.

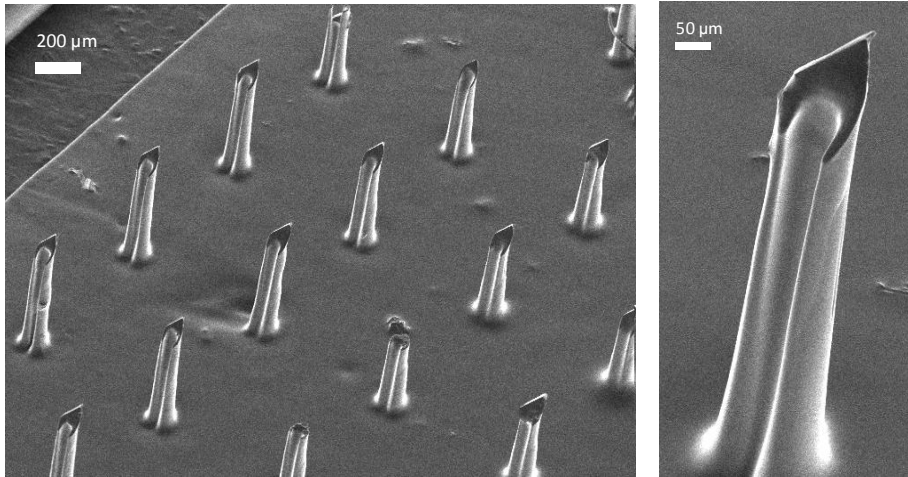


Figure 4.40: An array of microneedles with bevel-shaped tips with a slit through their entire heights (HSB) standing out-of-plane on a solid platform without any holes. Dimensions - (Microneedle) Height = $600\ \mu\text{m}$, Inner diameter = $66\ \mu\text{m}$, wall thickness = $25\ \mu\text{m}$; Platform thickness = $200\ \mu\text{m}$. (Left): An array of bevel-slit microneedles on platform; (Right): The sharp bevel-shaped tip of a single microneedle is observed. The slit is well-pronounced through the entire height. This can be used as a solid or semi-hollow microneedle.

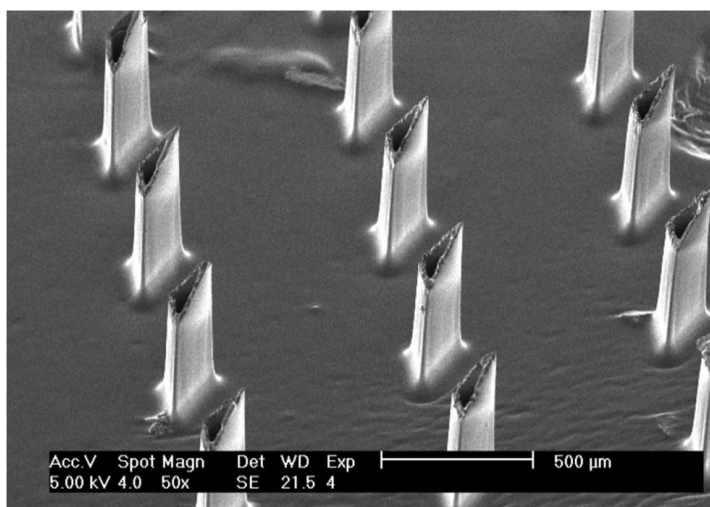


Figure 4.41: Triangular cross-section polymer microneedles with very well-defined wall edges, and a very clear hollow lumen, also standing on a polymer platform, all composed of a single material – SU-8; Cross-sectional shape: right-angled isosceles; Dimensions – Microneedle Height = 1000 μm; Outer height = outer base = 175 μm; Inner height = inner base = 100 μm; Platform thickness = 200 μm.

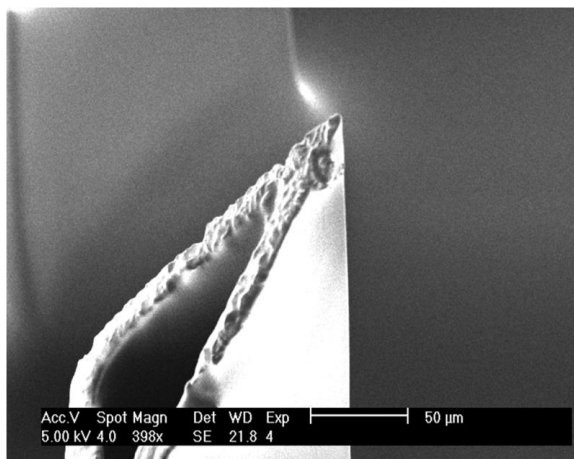


Figure 4.42: SEM picture of a close-up view of triangular cross-sectional microneedle tip. Tip diameter < 4 μm. The rough edge of the tip surface may have resulted from a hastened release step at the time of development.

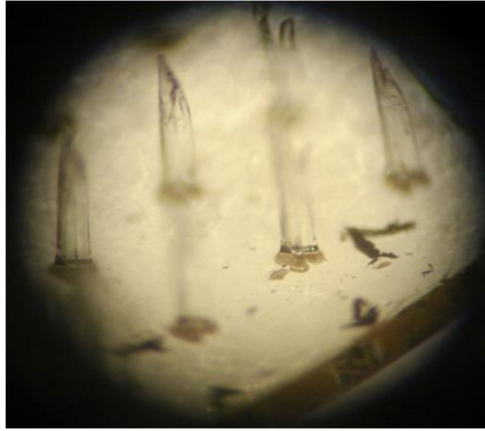


Figure 4.43: Picture of the entire microneedle array on a platform viewed under an optical microscope. Since the microscope can only focus at a certain depth at a given time, some of the microneedles appear to be blurred. What is clearly observable is the thickness of the platform, and the fact that both the needles and the platform are made of a singular material.

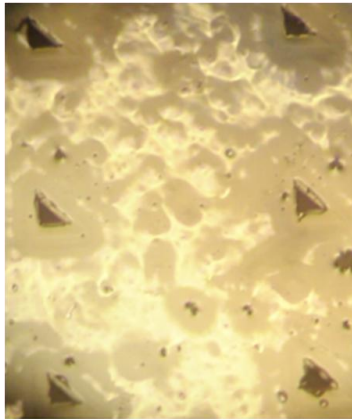


Figure 4.44: Openings at the rear end of the platform corresponding to the microneedle lumen bores, and are continuous through the thickness of the platform.

As can be observed from the above figures, the microneedles fabricated have met the initial process target goals. They are tall, hollow with clear lumens, sharp-tipped and standing on a platform made of the same material with hollow lumens continuous through the coinciding holes in the platform layer. It is to be stressed once again, that as per the process goals, both the

sharpening of the tips as well as formation of the platform layer were executed *in-situ* in the process itself, and the use of additional materials has been kept at a bare minimum. By being able to achieve this feat, the process can be qualified as a monolithic since both needles as well as platform are made of the same material without use of any “glue” to bond the two. Further, on inspecting the above figures, it can be surmised that in accordance with our initial “inspiration” of the “mosquito proboscis”, the shape of the needle tip does in fact, bear quite a striking resemblance to the same (see Figure 4.45). The bevel-shaped tips of the needles in Figure 4.37, Figure 4.38 and Figure 4.39, all bear testimony to this fact.

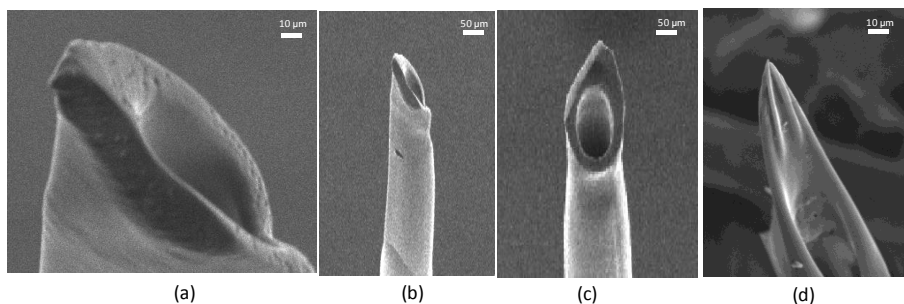


Figure 4.45: Already illustrated previously in the text individually, they are displayed here once again to bring out the comparison of the fabricated SU-8 bevel-shaped microneedle tip with the real mosquito fascicle. The biomimetic aspect is quite pronounced here. (a) Close-up side view of the fabricated tip indicating its sharpness; (b) Side view showing the 54.74° sloped angle of the sharp tip; (c) Front view of the bevel-shaped tip; (d) The actual mosquito fascicle tip. The bevel-shaped opening of the tip bears a striking similarity with the fabricated tips.

At this stage, it would be appropriate to dwell a bit on a certain aspect of the mask design which actually culminated in this excellent biomimetic shape. Though, the various designed cross-sections were already listed in Chapter 3, a word about the mask design for the bevel-shaped tip especially, should find a special mention. The bevel-shaped geometry as seen above in Figure 4.45 is the result of an innovative combination of three different shapes to result in this particular shape.

Also, the triangular cross-sectioned microneedle tip as illustrated in Figure 4.41 and Figure 4.42, highlights the sharpness of tips achieved by this process. Tip sharpness has been measured to be less than $4\ \mu\text{m}$ at tip diameter. Further, the openness of the lumen both at the tips as well as at the posterior end, that is on the back-side of the platform as displayed in Figure

4.44, indicate the robustness of the process in terms of producing clear unclogged hollow lumens even at such high aspect ratios. This was indeed a major challenge which has been met. Additionally, the process has a high yield (as noted over the repeated runs) averaging around 90% together with being quite repeatable. Thus, this also has the potential to be scaled up to a mass scale production line. Furthermore, given the relative simple processing tools and low-cost materials utilized along with the repeatability of the master Si mould, makes it a low-cost high throughput process and thus, economically quite viable. And last but certainly not the least, harking back to the initial process goals once again, it can be said that the process in itself lends a great deal of flexibility to the designer in terms of microneedle height, cross-sectional geometry, microneedle dimensions and even to freely select between solid (non-hollow) or hollow architectures without requiring any change whatsoever in the given process design. Only a change in the mask design would suffice to cater to the aforementioned changes in design (except microneedle height which is a function of the thickness of the SU-8 layer and can be tuned easily in the process).

4.8 Conclusion

The salient features of the fabrication process of microneedles may be listed as follows:

1. Simple, elegant process
2. Use of materials kept to a minimum – primarily monolithic
3. Flexibility of design – heights, dimensions, cross-sectional geometry, inter-needle spacing can be very easily altered.
4. Solid or hollow microneedles possible
5. Tall, hollow, high-aspect ratio structures
 - Microneedle Final Dimensions:
Height > 1000 μm , *Inner dia.* = 70 μm ,
Wall thickness = 25 μm ;
Platform thickness = 200 μm
Microneedle Aspect Ratio > 40
6. Sharpening of tips done *in-situ*. Final tip diameters achieved $\sim 5 \mu\text{m}$.
7. An anti-reflective Cr-black layer ensured minimum internal reflection thereby preventing cross-linking of the needle bore.
8. Platform layer made *in-situ*.

9. No additional bonding material required between microneedle and platform layer.
10. A novel and every efficient release mechanism
11. Repeatability of the Si wafer master moulds

In conclusion, it can be summed up that finally a process was designed and optimized in the most elegant manner keeping in mind the various constraints and challenges presented. Right from the outset, the target goals of the process were kept uppermost in mind and this helped to select and narrow down the best possible process design amongst the various options at-hand. It may be perhaps pertinent to note that though microneedles can be fabricated in a variety of methods as has been shown in literature studies, the process utilized herein is quite novel and unique given its salient points. It is in fact, a better process than the one used by Wang et al (84) since here Si moulds were utilized instead of PDMS moulds thereby resulting in much sharper tips. Also a multi-spin coating process was used here while they used a simple casting process. This ensued a thicker SU-8 layer which in turn produced taller microneedles, thereby resulting in a higher aspect ratio. An anti-reflective coating of Cr-black layer which was electrodeposited here, was not done by Wang et al. It is also worthwhile to note once again that most research groups worldwide focus mainly on making “solid microneedles” as they are for obvious process reasons much more hassle-free and involves less complexity. The main challenge faced here in this case was to design a process that would not only be robust and repeatable but would be simple as well. This simplicity is, well confounded, albeit a bit, when additional constraints of “tall, sharp, hollow” are thrown it as it translates into high-aspect ratio structures. Producing high-aspect ratio hollow structures using polymer processing without resorting to advanced techniques such as LIGA or Deep RIE (DRIE) in itself, is a formidable challenge which has also been met quite elegantly.

5

Device Tests & Characterization

Abstract

In this penultimate chapter, the various tests performed on the fabricated microneedle arrays, are discussed – the tests include those for mechanical strength and stability as well as basic microfluidic properties. From these test results, it can be determined that the microneedle array on platform is suitably strong enough to penetrate human stratum corneum. Penetration tests have been performed on agar gel and forces measured. Finally, preliminary biocompatibility tests for cytotoxicity and finger penetration were also performed.

5.1 Microneedle testing

Broadly speaking, from an engineering standpoint, microneedles need to be tested in two areas:

- 1) Mechanical strength
- 2) Microfluidics (if needle is hollow and serves as conduit for fluids)

While mechanical strength testing comprises measurement of critical load-bearing force or the failure force for an orthogonal load as well as shear testing for lateral shear forces during penetration into the stratum corneum, microfluidic testing comprises a basic measurement of flow rates through the microneedle, at a given pressure.

A noteworthy point to be borne in mind before dwelling on the following tests is that the testing and characterization should obviously reflect the true application of the device. For instance, if the microneedle architecture is a solid one, devoid of any hollow lumen, a microfluidic testing is not possible. In that case, since the drug would be coated onto the needle surface, what should be tested, rather is the adhesion of the drug to the surface of the needle, whether any surface pre-treatments are required to increase this adhesive force, whether during penetration into the skin if the drug still remains faithfully adhered to the surface of the needle or does it, due to the frictional forces acting upon it, delaminates from the needle surface in the process of skin penetration.

However, since the architecture of our microneedle is primarily hollow, the corresponding mechanical and microfluidic tests shall be dealt with herein.

5.1.1 Mechanical tests

The primary concern regarding testing mechanical characteristics of a microneedle for transdermal drug delivery is the ability of the microneedle to be able to penetrate the stratum corneum layer of the skin without undergoing mechanical failure. For this, it is essential to determine the critical load bearing force of the microneedle and, the penetration force required to puncture into the skin. The critical load bearing force (also known as the failure load) of the microneedle is the maximum applied load beyond which the microneedle undergoes failure and breaks as a result. There were three components to the mechanical tests:

- 1) Compressive mechanical test
 - a) On flat-top (unsharp) microneedle
 - b) On an array of sharp microneedles
 - c) On single sharp microneedle
- 2) Shear mechanical test
- 3) Penetration test

5.1.1.1 Compressive mechanical test

- a) On flat-top (unsharp) microneedle

This was a very preliminary test performed on the basic unsharp hollow microneedle structure more to just test the material properties of the SU-8 than to test the microneedle performance *per se*. In this test, a nanoindenter frustum of a cone having a radius of 110 μm was used to apply an axial load orthogonally on the top of the microneedle. This loading continued till the maximum applicable limit of the nanoindenter (i.e. 500 mN) and was then unloaded. This cycle of loading-unloading was repeated 5 times on a single microneedle of height 1540 μm , circular crosssection with a circular bore, inner diameter of 150 μm and an outer diameter of 250 μm . The resulting plot is illustrated in the following Figure 5.1.

Firstly, it is quite obvious that the loading-unloading curve follow a hysteresis pattern. Secondly, it is observed that with each loading-unloading cycle, the microneedle in effect becomes stiffer. Thirdly, from the graph of experiment 1 in Figure 5.1, the stress and strain values can be calculated. Taking the maximum applied force as 500 mN over the area of circular indenter directly gives the applied stress. On closely inspecting the graph where the unloading curve meets the x-axis (assuming the point of intersection to measure 4800 nm or 4.8 μm which is the change in length of the pillar compared to its original height of 1540 μm , the Young's modulus E, of SU-8 can be determined as follows:

$$E = \frac{\text{Stress}}{\text{Strain}} \quad 5-1$$

Calculating, E is determined to be 4.22 GPa which is well in agreement with SU-8's Young Modulus of 4 GPa (109).

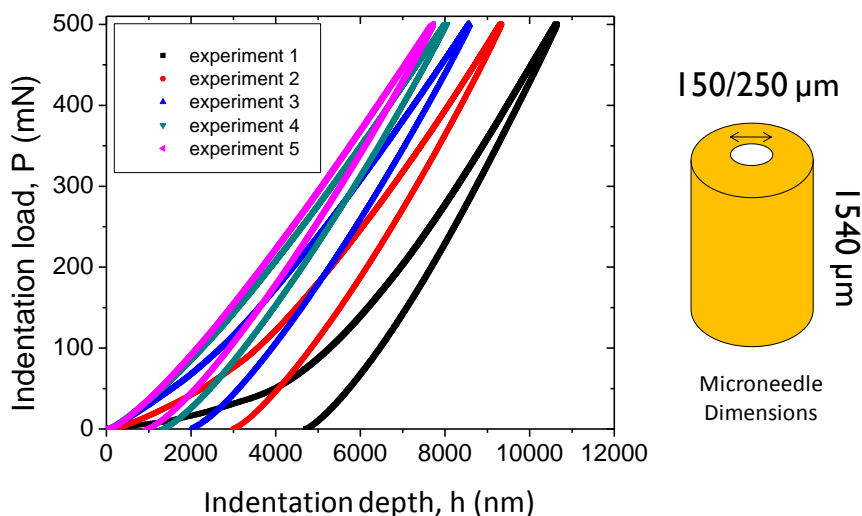


Figure 5.1: Cyclic loading-unloading of hollow SU-8 cylinders by a nanoindenter of 220 microns in diameter. A schematic of the tested microneedle dimensions are also given alongside – Inner diameter = 150 μm ; Outer diameter = 250 μm .

b) On an array of microneedles

In very simple terms, the objective of the compressive test was to determine the maximum compressive load which could be applied on the microneedle during insertion into skin, without it undergoing failure. This mechanical test experiment was carried out on a delaminator testing set-up. The platform-side of the microneedle array was glued onto a holder with epoxy and pressed down in order to ensure uniform spreading of the glue to the underside of the needle platform and allowed to dry. The affixation of the needle array to the holder by glue was important to ensure that the needle array remains in place and does not slip during the orthogonal application of force. The basic schematic of the arrangement was as illustrated in Figure 5.2.

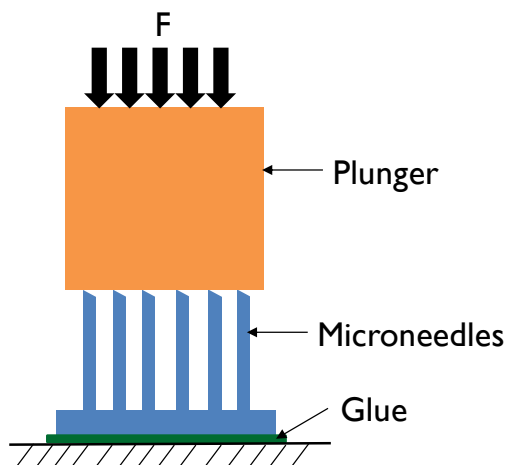


Figure 5.2: Schematic of failure force characterization on microneedle array

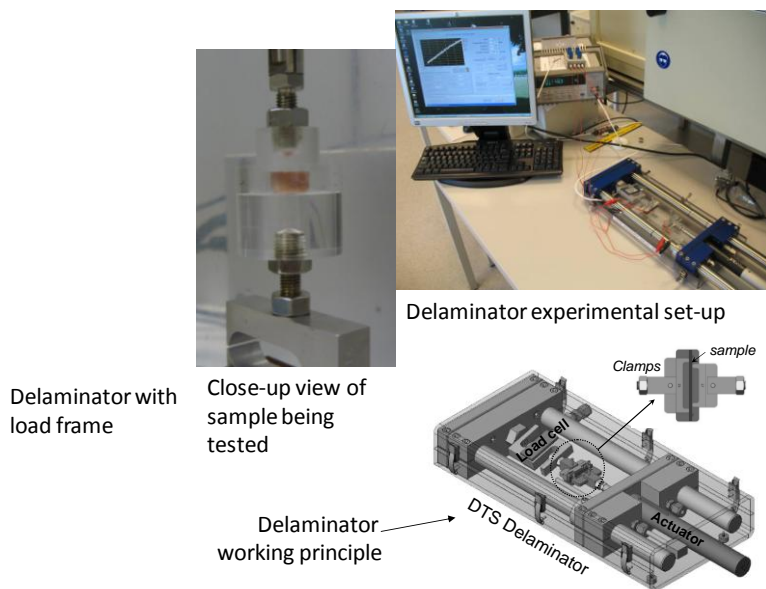


Figure 5.3: DTS Delaminator experimental set-up for measuring failure force of the microneedles.

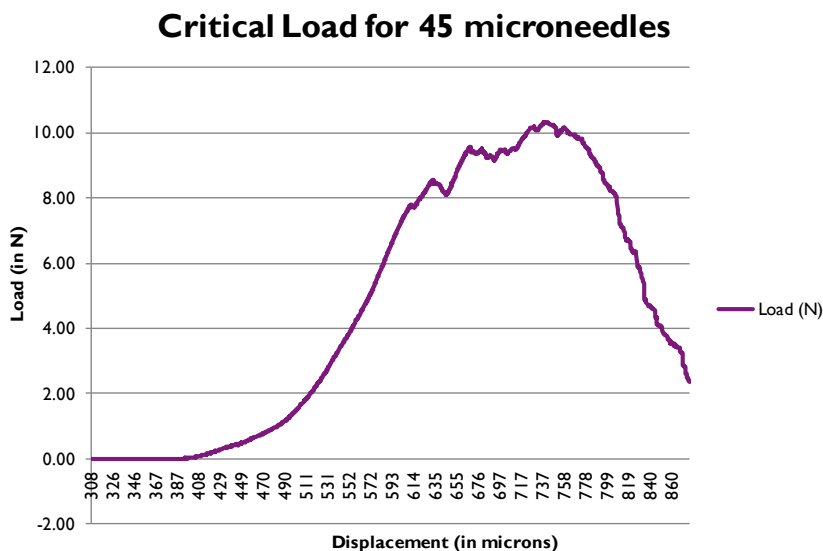


Figure 5.4: Load-displacement graph to determine the critical load bearing force of fabricated hollow microneedles. Load applied is measured in "Newtons" and displacement in "micrometers". This test was performed on an array of 45 microneedles in number, hollow lumen, triangular cross-section, 1000 μm in height as fabricated previously (see Figure 4.41). The maximum load applied is 10.35 N.

The name of the tool used is DTS (Dauskardt Technical Services) delaminator, as displayed in Figure 5.3. This system is a high precision micro-mechanical test system with full computer control and data analysis. The system is built around a mechanical stiff frame to improve test stability and yield. It includes an ultra-high-resolution linear actuator providing linear motion of 50 mm with a resolution 20 nm in a compact package. The speed is limited between 20 nm/s minimum and 3 mm/s maximum, while the load on the actuator is limited in the software to 180 N. This load can only be applied in the direction axis of the movement. The load cell has a maximum load of 222 N. The cell is connected to the data acquisition (DAQ) device with a standard 6 pin load cell connector. The system is capable of testing in compression and tension.

Effectually, the experimental set-up employs a force sensor which measures the reaction force. Obeying the principles of Newton's Third Law of Motion, as the applied load is increased progressively in steps by the plunger, the resulting reaction force is equal in magnitude but opposite in

direction – this continues till failure of the microneedle occurs by its breakage wherein the reaction force drops to 0 N. This is the basic operational principle. The highest peak in the applied force curve beyond which the curve drops, is the maximum load that can be withstood by the array of needles, or the critical load-bearing force of the microneedle array. For this experiment, the plunger steps were defined at the rate of 0.5 $\mu\text{m/s}$ orthogonal displacement, and the corresponding reaction force measured. It is no be noted that this experiment was carried out on an array of 45 microneedles, thus the total load bearing force must be divided by this number in order to arrive at the correct failure load per microneedle. The results can be observed from the load-displacement graph as displayed in Figure 5.4. From the above graph it can be observed that the maximum load applied was 10.35 N. Given that this was applied over a total number of 45 microneedles, it gives the critical load bearing force of each microneedle to be 230 mN per microneedle.

However, a more detailed look at the above graph raises several questions such as why is the drop in the curve not smooth? Why do sudden peaks occur during the rise of the force curve, and what do they signify? Why is there no single clearly defined peak? These questions certainly warrant a deeper discussion into the phenomenon of the failure process. One possible and most reasonable explanation is that due to certain fabrication process anomalies such as non-uniform thicknesses of the SU-8 at different areas on the wafer (resulting from possible levelling issues at the stage of reflow), it is likely that of the total number of 45 microneedles in the array, that some needles are slightly taller than the rest, and in all probability this phenomenon of a few needles taller than the average needle height is random. In effect, these microneedle tips might have been first in contact with the flat surface of the plunger and due to the randomness of the taller-than-average needle distribution; the plunger surface might have been sloped, thereby, contacting some of the taller needles on one side and some of the shorter needles on the other side. When these taller needles first undergo failure, the plunger surface gets re-aligned to the remaining needle tips, and this steps recurs till the entire needle array has been re-adjusted automatically to contact the plunger surface, and the avalanche of breakage commences at the 10.35 N mark. Thus, from an accurate scientific standpoint, it would be wiser to re-look at the critical load bearing force. If 10.35 N was the maximum load point for the final avalanche set in, the commencing load point for an initial failure can be marked as 7.8 N, the point of first significant drop in the rise of the force curve. Considering 7.8 N as the applied force on 45 needles, gives the failure load as 173.33 mN per

microneedle. Thus, in effect, the final load bearing force for each microneedle can be said to lie in the range of 173.33 mN to 230 mN.

Figure 5.5 below illustrates the array of needles before and after the failure testing. In fact, the very reason why this kind of testing on the entire array of microneedles was chosen was in order to get a realistic average value of the failure force. But as is observed, the results of the analysis is far from clear, and a full knowledge of the true failure force can be obtained only from testing of a singular microneedle, since the array might have several effects running in parallel which conceals the true failure force.

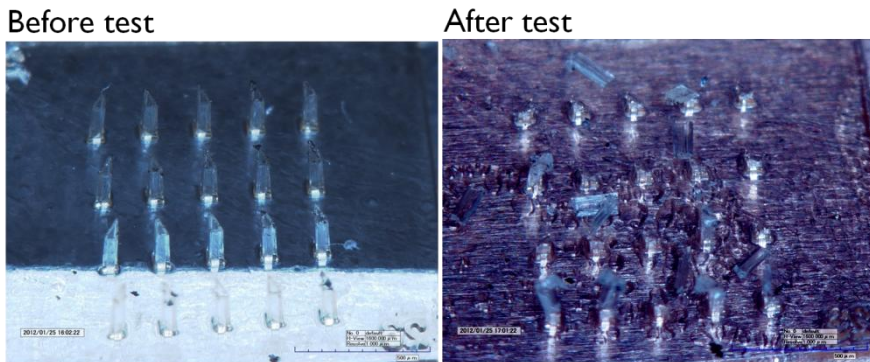


Figure 5.5: Before and after view of the compressive critical load bearing force test on the microneedle array. (Right): The entire needle array comprising all individual needles has undergone failure. (Left): The same needle array intact prior to testing.

It is to be borne in mind that the above microneedles were of the hollow variety with triangular section. This is one of the geometrical shapes which have repeatedly yielded very similar and desirable fabrication results, which is why this shape has been selected to be used in a final application.

However, it may be recalled that several other geometrical cross-sections were also fabricated such the one below in Figure 5.6.



Top View: CS of solid microneedle with slit along its entire height

Figure 5.6: Alternative solid microneedle cross-section - a bevel-shaped tip combined with a slit running through its entire length of the shaft.

Subjecting a microneedle array of the above cross-section of Figure 5.6 to the similar compressive test leads us to the following results as illustrated in the following graph of Figure 5.7.

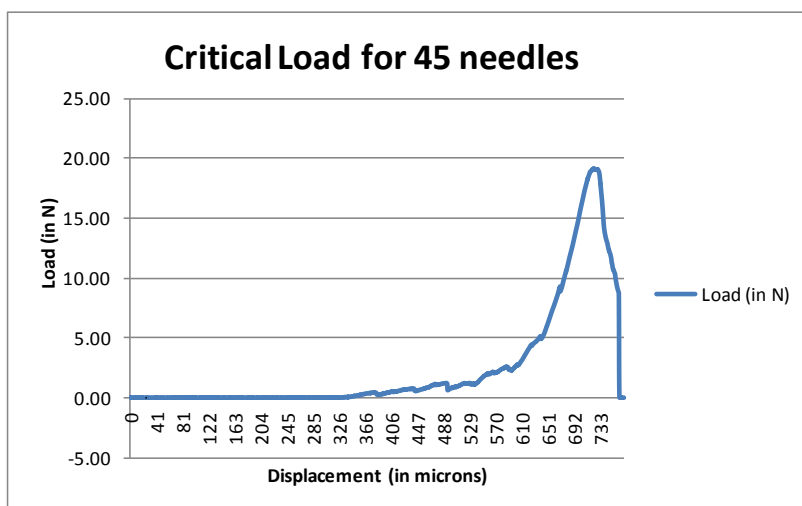


Figure 5.7: Load-displacement graph to determine the critical load bearing force of fabricated solid (with slit) microneedles. This test was performed on an array of 45 microneedles in number, of average height 650 μm , bevel-shaped cross-section with slit through entire shaft. The maximum applied load is 19.09 N.

As in the previous experiment, here the total maximum applied force (= 19.09 N) divided by the number of needles (= 45), or the critical load bearing force of each of the microneedles is ascertained to be 424.22 mN if the peak of the graph is considered. But if the curve is analyzed more carefully, it is observed that “bumps”, possibly signifying failure, start setting in from even as early on as 336 μm displacement corresponding to a

less than 1 N failure force. Again, as aforementioned the same fabrication process anomalies may be responsible for this erratic measurement.

Comparing with the triangular cross-section with hollow lumen, this solid bevel-shaped needle with slit *only appears* 2 times stronger simply because the average needle height fabricated here is about 650 μm . Moment of inertia calculations indicate as in Chapter 3 (Figure 3.6), that structurally the triangular cross-section microneedles are stronger than the bevel-shaped ones.

Further, an illustration of the microneedle array before and after the performance of the test is given below in Figure 5.8.

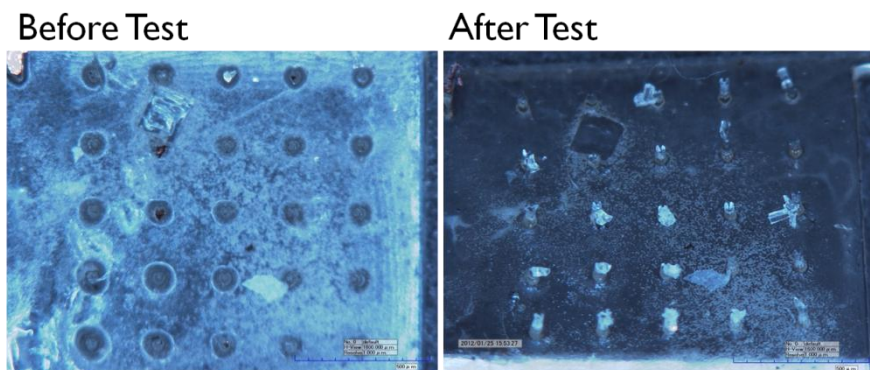


Figure 5.8: (Left) Top view of the intact solid bevel-shaped microneedles with slit before compressive test; (Right) Top view of the same after test, depicting breakage of all the microneedles in the array indicating complete failure.

Notwithstanding the initial failures in both graphs of Figure 5.4 and Figure 5.7, and just restricting the analyses to the modes of final failures, it can be reasoned that step-by-step failure in Figure 5.4 could be a result of a plastic deformation while the more or less abrupt drop in Figure 5.7 could have arisen due to a brittle failure. One possible explanation for this hypothesis could be that the solid SU-8 microneedles are more brittle than the hollow ones.

c) On a single microneedle

Keeping in mind the inconsistencies observed in the previous tests on arrays of microneedles, and in order to have a clearer insight into the mechanical

performance of a single microneedle, the same compressive test experiment was carried out on a single microneedle. The same experimental set-up of Figure 5.2 was used with the only difference that all except one microneedle in the array had been removed.

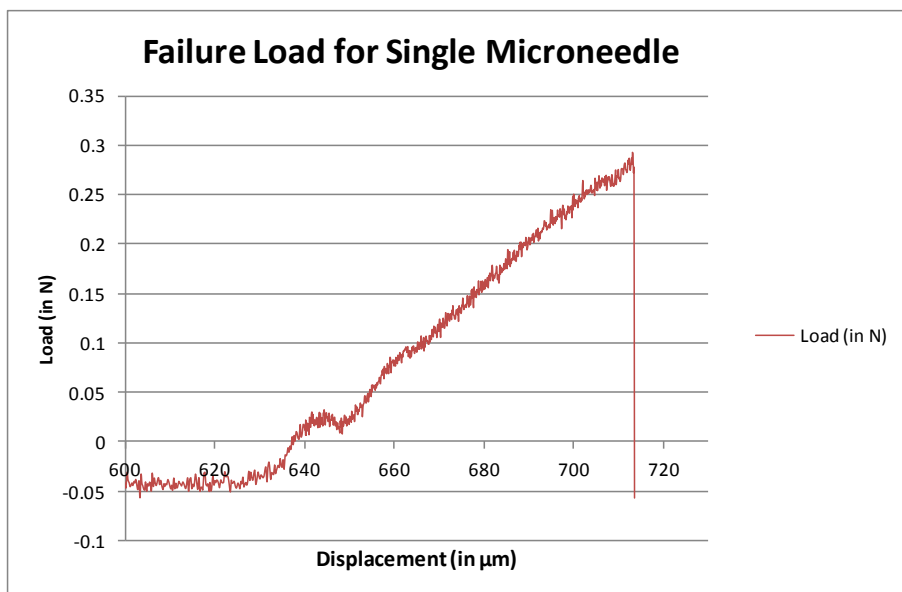


Figure 5.9: Load-displacement graph for single microneedle with hollow lumen, triangular cross-section, 1000 μm in height. The measured failure force is 0.277 N.

From the above Figure 5.9, it is observed that the critical failure load of the individual microneedle of triangular cross-section, hollow lumen and 1000 μm in height, is about 277 mN for this particular case. The apparent disturbance in the curve is due to a “noise” influence which otherwise holds no special significance. Furthermore, compared to the previous analyses on the arrays, here, the failure is quite explicitly reflected at 277 mN. In order to validate this reading, the test was repeated over 15 different microneedles of the same dimensions taken from 15 different arrays. The results are plotted in the following Figure 5.10.

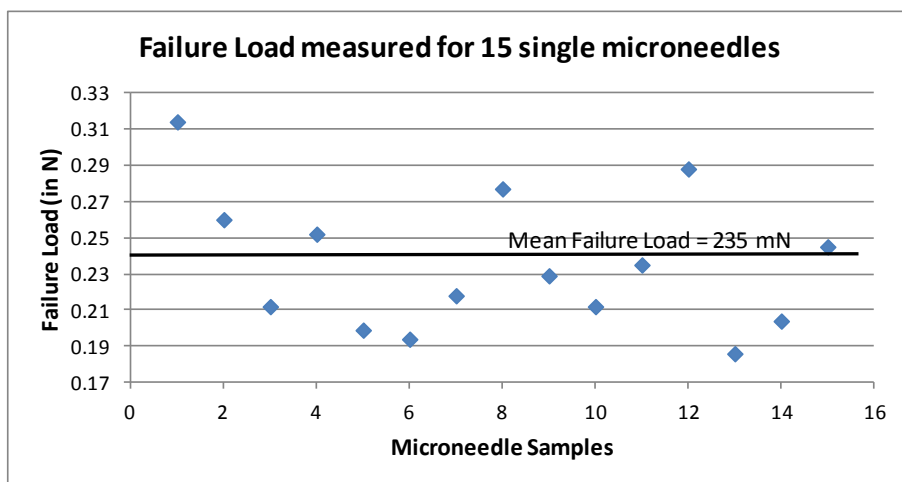


Figure 5.10: Failure load measured for 15 single microneedles of the same dimensions (1000 microns in height), hollow lumen and triangular cross-section taken from 15 different arrays; and the mean failure load of 235 mN is depicted with the help of a straight line.

The arithmetic mean of the failure load values obtained was 235 mN which is in good agreement with the theoretical calculated value of 230 mN. However, the range varied between 186 mN on the lower side and 314 mN on the higher side. This is a more realistic range of values of the critical failure force when compared to the compressive testing on the arrays.

Average failure load (compressive) of single hollow microneedles = 235 mN \pm 17%.

For practical purposes, the compressive failure load of each hollow microneedle can be designated as ~ approx. 186 mN.

It is of technical interest at this point to determine the failure stress of the microneedle and then compare it with the material properties of SU-8. Since the cross-sectional area of the microneedle may be calculated from the triangular shape ($= 10,312 \mu\text{m}^2$), and the given average failure force is 235 mN; then the measured stress is found to be about 23 MPa. Though the stress limits of SU-8 depends on a host of factors primarily, the manner of processing, still it can be said that the stress values range from about 20 MPa (thin films) to about 40 MPa (hard-baked) as per (128) (109). Thus, it can be observed that the value falls within the given range and therefore is in good agreement with the material stress properties.

5.1.1.2 Shear mechanical test

The skin being a visco-elastic structure exerts lateral forces on the microneedle during the orthogonal insertion of the latter inside it. Though the net lateral force on the microneedle still remains zero, however, it is during the insertion by the user, that there is a high chance that a non-orthogonal insertion might happen inadvertently. In such a case, it is necessary to know the shear forces that could be acting upon the microneedle tips . Thus, it becomes imperative to test the upper limit of these lateral shear forces which the microneedle can withstand. This is an important parameter indicating the strength of the bond between the microneedle shaft and the platform on which it stands perpendicularly. Since both the needle shaft and the platform are made of one material, it is but expected that the resulting bond between the two should be strong. The shear mechanical test measures this strength precisely.

The tool employed for this experiment was a “nanoindenter”. Broadly speaking, the working principle is also similar to the previously used delaminator except that in this case, the size of “plunger” is much reduced, can be applied locally on a wide range of regions on the sample surface, and is a “nanoindenter” instead. The nanoindenter used here is shaped quite like the frustum of a cone as depicted in Figure 5.11 below:

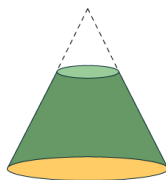


Figure 5.11: Shape of the nano-indenter used for this shear test – frustum of a cone. The force is applied on the sample by the smaller disc of radius $10\ \mu\text{m}$.

Unlike in the previous experiment wherein an entire array of needles was subjected to the orthogonal force, here only individual microneedles were probed by the nano-indenter near their tips in order to generate maximum lateral bending. Schematically, this can be represented in Figure 5.12 as follows:

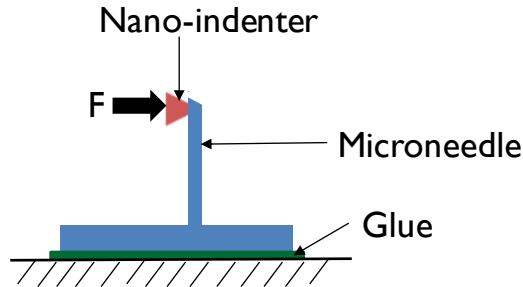


Figure 5.12: Principle of measuring shear force by nano-indenter.

For the hollow triangular cross-sectioned microneedle, 800 μm in height, the average maximum shear force, F_{max} that can be withstood by an individual microneedle is about 223 mN with an average maximum displacement of 217 μm . Modelling the microneedle as an approximate cantilever beam with a fixed-free end and with the applied load at its free tip;

$F_{\text{max}} = kx$, where k is the stiffness constant of the microneedle at/near its tip.

Thus, k can be determined to be about 1,028 N/m at the tip of the microneedle.

It is known (117) that for a fixed-free horizontal cantilever of length L , with a moment of inertia I , and composed of a material with a Young's modulus E , when a point load W ($=F_{\text{max}}$) is acting on its tip vertically,

$$\text{Maximum displacement, } y_{\text{max}} = \frac{WL^3}{3EI} \quad 5-2$$

It is to be noted that due to a non-regular geometry of the exact tip, the point load was positioned at 100 μm from the tip, thus, effective $L = 700 \mu\text{m}$. On substituting the other values, we obtain:

$$y_{\text{max}} = 274 \mu\text{m}$$

which is in relatively moderate agreement with the actually obtained value of 217 μm .

Further validation in the form of stiffness measurement results also confirm the above result. The stiffness was measured on different microneedles of 800 μm lengths and having the same dimensions and cross-section as the above tested microneedles.

The graph obtained in Figure 5.13 proves that the microneedle is much stiffer at its base compared to its tip as can be even surmised intuitively. Further, on comparing the value of stiffness at 700 μm from the graph (approximately between 600 N/m and 1000 N/m), we observe that it comes close to the calculated value of 1,028 N/m.

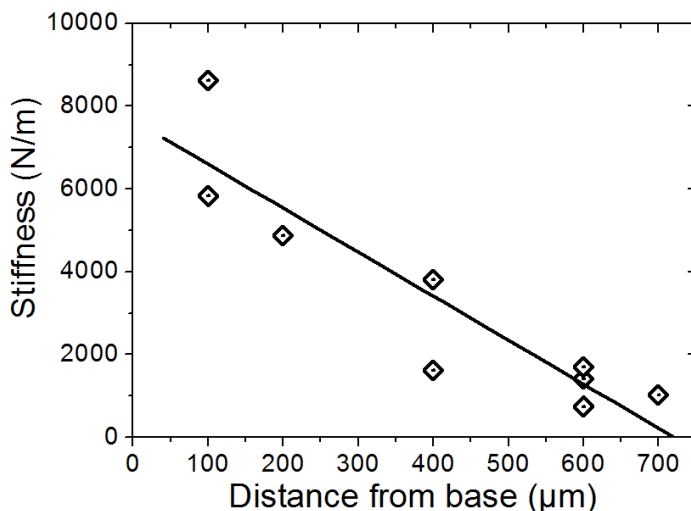


Figure 5.13: Stiffness of microneedle measured by a nano-indenter. Microneedle dimensions were 800 microns in height, triangular cross-section with hollow lumen. As the distance from the base of the needle increases the stiffness reduces rendering the microneedle much more flexible at its base than at its tip.

Thus, it can be safely stated that the:

Average critical shear failure force per hollow microneedle = 223 mN \pm 12%.

For practical purposes, the shear failure load of each hollow microneedle can be designated as ~ approx. 197 mN.

It is highly likely that the failure accrues from shear stresses rather than from bending of the microneedle, as could be observed from visual images during the nano-indentation.

The entire experimental set-up of the nano-indenter is as illustrated in Figure 5.14 below:

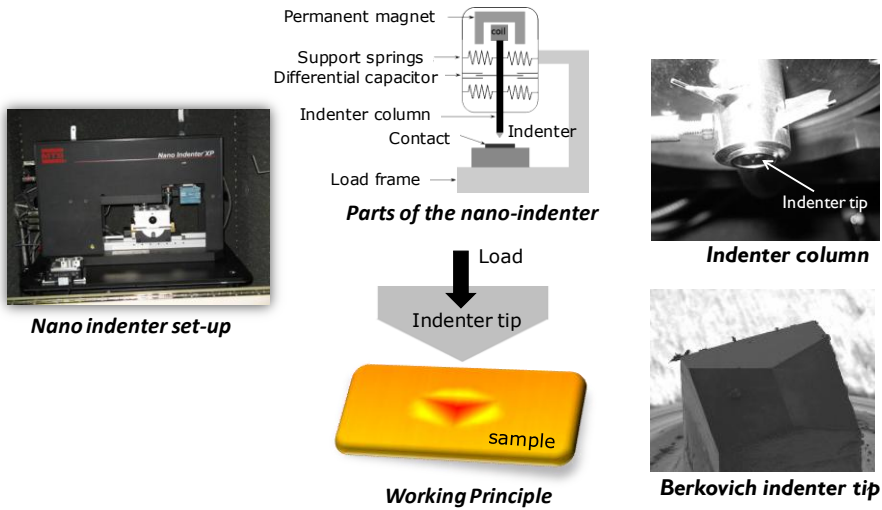


Figure 5.14: Nano-indenter experimental set-up, parts, working principle and example of a real indenter tip.

5.1.1.3 Penetration test

The objective of the penetration test was to primarily determine if the fabricated microneedles possessed sufficient strength to penetrate into an approximate skin equivalent. The approximate skin equivalent was taken to be commercially available agar gel. A thin slice of the agar gel of approximate thickness of 2 mm was placed on a fixed surface into which the microneedle array [3x3] was inserted from the top, in the same delaminator set-up of Figure 5.2. Schematically this can be illustrated as follows in Figure 5.15:

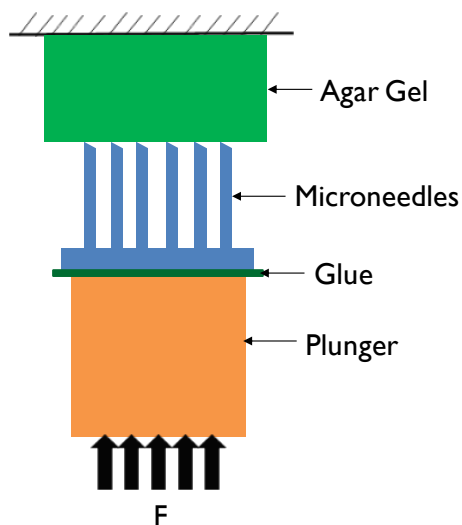


Figure 5.15: Schematic of penetration test characterization on fabricated microneedle array.

The mechanism of determination of the insertion force is slightly different from that of the failure force, as the failure force was being measured against a rigid body, namely the microneedles and the reaction force measured would be equal to the applied force. However, in this case, due to the viscoelastic properties of the agar gel, the applied force by the needles on the gel surface (open end of the agar gel) would not be equivalent to the reaction force at the bottom surface (fixed end of the agar gel). In this case, a manual mode of operation of the delaminator was chosen in which an initial impulse was imparted to the plunger and then it was allowed to freely experience the elastic reaction force of the agar gel on it. After a series of incremental increases in the force, the point at which the plunger doesn't experience any elastic reaction force anymore is when the microneedles have just penetrated the agar gel. This is also noted by visual inspection. Thus, the indicative measure of the penetration force into the agar gel by the [3x3] array of microneedles is 63 mN. Therefore, the critical penetration force for each hollow microneedle is ascertained from the above experiment to be about 7 mN which is unreasonably low. However, from literature values (74) we know that for a Si microneedle of 10 μm in tip diameter, the insertion force per microneedle was about 10 mN which is rather low due to its ultra-sharp tip. But widely used skin insertion force values for microneedles (118) range between 100 mN to 3 N depending on tip sharpness. The range of

sharpness of tip for our microneedle falls under the 100 mN skin insertion force regime and shall be used herein for further calculations.

From Section 5.1.1.1, we know that the critical failure force of each microneedle is about 186 mN. Taking a safety margin of 25% on this value gives a failure load limit of 140 mN. Assuming 100 mN as the maximum insertion force, safety factor for the microneedles (defined as the ratio of the critical failure force to the critical penetration force) is 1.4. This would still result in a safety factor greater than 1 (117) which is acceptable by mechanical engineering standards for skin insertion by microneedles (129).

Thus, safety factor = 1.4 (approx.)

The Figure 5.16 below illustrates the exact region (square outline) where the microneedles were inserted into the agar gel *vis-a-vis* other regions (darker in colour) where the agar gel is clearly unpenetrated.

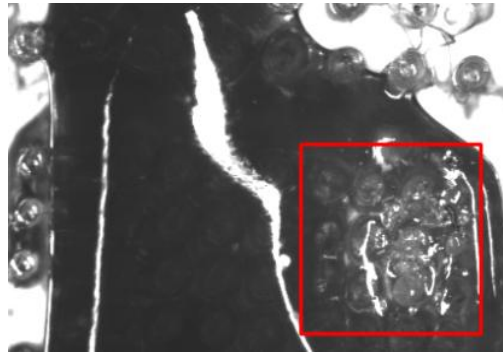


Figure 5.16: Penetration of microneedles into agar gel. The square outline indicates the area comprising an array of [3x3] hollow microneedles penetrated inside the agar gel by applying a force of 63 mN. Thus, insertion force of each microneedle is 7mN. The light gray coloured region shows that the microneedles have penetrated inside the agar gel in this region while the rest of the dark gray area signifies the agar gel lying in contact with the microneedle tips and not penetrated.

5.1.2 Microfluidic test

The primary objective of the microfluidic test was to determine if the microneedles were indeed hollow or not and if they provided a conduit for the flow of fluids, as intended to be. For this purpose, an array of microneedles was mounted on a syringe base, as shown in Figure 5.19, with epoxy glue for the purpose of injecting fluid through it.

5.1.2.1 Applicator design

The microneedle arrays as they are fabricated, stand-alone platforms comprising an array of needles are by itself incomplete from a system point of view. Not only can they not be utilized for drug delivery just as they are, but also they are not capable to being tested for their microfluidic characteristics without integrating them with additional contraptions. Though in literature examples abound about how fabricated microneedles have been mounted on plates (93) and assembled with a moulded and sealed platform made of PDMS (poly-dimethyl-siloxane) (130), the chief goal here was to conceptualize and design a contraption which could be utilized both for the microfluidic testing as well as for a real application of drug delivery. The key objectives to be met were: low-cost, easy to integrate, robust and reproducible. The final contraption that was designed was by modifying an off-the-shelf plastic (polypropylene) syringe. The base of syringe with the flat finger holder was converted into the platform for mounting the needle array. By doing this the needle array had a readymade horizontal surface on which it could be mounted. Next, the head of the syringe comprising the nozzle and a part of the body of the syringe was sawed off to produce an entry for the plunger. Thus, this looks like a syringe in reverse and works exactly like a normal syringe except that this has no nozzle and the plunger is pushed from the head side of the syringe instead of from the bottom side. Finally, the microneedle array was mounted onto the syringe flat base plate with glue ensuring that the glue didn't clog up the backside openings of the needles on the reverse side of the array, as illustrated in Figure 5.17. The advantage of this design is that not only could it be used for the microfluidic testing, but also could be utilized in future as an actual applicator for the microneedles. Though this is a very rudimentary design and leaves much scope for improvement, the primary objectives of microfluidic testing and that of injecting a fluid into skin for drug delivery could be met with this device.

5.1.2.2 Syringe force theory

Since the applicator to be used for performing the microfluidic tests is a syringe-based one, it is worthwhile to delve slightly into the background theory of the same. Consider a syringe as in Figure 5.18. If L is the length of the needle, R_b is the inner radius of the needle bore, R_p is the radius of the plunger, then the force F required to push a volume V_D of fluid of dynamic viscosity μ in time t_d is given by:

$$F = \frac{8\mu LV_D R_p^2}{t_d R_b^4} \quad 5-3$$

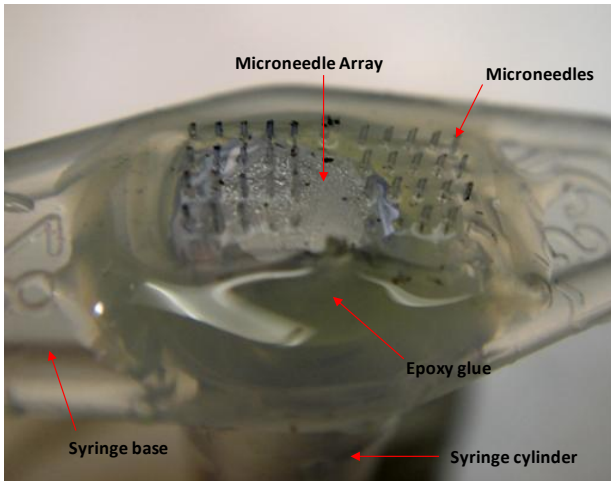


Figure 5.17: Designed applicator for microfluidic testing.

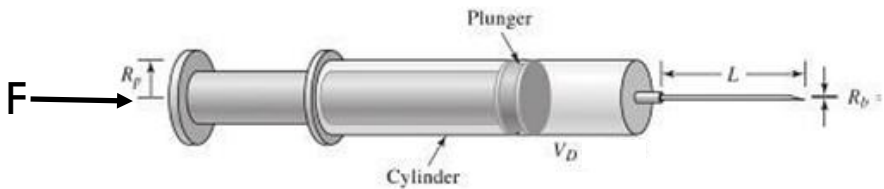


Figure 5.18: Syringe pumping force for fluid flow.



Figure 5.19: (Left) Array of microneedles mounted on a platform. (Right) Coloured water being ejected through the hollow microneedles.

5.1.2.3 Determination of flow rate, pressure drop

Experimentally, it was determined from the applicator setup with just one microneedle in place, that the maximum flow rate achieved was about 1000 μl in 1000 s or, 1 $\mu\text{l/s}$ per microneedle for distilled water at room temperature. Any rate higher than this resulted in a mechanical breakdown of the microneedle due to the high fluidic pressure. Substituting the following values into the above

$$\text{Equation } F = \frac{8\mu LV_D R_p^2}{t_d R_b^4} \quad 5-3$$

$$E = \frac{\text{Stress}}{\text{Strain}} \quad 5-1$$

we get:

- μ (for water) = 10^{-3} kg/ms
- $L = 1000 \mu\text{m} = 10^{-3}$ m
- $V_D = 1 \text{ ml} = 10^{-3}$ l
- $R_p = 2.5 \text{ mm} = 2.5 \times 10^{-3}$ m
- $t_d = 1000$ s
- $R_b = 33 \mu\text{m} = 33 \times 10^{-6}$ m

F = 42 N for 1 microneedle for maximum flow rate of 1 $\mu\text{l/s}$.

However, as mentioned in Chapter 3, there is an important trade-off between the number of microneedles (and thus, the total insertion force) and the total

flow rate, the optimal number of needles has been decided to be 4, in an array of [2x2]. Using, this array, at various flow rates, the applied force for injecting the fluid through the array of microneedles is computed to be as follows:

for 1 $\mu\text{l/s}$ per needle or 4 $\mu\text{l/s}$ for array $\rightarrow F_1 = F/4 = 11 \text{ N}$

for 0.5 $\mu\text{l/s}$ per needle or 2 $\mu\text{l/s}$ for array $\rightarrow F_2 = F_1 \times 0.5 = 5 \text{ N}$

for 0.33 $\mu\text{l/s}$ per needle or 1.32 $\mu\text{l/s}$ for array $\rightarrow F_3 = F_1 \times 0.33 = 3 \text{ N}$

for 0.17 $\mu\text{l/s}$ per needle or 0.68 $\mu\text{l/s}$ for array $\rightarrow F_4 = F_1 \times 0.17 = 2 \text{ N}$

Thus, the range of flow rates that can be achieved per array of [2x2] needles varies from about 41 $\mu\text{l/min}$ to 240 $\mu\text{l/min}$ for water-like fluids. Of course, as the fluid viscosity increases, the flow rate decreases, if the applied force is kept more or less constant or reduced, and vice versa.

Considering maximum flow rate per microneedle to be 1 $\mu\text{l/s}$, the velocity of flow can be computed from:

$$\text{Flow rate} = \text{Flow velocity} \times \text{Cross-sectional area} \quad 5-4$$

$$\text{Thus, Flow velocity } (\bar{w}) = \frac{\text{Flow rate}}{\text{Cross-sectional area}} \quad 5-5$$

Substituting the value of the above flow rate and the cross-sectional area of the microneedle, we get $\bar{w} = 0.292 \text{ ms}^{-1}$

$$\text{Reynold's number, } Re = \frac{\bar{w} \times D}{\nu} \quad 5-6$$

where D is the diameter of the microneedle (66 μm in this case), ν is the kinematic viscosity of water ($10^{-6} \text{ m}^2/\text{s}$)

$$\therefore \text{From Reynold's number, } Re = \frac{\bar{w} \times D}{\nu}$$

$$5-6 \text{ we get } \mathbf{Re = 19.272}$$

Since $Re < 2320$, this is in the regime of laminar flow.

$$\text{Next, Pipe friction coefficient, } \lambda = \frac{64}{Re} \quad 5-7$$

Substituting Re, we get $\lambda = 3.32$

Given that density ρ of the fluid injected (water) is 1000 kgm^{-3} , calculating pressure drop (Δp) across the length of the microneedle,

$$\Delta p = \lambda \times \frac{L}{D} \times \frac{\rho}{2} \times \bar{w}^2 \quad 5-8$$

Substituting the aforementioned values, we get $\Delta p = 2.1 \text{ kPa}$

Thus, the maximum pressure that can be withstood by each microneedle is 2.1 kPa at maximum flow rate of 1 $\mu\text{l/s}$ per microneedle without any back pressure that might arise when injecting into skin. Further, a higher pressure leads to the risk of fluid leakage at the glue interface of the platform and the applicator.

5.1.3 Preliminary biological tests

5.1.3.1 Preliminary cytotoxicity tests for SU-8 microneedles

Preliminary cytotoxicity tests done on the fabricated SU-8 microneedles were deemed successful. Primary mouse embryo fibroblast cells were grown on the SU-8 microneedle array substrates by direct contact. While PLL protein has been used to promote cell adhesion, a standard polystyrene well has been used as a control. Fluorescent staining shows green colour largely indicating calcein-am stained live cells, red colour denotes dead cells while blue denotes Hoechst stain, cell nucleus. The following Figure 5.20 illustrates the essential results:

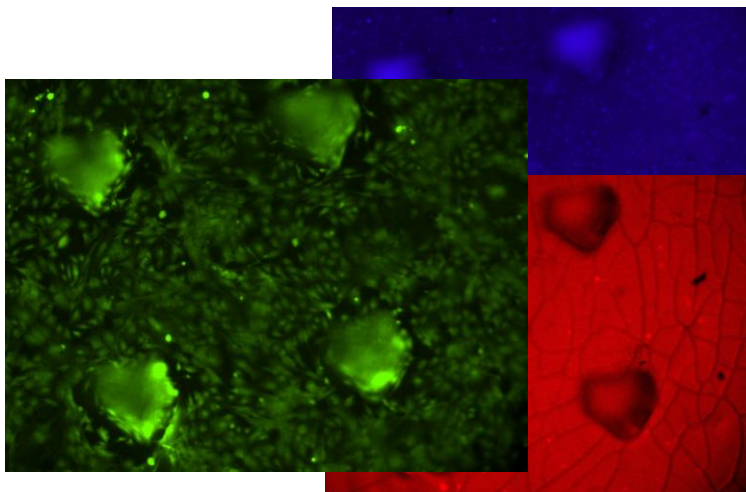


Figure 5.20: SU-8 substrate stained with PLL to promote cell adhesion on frontside. Bulk of the surface is predominantly green indicating calcein-am stained live cells.[

5.1.3.2 Preliminary finger penetration tests

Preliminary finger penetration tests were performed as shown in the Figure 5.21 and it was “felt” that the microneedles were penetrating into the stratum corneum layer of the skin. Of course, the finger penetration tests are not conclusive and further tests are required to substantiate whether the microneedles really penetrate the skin or not and if a fluid can be injected into the skin via the hollow microneedles. It is envisaged that these tests would be carried out in the near future to validate the system as fully functional. The platinum coated microneedles serve to explore another possible application of the microneedles in the realm of dry electrodes. The sputtered platinum has a thickness of 20 nm and does not alter the mechanical properties of the microneedle noticeably.

5.2 Conclusion

A quick recapitulation from design to fabrication to testing demonstrates that all the designs of microneedles were fabricated and of them, only a few have been finally selected as the best designs, in terms of ease of fabrication and

performance. A tabular comparison of the same in Table 5.1 shall reinforce this further.

The mechanical and microfluidic tests were duly performed on the fabricated microneedles. In essence, the results demonstrated were encouraging in terms of mechanical performance. Thus, the microneedle array should be able to penetrate the skin without undergoing failure. The fabricated hollow microneedles had a measured average load-bearing strength of 235 mN per needle which is sufficient for penetration into the stratum corneum. Furthermore, microfluidic tests have proven that upto 240 $\mu\text{l}/\text{min}$ can be delivered for water-like viscous fluids when injecting into air. It needs to be determined how this maximum rate shall vary while injecting the same into skin. Subsequent tests are still required for more viscous fluids as well as simultaneous testing of penetration of microneedle array and drug delivery through the penetrated microneedles.

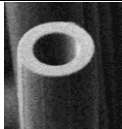


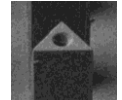
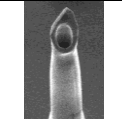
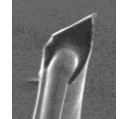
Cross-section geometry	SEM of fabricated microneedle	Computed Failure Force (in mN for $l=600 \mu\text{m}$)	Computed Failure Force (in mN for $l=1000 \mu\text{m}$)	Actual Measured Failure Force (in mN)	Remarks
HC		47	<u>17</u>	<u>15</u>	Too weak
CS		31	11	–	Too weak
HTTC		641	<u>231</u>	<u>235</u>	Good strength
HTCC		676	243	–	Process issues
HB		<u>370</u>	133	<u>355</u>	Good for 600 μm
HSB		<u>506</u>	182	<u>424</u>	Good for solid, for both heights

Table 5.1: Comparison of fabricated microneedles in terms of mechanical failure force. The three categories highlighted in **bold** signify the types selected for further work. Underlined values indicate which one of the two heights (600 μm or 1000 μm) were tested.

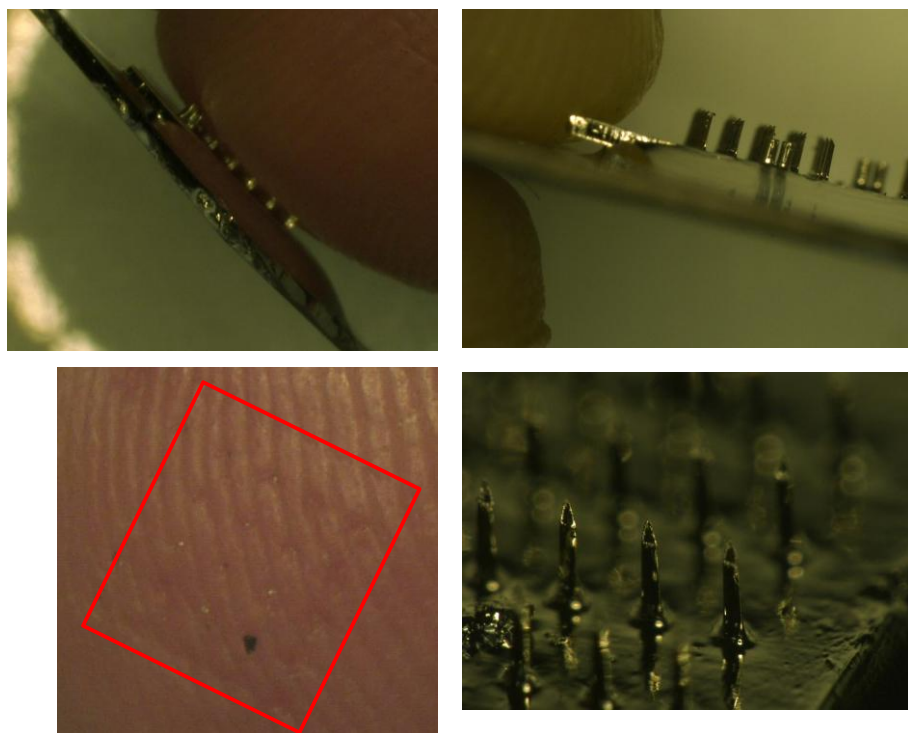


Figure 5.21: Finger tip insertion test with fabricated microneedle array. (Top-left): Finger insertion into needle tips. (Top-right, Bottom-right): Side view of platinum coated microneedles, close-up perspective view of the same microneedle array, respectively. (Bottom-left): Markings of the microneedle insertions into the skin. The dark patch signifies a slight bleeding caused by one microneedle.

6

Conclusion & Future Work

Abstract

In this ultimate chapter, inferences are drawn and the total journey starting from design to process to testing is summed up in a nutshell. The initial design objectives as listed out in Chapter 3 are compared with the fabricated results. Further work is discussed: the present state of the device is compared to what remaining work still needs to be done.

6.1 Key contributions

- Sharp-tipped, tall ($\sim 1000 \mu\text{m}$ in height) polymeric (made of SU-8 epoxy) microneedles with a hollow lumen, standing on a platform have been fabricated.
- Aspect ratios higher than 40 have been achieved. Such high aspect ratios for hollow polymeric microneedles have not yet been reported so far. Wang et al (84) achieved an aspect ratio of about 16.
- The use of an anti-reflection layer, to prevent internal cross-linking of the hollow lumen is a notable feature of the fabrication process.
- Moulding on KOH-etched Si wafers directly instead of on PDMS moulds (84) have consistently resulted in much sharper tips ($< 10 \mu\text{m}$ tip diameter) compared to $15 \mu\text{m}$ to $25 \mu\text{m}$ tip diameters reported by Wang et al at Georgia Tech (84).
- Unique cross-sectional geometries of the microneedles were designed to mimic the mosquito fascicle as far as possible.
- No sacrificial layer has been used for the release of the microneedles from the substrate.
- Mechanical compressive tests performed showed encouraging results of high microneedle failure forces averaging 235 mN with a practical usage limit set at 140 mN.
- Mechanical shear stress showed strong bonding between needle shaft and platform.
- Preliminary microfluidic tests demonstrated that the bores of the microneedles are open.
- A simple novel applicator was also developed for integration with the microneedle array for liquid infusion.
- Overall, the fabrication process developed that has been developed for producing the microneedles is quite robust and repeatable.
- The process lends significant flexibility to the design in terms of: microneedle height and other dimensions, platform thickness, cross-sectional shape, whether solid or hollow architecture, number of needles per array.

6.2 Concluding remarks

Table 5.1 gives a snapshot of most of the different basic architectures of microneedles that were designed, fabricated and tested for mechanical failure. Of these, HTTC, HB and HSB performed the best not only in mechanical failure but also with respect to ease of fabrication, clear hollow lumens and inconsistency of results. In terms of structural shape too, these three were the closest to come to the mosquito fascicle tip. HSB is the most versatile in that it can be employed both as a solid microneedle as well as a hollow one due to the unique design of the slit running through the entire microneedle shaft length. HTCC, as can be seen from the table also has a good mechanical strength but however, the fabrication process of the same leads to the hollow lumen of the needle being blocked after development most of the times. Also, due to their specific geometries, the sharpness they exhibit is also enhanced – tip diameters ranging between 4 μm and 8 μm . The measured failure force vs. computed failure forces indicates an error range of 5 to 15% less than the computed values. Given the nature of the process of fabrication, it is a considerably good fit and thus, validates the design. Thus, the three best microneedles HTTC, HB and HSB have been selected to be pursued for further work.

Tall, sharp, hollow, polymeric microneedles on a platform were designed, fabricated and characterized. It is also noteworthy to mention that the fabricated results are quite consistent with the design specifications as listed out in Section 3.2. Besides this, the microneedles were also tested successfully for their hollowness and approximate flow rates were measured. In fact, it should be noted that though polymeric microneedles with a hollow lumen, sharp tip and an integrated platform produced by a moulding technique have been reported earlier in literature (84) the aspect ratios achieved by them are much lower (around 16) while ours is greater than 40. Further, such HAR microneedles were also proven to be mechanically sufficiently strong to penetrate the skin. The monolithic nature of the whole device, that is, both microneedle and its platform being made of the same polymer, SU-8, without introduction of any other material, adds further elegance to the fabrication process. The process employed in itself is simple, repeatable, robust and is economical for scaling up to mass scale production. Also, due to the nature of the process, some of the design parameters such as the geometry of microneedles, height, wall-thickness, inner and outer diameter can be changed within certain permissible limits without having to

change the process parameters. Not just this, even the very architecture of the microneedles, that is, solid or hollow, can also be altered easily. It is this very facet lends this process a great deal of flexibility as well as versatility, and makes it unique from various other polymeric microneedle fabrication approaches.

The process hurdles during the fabrication were overcome and the challenges were met thereby fine-tuning the process parameters and making the fabrication process more robust, repeatable and high-yielding.

6.3 Future work

6.3.1 Broad issues

Still a considerable amount of work needs to be done in future in order to take the fabricated microneedle device to mass-scale production and thereon, to market. In keeping with this, an IWT (agentschap voor Innovatie door Wetenschap en Technologie) Innovation Mandate (a Flemish Government initiative) funding has been obtained in order to pursue a spin-off trajectory. In the context of the IWT-IM post-doctoral framework, following are the main broad issues that need to be addressed:

1) Development of a more automated process for vacuum oven degassing step.

A special arrangement could be conceptualized for picking up the substrate from the hotplate and placing it in a special container and inside the vacuum oven, to prevent spill-overs. Another robotic arm needs to take the substrate out from the vacuum oven after the degassing step is finished, and release the substrate from the container into which it was placed, prior to loading it in the vacuum oven chamber. At this stage, the thickness of the polymer material can be measured manually and should the thickness measured be lower than the tolerable limits, the process may be repeated one more time.

2) Automating the process to collect the dispersed microneedle array platforms from the solution.

Currently, this step is carried out manually using tweezers. This can be critical as there is high risk of a chance of mechanical damage to be inflicted upon the sharp needles. A possible approach here could lie in using a sieve-like material to first filter out the developer solution and then using a special pair of tweezers to individually pick up the needle platforms and place it under a steady though slow stream of nitrogen air, for drying. It is also important to consider that it should be simple to pick up the individual platforms and place them down on the surface to be dried with the platforms at the bottom and the needle tips on top (so just as normal needles standing on the base platform). Otherwise, if the needle tips are in contact with the surface instead, due to high surface tension, the tips shall stick to the surface and any force exerted to remove the tips from the surface, shall only damage the tips. Also, another approach could be that the individual platforms are connected to each other by breakable arms which would ensure that all platforms be collected together as one entity.

3) Developing an applicator technology facilitating quick snap-n-fit eliminating the tedious glue and bonding technique.

The applicator technology comes in use when the microneedle array is to be used more like a replacement for the hypodermic needles. When this is the case, the drug needs to be injected through the microneedles and for this purpose, an applicator is required. Though a rudimentary applicator has been developed for our microneedle array platform, much is still left to be desired with respect to improving the “feel” and “ergonomics” of the system. Ideal approach to this problem would be to conceptualize a snap-fit system whereby the needle array platform snugly fits into the applicator top with minimal effort. Of course, for this also the platform design itself of the microneedle needs to be tweaked so as to accommodate a snap-fit kind of mechanism. Plus, given the brittle nature of SU-8 polymer, it is yet to be seen if such a snap-n-fit mode can be handled by the polymer material itself. If not, how best the applicator technology can be improved to ensure a smooth and hassle-free bonding process, of course, ensuring at the same time that leaks don't occur in the glue. Leaks occurring in the glue are absolutely detrimental to the

functioning of the entire system as then the fluid (drug) would just find the path of least resistance (in this case, the leak itself) and flow out through the leak, rendering the microneedles completely redundant! Thus, it is vital that no leaks exist after bonding, and one way to ensure this (as also previously mentioned), is to increase the dead area of the platform itself, so that the glue has more surface area to act on, also in turn preventing the glue from flowing down below the platform and inadvertently sealing the backside openings of the platform.

4) Biological skin puncturing testing

Once the 2x2 or 4 numbers of needles are on a platform, with sufficient mechanical testing done successfully, biological skin puncturing is the next logical step. The number of needles per array need to be reduced in order to require a lower insertion force for puncturing the skin, due to the afore mentioned fakir-bed effect (see Fig. 8). In this direction, porcine skin should be prepared according to standard testing protocols and the needle array mounted on the applicator should be inserted into the skin, and a coloured liquid injected. Once the needles are retracted from the skin surface, the region of the skin should be observed closely under a microscope to check if the fluid has really passed into the skin or not. Also the microneedles after being retracted need to be studied to see if they are still intact or not, or if they have suffered any mechanical damage. The same approach needs to be followed for the human cadaver skin. For live human skin, special permissions will need to be taken from the UZ Gaasthuisberg or perhaps this will come at a much later stage after medical regulatory bodies have approved of the product.

5) Microfluidic testing

Once skin puncturing has been proven, the next stage is microfluidic testing (or it could also be undertaken earlier than skin puncturing). Here, not just the basic passage of fluid through the microneedles would be tested but also flow rates ranging from 5 $\mu\text{l}/\text{min}$ to 500 $\mu\text{l}/\text{min}$ would be experimented with. Precisely speaking, both the upper and lower limits of the flow rates would be experimentally determined within reasonable ranges of pressure, as can be exerted by a normal human

hand. These experimentally obtained values shall be compared with those determined analytically and a comparison drawn. Currently, basic microfluidic testing has been done to test passage of fluid through needle array.

Another very vital area of testing is using fluids of different viscosities, and the pressure required to be exerted to pump the same, and the flow rates thus obtained. Again here, an upper and lower practical limit based on experiments, should be fixed on the viscosities. Same should be repeated using suspensions, and checking if the same flow rates (as with non suspensions) and pressures are achievable as the flow profile of the liquid could possibly change from laminar to non-laminar when the nature of the fluid changes.

6) Time dosage profile of drug infused into the skin to be studied and graphs plotted.

When the microneedle array is to be applied as patch on the skin – it can come in two forms: a) solid coated microneedles and b) hollow pre-filled microneedles with a drug reservoir (if required, depending on the volume of the drug to be delivered). In the former case, a drug coating requires an entirely new medication in turn requiring an entire set of completely new regulatory approvals which are quite long drawn. Comparatively, hollow pre-filled microneedles on patch are more attractive (of course, provided it is demonstrated that no reaction occurs between the structural material of the microneedle and the active drug component) for a long-term based drug delivery typically requiring a very long time dosage profile. Two drugs, say, fentanyl and nicotine could be used to check for infusion inside porcine or cadaver skin over a period of few hours and the results noted. This would give a clearer picture of the rate of infusion of the drug into the skin from the microneedle, and a time dosage profile could be obtained for these two drugs as well.

7) Complete mechanism to be developed for sterilizing and pre-filling a microneedle-patch (including drug reservoir system) with a drug (typically a large molecule drug such as a protein drug/vaccine) such that the patch can deliver the drug for long duration ranging from a few hours to a few days (under a week).

Firstly, a drug reservoir system needs to be conceptualized and integrated into the design of the microneedle array. Several approaches could be followed here: one, an external chamber is placed underneath the platform array or two, no external chamber but microneedle itself could be used as the drug reservoir. But before the drug is filled, the hollow microneedle array has to be sterilized. The process of sterilization shall be tested with heat (boiling water at 100°C), ultraviolet (UV) radiation as well as gamma radiation. For each of the above methods of sterilization it needs to be observed if the needle structural material displays any sign of a physical or chemical reaction in response. If this is successful, then a method needs to be conceptualized to fill in the drug in the needle. One such idea is to “dip fill” the needles by simply dipping the sterilized needles into a bath of the drug under stringent conditions, and the needles drawing up the drug by capillary force. Alternate designs of the needle structure itself could be incorporated to facilitate such a kind of capillary force. Once the drug (either a large molecule protein or a vaccine) is pre-filled in the needle, the microneedle array shall be inserted into cadaver or porcine skin and the time dosage profile of the drug will need to be studied and monitored over the next few days. It needs to be studied that in case if this kind or a similar pre-filled arrangement, does the drug actually enter the stratum corneum even without the use of any external pumping force? If so, how long would it take to diffuse out into the surrounding of the needle array and finally how long would it take to enter the blood flow.

An ideal vision for the complete final device is as illustrated in

8) Investigate and explore the choice of target drugs: vaccines, biologics or others which may be used in conjunction with the needle array system.

As mentioned right at the outset, large molecule drugs are the biggest motivation to switch from conventional drug delivery systems to a microneedle-based transdermal drug delivery system. Thus, biologics or protein drugs fall under this category. It is a vital objective to be able to identify at least one single large molecule of interest which can be combined with the microneedle-on-patch based system. The choice of this drug will depend on existence of present alternative modes of delivery for the same in market today, as well as the business potential for the health condition that is being treated by the particular drug.

Vaccines, on the other hand, are also a very interesting drug class to be combined in usage with the microneedle array system primarily because

of rich concentration of immune cells present in the intradermal layer which can initiate a much more efficient immunological response compared to when the vaccine is injected by intra-venous or intra-muscular route.

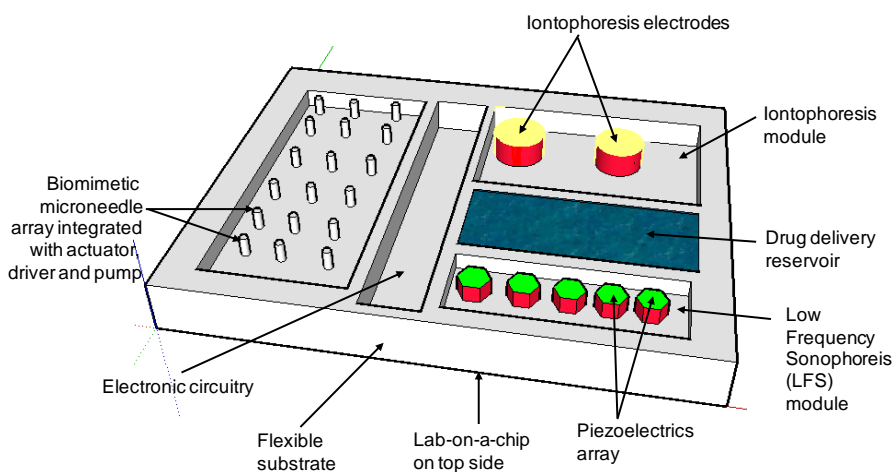


Figure 6.1: A future vision for the final device culminating from this work: a closed-loop comprehensive transdermal drug delivery and blood extraction (using microneedles) system. The LFS and iontophoresis modules complement the microneedles in drug delivery and simple enhance the efficiency of the device.

Appendix I: List of Abbreviations

GI – Gastro-intestinal
LFS – Low Frequency Sonophoresis
TDD – Transdermal Drug Delivery
IV – Intravenous
IM – Intra-muscular
SC – Sub-cutaneous
MN – microneedles
RF – Radio frequency
UK – United Kingdom
PMMA – Polymethylmethacrylate
LIGA – Lithography, Electroplating and Moulding
UV – Ultra-violet
PDMS - Polydimethylsiloxane
SEM – Scanning electron micrograph
CMC – Carboxy-methyl cellulose
PLGA – Poly-lacto-gycolic acid
PU – Poly-urethane
MEMS – Microelectromechanical Systems
FDA – Food and Drug Agency
US – United States of America
DRIE – Deep Reactive Ion Etching
ICP – Inductive coupled plasma
DNA – Deoxyribonucleic acid
RNA – Ribonucleic acid
EPO - erythropoietin
PTH – Parathyroid Hormone
3-D – Three-dimensional

PGMEA – Poly glycol methyl ether acetate
HAR – High Aspect Ratio
FIB – Focussed Ion Beam
RIE – Reactive ion etching
CG – centre of gravity
dia. – diameter
tri. – triangle
circ. – circle or circular
ht. - height
rect. – rectangle
CS – cross-section
SC – solid-circular
HC – hollow-circular
CS – C-shaped
HTTC – hollow triangular with triangular cross-section
HTCC – hollow triangular with circular cross-section
HB – hollow-bevel
HBS – hollow bevel with slit
USP – United States Pharmacopeia
approx. – approximately
w.r.t. – with respect to
eg. – example

Appendix II: List of Symbols

1 μm = 1 micron = 1 micrometer = 1×10^{-6} m

kg = kilogram = 1×10^3 kilogram

Da = Dalton

GPa = Gigapascals = $\times 10^9$ Pa

MPa = Megapascal = $\times 10^6$ Pa

Al = Aluminium

Si = Silicon

SiO₂ = Silicon dioxide

KOH = Potassium hydroxide

Cr = Chromium

Cu = Copper

nm = nanometer = $\times 10^{-9}$ m

Hz – Hertz

Appendix III: List of Publications

Journal Publications.

- **B. P. Chaudhri**, F. Ceyskens, P. de Moor, C. Van Hoof, R. Puers, "A high aspect ratio SU-8 fabrication technique for hollow microneedles for transdermal drug delivery and blood extraction," *Journal of Micromechanics and Microengineering*, Vol. 20, June 2010.
- **B. Paul Chaudhuri**, B. Thubtimthong, F. A. Chollet, "*Development of fabrication process and electrostatic actuator for a mechanically tunable 2-D photonic crystal*", *Advanced Materials Research*, Vol. 31 (online at <http://www.scientific.net/0-87849-471-5/179/>) (2007) 179-181.

Conference Proceedings

- **B. Paul Chaudhuri**, F. Ceyskens, H. Neves Pereira, K. Vanstreels, M. Gonzalez, A. La Manna, C. Van Hoof, R. Puers, "*Design and Characterization of a Monolithic System: Polymer Microneedle on a Polymer Platform*," *Microneedles conf.*, May 2012, Cork, IR.
- **B. P. Chaudhri**, F. Ceyskens, H. Neves Pereira, T. Guan, A. La Manna, C. Van Hoof, R. Puers, "*High strength polymer microneedles for transdermal drug delivery*," *Euroensors XXV conf.*, Sept. 2011, Athens, GR
- **B. P. Chaudhri**, F. Ceyskens, H. Neves Pereira, A. La Manna, C. Van Hoof, R. Puers, "*Out-of-plane, high strength, polymer microneedles for transdermal drug delivery*," *IEEE Engineering in Medicine and Biology Conference (EMBC)*, Aug. 2011, Boston, US.
- **B. P. Chaudhri**, F. Ceyskens, P. de Moor, C. Van Hoof, R. Puers, "*Low cost bevel-shaped, sharp tipped, hollow polymer-based microneedles for transdermal drug delivery*," *Micromechanics Europe (MME) conf.*, Sept.

2010, Enschede, NL.

- **B. P. Chaudhri**, F. Ceysens, P. de Moor, C. Van Hoof, R. Puers, "*Low-cost, polymer-based, high aspect ratio, hollow microneedles for transdermal drug delivery and blood extraction,*" Micromechanics Europe (MME) conf., Sept. 2009, Toulouse, FR (***Won Best Poster Award***)

Appendix IV: Curriculum Vitae

BUDDHADEV PAUL CHAUDHURI

Tervuursevest23/1101, Heverlee 3001, BE • Mob: +32488604346 • buddhadevpc@gmail.com

PROFILE

Currently final-phase PhD student at MICAS, ESAT, Department of Electrical Engineering, KU Leuven, and IMEC, Belgium, undertaking research in transdermal drug delivery using polymer-based microsystems.

WORK HISTORY

Research Scientist

Philips Research N.V.

Eindhoven, Holland
June 2012 to Oct 2012

Worked on Thin-Film Process Design for neuroprobe fabrication.

Research Assistant

Indian Institute of Science (IISc)

Bangalore, India
Aug 2005 to Dec 2005

Worked on the design and simulation of a wide range of micromirrors for optical fiber communications.

EDUCATION

IMEC / KU Leuven

Ph.D. (ongoing)

Leuven, Belgium
June 2008 to Present

Working on developing biomedical microsystems for transdermal drug delivery. The aim is to develop a low cost integrated microdevice (comprising microneedles) on a flexible patch which can be laid atop the human skin, while it delivers drugs inside the skin, painlessly. Experienced with hands-on fabrication of polymer microneedles using semiconductor processing principles.

- Ph.D. Research Topic: Miniaturized painless transdermal drug delivery system using polymer microneedles

Expected Date of Graduation: December 2012

- *Conceptualized and guided Masters students' coursework project*: Design of a miniaturized wearable perfume dispenser

Nanyang Technological University (NTU)

Dual Master of Science in Microsystems Engineering

Singapore
Jul 2006 to Dec 2006

APPENDIX IV: CURRICULUM VITAE

Pursued a Dual Masters of Science program in Microsystems (MEMS) Engineering from ESIEE, Paris and Nanyang Technological University (NTU), Singapore. It was a total one year program split between ESIEE's Paris campus and NTU's Singapore campus. First part of the program was held in Paris and the second part was in Singapore.

Effectively graduated in April 2007 with *Distinction*.

- Masters Thesis Project: Design and fabrication of tunable photonic crystals using SU-8 polymer

Ecole Supérieure d'Ingenieurs en Electronique et Electrotechnique (ESIEE)

Paris, France
Jan 2006 to Jun 2006

Dual Master of Science in Microsystems Engineering

- Project: A novel design for a miniaturized Solid Oxide Fuel Cell (SOFC) for operating at room temperatures

Vellore Institute of Technology University (VIT)

Vellore, India
Sep 2001 to Jun 2005

Bachelor of Technology, Electronics & Communication Engineering

Graduated with a *first-class distinction*.

Bachelors Thesis Project: Design, Simulation and Analysis of 2x2 micromirror arrays for application in optical communication networks || Carried out at Indian Institute of Science (IISc), Bangalore, India.

Bishop Cotton Boys' School

Bangalore, India
Jun 1997 to Apr 2001

High School: Grades 9, 10, 11, 12

Passed the Grade 10 board examination, Indian Certificate For Secondary Education (ICSE) in 1999.

Passed the Grade 12 board examination, Indian School Certificate Examination (ISC) in 2001, with subjects Mathematics, Physics, Chemistry, Electronics and English.

SOFTWARE/SYSTEM SKILLS

- C, C++, ANSYS, MATLAB
- CoventorWare
- Intellisuite
- MS Office

ACADEMIC AWARDS

- Won the Best Poster Award at the Micromechanics Europe (MME) 2009, in Toulouse, France.
- Awarded the First General Proficiency prize every consecutive year in school from Kindergarten to Grade 11 (12 consecutive years in two different schools in two cities), India.

EXTRACURRICULAR ACTIVITIES & INTERESTS

- First Social Chair of newly-founded PhD Society Leuven (2010-2011) – organized various events for PhD students of KUL: dinners, cooking workshops, movie nights, Latino dance workshop, social weekly drinks, summer barbeque, canal cruise, joint social event with PhD Academy of Maastricht.
- Participated and qualified up to second round in Cleantech Business Challenge at Leuven (2012).
- Participated and qualified up to second round in Business Plan Competition at NTU, Singapore (2006).
- Founding member of Debate and Dramatics club in VIT University (2002-2003).
- Member of Editorial Committee of "Cottonian" magazine in High School (1999-2000).
- Poetry, latino dancing, debates, cooking
- Horse-riding, swimming, golf, chess

PROFESSIONAL MEMBERSHIPS

- Institute of Electrical and Electronics Engineers (IEEE)
- IEEE - Engineering in Medicine and Biology Society (EMBS)

Bibliography

1. **F. Bath-Hextall.** *School of Nursing, Midwifery and Physiotherapy, University of Nottingham.* [Online] <http://www.nottingham.ac.uk/nursing/sonet/rlos/bioproc/metabolism/01.html>
2. **R. Nassiri - Medical Mission Trip, Dominican Republic.** Introduction to Pharmacology . *Michigan State University.* [Online] <https://www.msu.edu/~iih/docs/introtopharmacology.pdf>.
3. *First-pass metabolism of peptide drugs in rat perfused liver.* **Taki Y, Sakane T, Nadai T, Sezaki H, Amidon GL, Langguth P, Yamashita S.** 9, Sep 1998, *J Pharm Pharmacol.*, Vol. 50, pp. 1013-8.
4. *Transdermal drug delivery.* **M. Prausnitz, R. Langer.** 11, November 2008, *Nat Biotechnol.*, Vol. 26, pp. 1261–1268. doi: 10.1038/nbt.1504.
5. *Immunization without Needles.* **S. Mitragotri.** December 2005, *Nature Reviews Immunology*, Vol. 5, pp. 905-916. doi:10.1038/nri1728.
6. *Cutaneous and transdermal delivery: Processes and systems of delivery.* **G.L. Flynn.** s.l. : Banker, G.S & Rhodes, C.T, eds. New York, NY: Marcel Dekker, 1996, *Modern Pharmaceutics*, pp. 239-299.
7. *Modulation of the barrier function of the skin.* **J. Hadgraft.** 1, 2001, *Skin Pharmacol Appl Skin Physiol.* , Vol. 14, pp. 72-81.
8. **J.A. McGrath, R.A. Eady, F.M. Pope.** *Rook's Textbook of Dermatology.* 7. s.l. : Blackwell Publishing. pp. 3.1–3.6. ISBN 978-0-632-06429-8.
9. **G.J. Marks, J. Miller.** *Lookingbill and Marks' Principles of Dermatology.* 4. s.l. : Elsevier Inc., 2006. pp. 8–9. ISBN 1-4160-3185-5.
10. **O.H. Petersen.** *Lecture Notes: Human Physiology.* s.l. : Blackwell Publishing, 2009.
11. *Dendritic type accessory cells within the mammalian thymic microenvironment. Antigen presentation in the dendritic neuro-endocrine-immune cellular network.* . **B. Bodey, B. Bodey Jr., H.E. Kaiser.** 11, 1997, *In Vivo*, pp. 351-370.
12. *Micro-scale devices for transdermal drug delivery.* **A. Arora, M.R. Prausnitz, S. Mitragotri.** 2, s.l. : ScienceDirect, 8 December 2008,

- International Journal of Pharmaceutics, Vol. 364, pp. 227-236. <http://dx.doi.org/10.1016/j.ijpharm.2008.08.032>.
13. —. **S. Mitragotri et al.** 2008, International Journal of Pharmaceutics, Vol. 364, pp. 227-236.
14. *Keynote: Evaluation of microneedles in human subjects.* **M. Prausnitz.** Cork, IE : s.n., 2012. Microneedles.
15. *Microneedles for drug and vaccine delivery.* **Y.-C. Kim, et al.** 2012, Adv. Drug Deliv. Rev., Vol. (In press). doi:10.1016/j.addr.2012.04.005.
16. *Microfabricated needles for transdermal delivery of macromolecules and nanoparticles: Fabrication methods and transport studies.* **D.V. McAllister, P.M. Wang, S.P. Davis, J-H Park, P.J. Canatella, M.G. Allen, M.R. Prausnitz.** 24, 25 November 2003, Proceedings of the National Academy of Sciences (PNAS), Vol. 100, pp. 13755–13760.
17. **SensiVida Medical Technologies.** [Online] <http://www.sensividamedical.com/technology>.
18. *Fabrication of microneedles.* **Y.T. Chen, C.C. Hsu, C.H. Tsai, S.W. Kang.** 2010, J. Mar. Sci. Technol. , Vol. 18, pp. 243–248.
19. *Process optimization and characterization of silicon microneedles fabricated by wet etch technology.* **N. Wilke, A. Mulcahy, S.R. Ye, A. Morrissey.** 2005, Microelectron. J., Vol. 36, pp. 650–656.
20. *Evaluation needle length and density of microneedle arrays in the pretreatment of skin for transdermal drug delivery.* **G. Yan, K.S. Warner, J. Zhang, S. Sharma, B.K. Gale.** 2010, Int. J. Pharm., Vol. 391, pp. 7–12.
21. *Microfabricated silicon microneedle array for transdermal drug delivery.* **J. Ji, F.E.H. Tay, J.M. Miao, C. Iliescu.** Bristol : IOP Publishing Ltd., 2006, International MEMS Conference, pp. 1127–1131.
22. *Silicon Microneedles for Painless Percutaneous Penetration.* **C. O'Mahony, A. Blake: J. Scully, J. O'Brien, A.C. Moore.** La Grande Motte, France : s.n., 2010. Proc. Perspectives in Percutaneous Penetration. Vol. 12, p. 66.
23. *Microfabricated Silicon Microneedle Array for Transdermal Drug Delivery.* **J. Ji, F.E.H Tay, M. Jianmin, C. Iliescu.** 2006, Journal of Physics: Conference Series (International MEMS Conference 2006), Vol. 34, pp. 1127-1131.
24. **S. Chakraborty, K. Tsuchiya.** 2008, J. Appl. Phys., Vol. 103, pp. 114701-9. <http://dx.doi.org/10.1063/1.2936856>.
25. *Fabrication and characterization of flexible neural microprobes with improved structural design.* **A.A. Fomani, R.R. Mansour.** 2011, Sens. Actuators A Phys., Vol. 168, pp. 233–241.

26. *An electrically active microneedle array for electroporation.* **S.O. Choi, Y.C. Kim, J.H. Park, J. Hutcheson, H.S. Gill, Y.K. Yoon, M.R. Prausnitz, M.G. Allen.** *Biomed. Microdevices* : s.n., 2010, Vol. 12 , pp. 263–273.
27. *Industrial applications of laser micromachining.* **M.C. Gower.** 2000, *Opt. Express*, Vol. 7, pp. 56–67.
28. *Macroflux (R) microprojection array patch technology: a new and efficient approach for intracutaneous immunization.* **J.A. Matriano, M. Cormier, J. Johnson, W.A. Young, M. Buttery, K. Nyam, P.E. Daddona.** 2002, *Pharm. Res.*, Vol. 19, pp. 63-70.
29. *A novel fabrication process for out-of-plane microneedle sheets of biocompatible polymer.* **M. Han, D.H. Hyun, H.H. Park, S.S. Lee, C.H. Kim, C. Kim.** 2007, *J. Micromech. Microeng.*, Vol. 17 , pp. 1184–1191.
30. *A novel fabrication method of a microneedle array using inclined deep X-ray exposure.* **S.J. Moon, S.S. Lee.** 2005, *J. Micromech. Microeng.* , Vol. 15, pp. 903–911.
31. *Tapered conical polymer microneedles fabricated using an integrated lens technique for transdermal drug delivery.* **J.H. Park, Y.K. Yoon, S.O. Choi, M.R. Prausnitz, M.G. Allen.** 2007, *IEEE Trans. Biomed. Eng.*, Vol. 54, pp. 903–913.
32. *Microfabricated microneedles: a novel method to increase transdermal drug delivery.* **S. Henry, D. McAllister, M.G. Allen, M.R. Prausnitz.** 1998, *J. Pharm. Sci.*, Vol. 87, pp. 922–925.
33. *Determination of parameters for successful spray coating of silicon microneedle arrays .* **M.G. McGrath, A. Vrdoljak, C. O'Mahony, J.C. Oliveira, A.C. Moore, A.M. Crean.** 2011, *Int. J. Pharm.*, Vol. 415 , pp. 140–149.
34. *Chronic intracortical microstimulation of cat auditory cortex using a 100 penetrating electrode array.* **P.J. Rousche, R.A. Normann.** 1997, *J. Physiol.*, Vol. 499, pp. 87–88.
35. *Microfabricated polysilicon microneedles for minimally invasive biomedical devices.* **J.D. Zahn, N.H. Talbot, D. Liepmann, A.P. Pisano.** 2, 2000, *Biomed. Microdevices*, pp. 295–303.
36. *Effect of applying modes of the polymer microneedle-roller on the permeation of L-ascorbic acid in rats.* **S.K. You, Y.W. Noh, H.H. Park, M. Han, S.S. Lee, S.C. Shin, C.W. Cho.** 18 , 2010, *J. Drug Target*, pp. 15–20.
37. *Multidirectional UV lithography for complex 3-D MEMS structures.* **Y.K. Yoon, J.H. Park, M.G. Allen.** 2006, *J. Microelectromech. Syst.*, Vol. 15, pp. 1121–1130.

38. *Two photon polymerization of polymer–ceramic hybrid materials for transdermal drug delivery.* **A. Ovsianikov, B. Chichkov, P. Mente, N.A. Monteiro-Riviere, A. Doraiswamy, R.J. Narayan.** 2007, *Int. J. Appl. Ceram. Tec.*, Vol. 4, pp. 22–29.
39. *Metal microneedle fabrication using twisted light with spin.* **T. Omatsu, K. Chujo, K. Miyamoto, M. Okida, K. Nakamura, N. Aoki, R. Morita.** 2010, *Opt. Express*, Vol. 18, pp. 17967–17973.
40. *Fabrication of microneedle array using LIGA and hot embossing process.* **S.J. Moon, S.S. Lee, H.S. Lee, T.H. Kwon.** 2005, *Microsyst. Technol.*, Vol. 11, pp. 311–318.
41. *A microneedle roller for transdermal drug delivery.* **J.H. Park, S.O. Choi, S. Seo, Y.B. Choy, M.R. Prausnitz.** 2010, *Eur. J. Pharm. Biopharm.*, Vol. 76, pp. 282–289.
42. *Micromolding for ceramic microneedle arrays.* **S. Bystrova, R. Luttge.** 2011, *Microelectronic Engineering*, Vol. 88, pp. 1681–1684. doi:10.1016/j.mee.2010.12.067.
43. **R.J. Stokes, D.F. Evans, M. Errico.** *Liquid Coating Processes.* s.l. : Wiley-VCH.
44. *Coated microneedles for transdermal delivery.* **H.S. Gill, M.R. Prausnitz.** 2007, *J. Control Release*, Vol. 117, pp. 227–237.
45. *Parathyroid hormone PTH(1–34) formulation that enables uniform coating on a novel transdermal microprojection delivery system.* **M. Ameri, S.C. Fan, Y.-F. Maa.** 2010, *Pharm. Res.*, Vol. 27, pp. 303–313.
46. *Formulation and coating of microneedles with inactivated influenza virus to improve vaccine stability and immunogenicity.* **Y.C. Kim, F.S. Quan, R.W. Compans, S.M. Kang, M.R. Prausnitz.** 2010, *J. Control. Release*, Vol. 142, pp. 187–195.
47. *Coating formulations for microneedles.* **H.S. Gill, M.R. Prausnitz.** 2007, *Pharm. Res.*, Vol. 24, pp. 1369–1380.
48. *Poly[di(carboxylatophenoxy)phosphazene]is a potent adjuvant for intradermal immunization.* **A.K. Andrianov, D.P. DeCollibus, H.A. Gillis, H.H. Kha, A. Marin, M.R. Prausnitz, L.A. Babiuk, H. Townsend, G. Mutwiri.** 2009, *Proc. Natl. Acad. Sci. USA*, Vol. 106, pp. 18936–18941.
49. *Formulation of microneedles coated with influenza virus-like particle vaccine.* **Y.C. Kim, F.S. Quan, R.W. Compans, S.M. Kang, M.R. Prausnitz.,** 2010, *AAPS PharmSciTech*, Vol. 11, pp. 1193–1201.
50. *Enhanced memory responses to seasonal H1N1 influenza vaccination of the skin with the use of vaccine-coated microneedles.* **Y.C. Kim, F.S. Quan, D.G. Yoo, R.W. Compans, S.M. Kang, M.R. Prausnitz.** 2010, *Journal of Infectious Diseases*, Vol. 201, pp. 190–198.

51. *Improvement in antigen-delivery using fabrication of a grooves-embedded microneedle array.* **M. Han, D.K. Kim, S.H. Kang, H.R. Yoon, B.Y. Kim, S.S. Lee, K.D. Kim, H.G. Lee.** 2009, *Sens. Actuators B Chem.*, Vol. 137, pp. 274–280.
52. *Dissolving microneedles for transdermal drug delivery.* **J.W. Lee, J.H. Park, M.R. Prausnitz.** 2008, *Biomaterials*, Vol. 29, pp. 2113–2124.
53. *Sustained-release self-dissolving micropiles for percutaneous absorption of insulin in mice.* **Y. Ito, E. Hagiwara, A. Saeki, N. Sugioka, K. Takada.** 2007, *J. Drug Target.*, Vol. 15, pp. 323–326.
54. *Evaluation of self-dissolving needles containing low molecular weight heparin (LMWH) in rats.* **Y. Ito, A. Murakami, T. Maeda, N. Sugioka, K. Takada.** 2008, *Int. J. Pharm.*, Vol. 349, pp. 124–129.
55. *Minimally invasive protein delivery with rapidly dissolving polymer microneedles.* **S.P. Sullivan, N. Murthy, M.R. Prausnitz.** 2008, *Adv. Mater.*, Vol. 20, pp. 933–938.
56. *Fabrication of dissolving polymer microneedles for controlled drug encapsulation and delivery: bubble and pedestal microneedle designs.* **L.Y. Chu, S.O. Choi, M.R. Prausnitz.** 2010, *J. Pharm. Sci.*, Vol. 99, pp. 4228–4238.
57. *Biodegradable polymer microneedles: fabrication, mechanics and transdermal drug delivery.* **J.H. Park, M.G. Allen, M.R. Prausnitz.** 2005, *J. Control. Release*, Vol. 104, pp. 51–66.
58. *Rapidly dissolving fibroin microneedles for transdermal drug delivery.* **X. You, J.-h. Chang, B.-K. Ju, J.J. Pak.** 2011, *Mat. Sci. Eng. C.*, Vol. 31, pp. 1632–1636.
59. *Low temperature fabrication of biodegradable sugar glass microneedles for transdermal drug delivery applications.* **C.J. Martin, C.J. Allender, K.R. Brain, A. Morrissey, J.C. Birchall.** 2012, *J. Control. Release*, Vol. 158, pp. 93–101.
60. *Two-layered dissolving microneedles for percutaneous delivery of peptide/protein drugs in rats.* **K. Fukushima, A. Ise, H. Morita, R. Hasegawa, Y. Ito, N. Sugioka, K. Takada.** 2011, *Pharm. Res.*, Vol. 28, pp. 7–21.
61. *Feasibility of microneedles for percutaneous absorption of insulin.* **Y. Ito, E. Hagiwara, A. Saeki, N. Sugioka, K. Takada.** 2006, *Eur. J. Pharm. Sci.*, Vol. 29, pp. 82–88.
62. *Self-dissolving microneedles for the percutaneous absorption of EPO in mice.* **Y. Ito, J.I. Yoshimitsu, K. Shiroyama, N. Sugioka, K. Takada.** 2006, *J. Drug Target.*, Vol. 14, pp. 255–261.

63. *Hydrogel swelling as a trigger to release biodegradable*. **M. Kim, B. Jung, J.-H. Park**. 2012, *Biomaterials*, Vol. 33, pp. 668–678.
64. *Polymer microneedles for controlled release drug delivery*. **J.H. Park, M.G. Allen, M.R. Prausnitz**. 2006, *Pharm. Res.*, Vol. 23, pp. 1008–1019.
65. *Improved DNA vaccination by skin-targeted delivery using dry-coated densely-packed microprojection arrays*. **X.F. Chen, A.S. Kask, M.L. Crichton, C. McNeilly, S. Yukiko, L.C. Dong, J.O. Marshak, C. Jarrahan, G.J.P. Fernando, D.X. Chen, D.M. Koelle, M.A.F. Kendall**. 2010, *Journal of Controlled Release*, Vol. 148, pp. 327–333.
66. *Polymer particle-based micromolding to fabricate novel microstructures*. **J.H. Park, S.O. Choi, R. Kamath, Y.K. Yoon, M.G. Allen, M.R. Prausnitz**. 2007, *Biomed. Microdevices*, Vol. 9, pp. 223–234.
67. *Nickel microneedles fabricated by sequential copper and nickel electroless plating and copper chemical wet etching*. **P.G. Jung, T.W. Lee, D.J. Oh, S.J. Hwang, I.D. Jung, S.M. Lee, J.S. Ko**. 2008, *Sens. Mater.*, Vol. 20, pp. 45–53.
68. *Permeation enhancement of ascorbic acid by self-dissolving micropile array tip through rat skin*. **Y. Ito, T. Maeda, K. Fukushima, N. Sugioka, K. Takada**. 2010, *Chem. Pharm. Bull.*, Vol. 58, pp. 458–463.
69. *Separable arrowhead microneedles*. **L.Y. Chu, M.R. Prausnitz**. 2011, *J. Control. Release*, Vol. 149, pp. 242–249.
70. *Fluid injection through out-of-plane microneedles*. **B. Stoeber, D. Liepmann**. 2000. Proceedings of the International IEEE-EMBS: Special Topic Conference on Microtechnologies in Medicine and Biology. Vol. No. 34.
71. *Review of Patents on Microneedle Applicators*. **T.R.R. Singh, N.J. Dunne, E. Cunningham, R.F. Donnelly**. 1, s.l.: Bentham Science Publishers, January 2011, *Recent Patents on Drug Delivery & Formulation*, Vol. 5, pp. 11–23.
72. **K.V.I.S. Kaler, G. Gattiker, M. P. Mintchev**. *Fluid Sampling Analysis and Delivery System*. US 2005/0228313 US, 13 Oct 2005. A1.
73. *Development and fluidic simulation of microneedles for painless pathological interfacing with living systems*. **S. Chakraborty, K. Tsuchiya**. 2008, *J. Appl. Phys.*, Vol. 103, p. 114701. DOI:10.1063/1.2936856.
74. *Penetration-enhanced Ultra-sharp Microneedles and Prediction on Skin Interaction for Efficient Transdermal Drug Delivery*. **N. Roxhed, T.C. Gasser, P. Griss, G.A. Holzapfel, G. Stemme**. s.l.: IEEE, 2007, *Journal of Microelectromechanical Systems*, Vol. 16, pp. 1429–1440.
75. *Silicon micromachined hollow microneedles for transdermal liquid transport*. **H. Gardeniers, R. Luttge, E. Berenschot, M. de Boer, S.**

- Yeshurun, M. Hefetz, R. van't Oever, A. van den Berg.** 6, 2003, IEEE ASME J. Microelectromech. Syst., Vol. 12, pp. 855-862.
76. *Hollow metal microneedles for insulin delivery to diabetic rats.* **S.P. Davis, W. Martanto, M.G. Allen, M.R. Prausnitz.** 5, 2005, IEEE Trans. Biomed Eng., Vol. 52, pp. 909-915.
77. *A PZT insulin pump integrated with a silicon microneedle array for transdermal drug delivery.* **B. Ma, S. Liu, Z. Gan, G. Liu, X. Cai, H. Zhang, Z. Yang.** 2006, Microfluid. Nanofluid., Vol. 2, pp. 417-423.
78. *Sharp beveled tip hollow microneedle arrays fabricated by LIGA and 3D soft lithography with polyvinyl alcohol.* **F. Perennes, B. Marmioli, M. Matteucci, M. Tormen, L. Vaccari, E. Di Fabrizio.** 2006, J. Micromech. Microeng. 16 (2006) 473-479., Vol. 16, pp. 473-479.
79. *Three-dimensional hollow microneedles and microtube arrays.* **D.V. McAllister, F. Cros, S.P. Davis, L.M. Matta, M.R. Prausnitz, M.G. Allen.** Sendai, Japan : s.n., 1999. Transducers' '99. The 10th Intl. Conf. on Solid-state Sensors and Actuators. pp. 1098-1101.
80. *Polymolding: two wafer polysilicon micromolding of closed-flow passages for microneedles and microfluidic devices.* **N.H. Talbot, A.P. Pisano.** Hilton Head Island, SC, USA : s.n., 1998. Technical Digest. Solid-State Sensor and Actuator Workshop. pp. 265-268.
81. *Fabrication of microneedle for a trace blood test.* **K. Oka, S. Aoyagi, Y. Arai, Y. Isono, G. Hashiguchi, H. Fujita.** 2002, Sensors and Actuators A, Vols. 97-98, pp. 478-485.
82. *Precise microinjection into skin using hollow microneedles.* **P.M. Wang, M. Cornwell, J. Hill, M.R. Prausnitz.** 2006, J. Invest. Dermatol., Vol. 126, pp. 1080-1087.
83. *Evaluation of the clinical performance of a new intradermal vaccine administration technique and associated delivery system.* **P.E. Laurent, S. Bonnet, P. Alchas, P. Regolini, J.A. Mikszta, R. Pettis, N.G. Harvey.** 52, 17 Dec 2007, Vaccine, Vol. 25, pp. 8833-8842.
84. *Hollow Polymer Microneedle Array Fabricated by Photolithography Process Combined with Micromolding Technique.* **P-C Wang, B.A. Wester, S. Rajaraman, S-J Paik, S-H Kim, M.G. Allen.** Minneapolis, Minnesota, USA, September 2-6, 2009 : s.n. 31st Annual International Conference of the IEEE EMBS. pp. 7026-7029.
85. *An interconnect for out-of-plane assembled biomedical probe arrays.* **A. Aarts, H.P. Neves, C. Van Hoof, R. Puers.** 6, s.l. : IOP, Journal of Micromechanics and Microengineering , Vol. 18, pp. 1-7. 0960-1317.

86. *Structural and microfluidic analysis of hollow side-open polymeric microneedles for transdermal drug delivery applications.* **D.W. Bodhale, A. Nisar, N. Afzulpurkar.** 2010, *Microfluid. Nanofluid.*, Vol. 8, pp. 373-392.
87. *Silicon microneedle electrode array with temperature monitoring for electroporation.* **N. Wilke, C. Hibert, J. O'Brien, A. Morrissey.** 2005, *Sens. Actuators A Phys.*, Vols. 123–24, pp. 319-325.
88. *Microneedle array for transdermal biological fluid extraction and in situ analysis.* **E. Mukerjee, S.D. Collins, R.R. Isseroff, R.L. Smith.** 2004, *Sens. Actuators A Phys.*, Vol. 114, pp. 267–275.
89. *Design and fabrication of MEMS-based microneedle arrays for medical applications.* **P.Y. Zhang, C.L. Dalton, G. Jullien.** 2009, *Microsyst. Technol.*, Vol. 15, pp. 1073-1082.
90. *Investigations of development process of high hollow beveled microneedles using a combination of ICP RIE and dicing saw.* **N. Baron, J. Passave, B. Guichardaz, G. Cabodevila.** 2008, *Microsyst. Technol.*, Vol. 14, pp. 1475-1480.
91. *Geometrical strengthening and tip-sharpening of a microneedle array fabricated by X-ray lithography.* **S. Khumpuang, M. Horade, K. Fujioka, S. Sugiyama.** 2007, *Microsyst. Technol.*, Vol. 13, pp. 209-214.
92. *Microinfusion using hollow microneedles.* **W.Martanto, J.S.Moore, O. Kashlan, R. Kamath, P.M.Wang, J.M. O'Neal, M.R. Prausnitz.** 2006, *Pharm. Res.*, Vol. 23, pp. 104-113.
93. *Assembled microneedle arrays enhance the transport of compounds varying over a large range of molecular weight across human dermatomed skin.* **F.J. Verbaan, S.M. Bal, D.J. van den Berg, W.H.H. Groenink, H. Verpoorten, R. Lüttge, J.A. Bouwstra.** 2007, *Journal of Controlled Release*, Vol. 117, pp. 238-245.
94. *Minimally invasive insulin delivery in subjects with type 1 diabetes using hollow microneedles.* **J. Gupta, E.I. Felner, M.R. Prausnitz.** 2009, *Diab. Technol. Ther.*, Vol. 11, pp. 329–337.
95. *Microfabricated microneedles: a novel approach to transdermal drug delivery.* **S. Henry, D.V. McAllister, M.G. Allen, M.R. Prausnitz.** 1998, *J. Pharm. Sci.*, Vol. 87, pp. 922–925.
96. **J.K. Hickling, K.R. Jones, M. Friede, D. Zehring, D. Chen, D. Kristensen.** *Intradermal Delivery of Vaccines.* World Health Organization & PATH. 2009. Study.
97. *Combined Effect of Low-Frequency Ultrasound and Iontophoresis: Applications for Transdermal Heparin Delivery.* **L. Le, J. Kost, S. Mitragotri.** 2000, *Pharm. Res.*, Vol. 17, pp. 1354-1557.

98. *Transdermal delivery of antisense oligonucleotides with microprojection patch (Macroflux (R)) technology.* **W.Q. Lin, M. Cormier, A. Samiee, A. Griffin, B. Johnson, C.L. Teng, G.E. Hardee, P.E. Daddona.** 2001, *Pharm. Res.*, Vol. 18, pp. 1789-1793.
99. **M. Cormier, P.E. Daddona.** Macroflux technology for transdermal delivery of therapeutic proteins and vaccines, in. [book auth.] J. Hadgraft, M.S. Roberts M.J. Rathbone. *Modified-Release Drug Delivery Technology.* New York : Marcel Dekker, 2003.
100. *Coated microneedles for drug delivery to the eye.* **J. Jiang, H.S. Gill, D. Ghate, B.E. McCarey, S.R. Patel, H.F. Edelhauser, M.R. Prausnitz.** 2007, *Invest. Ophthalmol. Vis. Sci.*, Vol. 48, pp. 4038–4043.
101. *Intrascleral drug delivery to the eye using hollow microneedles.* **J. Jiang, J.S. Moore, H.F. Edelhauser, M.R. Prausnitz.** 2009, *Pharm. Res.*, Vol. 26, pp. 395-403.
102. *Micromechanical devices for intravascular drug delivery.* **M.L. Reed, C.Wu, J. Kneller, S.Watkins, D.A. Vorp, A. Nadeem, L.E. Weiss, K. Rebello, M. Mescher, A.J.C. Smith, W. Rosenblum, M.D. Feldman.** 1998, *J. Pharm. Sci.*, Vol. 87, pp. 1387-1394.
103. *Feeding strategy and the mechanics of blood sucking in insects.* **T. L. Daniel, J.G. Kingsolver.** 1983, *J. Theor.Biol.*, Vol. 105, pp. 661–72.
104. *Mechanics of a mosquito bite with applications to microneedle design.* **M.K. Ramasubramanian, O.M. Barham, V. Swaminathan.** 3, 2008, *Bioinsp. Biomim.* , pp. 046001-10.
105. **V.S. Swaminathan.** *Mechanics of a Mosquito Bite - MS Thesis.* Department of Mechanical and Aerospace Engineering, North Carolina State University. 2006.
106. *Design and mechanical properties of insect cuticle.* **J.F.V. Vincent, U.G.K. Wegst.** 2004, *Arthropod Struct. Dev.*, Vol. 33, pp. 187-99.
107. *High aspect ratio features in poly(methylglutarimide) using electron beam lithography and solvent developers.* **G. Karbasian et al.** *J. Vac. Sci. Technol. B* 30, 06FI01 (2012). <http://dx.doi.org/10.1116/1.4750217>.
108. *TOPICAL REVIEW - SU-8: a photoresist for high-aspect-ratio and 3D submicron lithography.* **A. del Campo, C. Greiner.** s.l. : IOP, 2007, *J. Micromech. Microeng.* , Vol. 17, pp. R81–R95. doi:10.1088/0960-1317/17/6/R01.
109. **MIT Material Property Database.** [Online] <http://www.mit.edu/~6.777/matprops/su-8.htm>.
110. *Determining the Young's modulus and creep effects in three different photodefinable epoxies for MEMS applications.* **K. Wouters, R. Puers.** 2009, *Sensors and Actuators A: Physical.* 10.1016/j.sna.2009.03.021.

111. Georgia Tech Webpage on SU-8. [Online] http://mems.mirc.gatech.edu/msmawebwebsite/members/processes/processes_files/SU8/SU-8.htm#physical.
112. *Young's modulus and interlaminar fracture toughness of SU-8 film on Si wafer*. **S-F Hwang, J-H Yu, B-J Lai, H-K Liu**. s.l. : Elsevier, 2008, *Mechanics of Materials*, Vol. 40, pp. 658–664. doi:10.1016/j.mechmat.2008.02.005.
113. *The mechanical efficiency of natural materials*. **U.G.K. Wegst, M.F. Ashby**. 21, 2004, *Philosophical Magazine*, Vol. 84, pp. 2167-2186. <http://dx.doi.org/10.1080/14786430410001680935>.
114. *Microstructuring of SU-8 Resist for MEMS and Bio-Applications*. **P.K. Dey, B. Pramanick, A. RaviShankar, P. Ganguly, S. Das**. 1, s.l. : International Journal on Smart Sensing and Intelligent Systems, March 2010, *International Journal on Smart Sensing and Intelligent Systems*, Vol. 3.
115. *Characterization of chemically amplified resist for X-ray lithography by Fourier transform infrared spectroscopy*. **T.L. Tan, D. Wong, P. Lee, R.S. Rawat, S. Springham, A. Patran**. 1-2, s.l. : Elsevier, 10 May 2006, *Thin Solid Films*, Vol. 504, pp. 113-116.
116. **S. Timoshenko**. *Theory of Elastic Stability*. New York : McGraw-Hill, 1961.
117. **R.S. Khurmi**. *Strength of Materials*. s.l. : S. Chand, 2010. pp. 491-492. ISBN 81-219-2822-2.
118. *Insertion of microneedles into skin: measurement and prediction of insertion force and needle fracture force*. **S.P. Davis, B.J. Landis, Z.H. Adams, M.G. Allen, M.R. Prausnitz**. 2004, *Journal of Biomechanics*, Vol. 37, pp. 1155-1163.
119. *Biomedical and Fluid Flow Characterization of Microneedle-based Drug Delivery Devices*. **I. Haider, R. J. Pettis, N. Davison, C. Richard, D. Jeffrey**. San Diego, CA : s.n., 2001. Proceedings from the 25th Annual Meeting of the American Society of Biomechanics.
120. *Fabrication of multi-layer SU-8*. **A. Mata, A.J. Fleischman, S. Roy**. 2006, *J. Micromech. Microeng.*, Vol. 16, pp. 276–284.
121. *Side-Opening Hollow Microneedles for Transdermal Drug Delivery*. **Wijaya Martanto et al.** s.l. : IEEE Proceedings, 2005.
122. *Hollow Polymer Microneedle Array Fabricated by Photolithography Process Combined with Micromolding Technique*. **Po-chun Wang et al.** Minneapolis : s.n., Sept 2-6, 2006. 31st Annual International Conference of the IEEE EMBS, US.
123. *A high aspect ratio SU-8 fabrication technique for hollow microneedles for transdermal drug delivery and blood extraction*. **B. Paul Chaudhri, F.**

- Ceyssens, P. De Moor, C. Van Hoof, and R. Puers.** 2010, J. Micromech. Microeng., Vol. 20, p. 064006 (6pp).
124. **R. Hull.** *Properties of Crystalline Silicon.* London : INSPEC, 1999.
125. *Design of chemical composition and optimum working conditions for trivalent black chromium electroplating bath used for solar thermal collectors.* **M.R. Bayati et al.** 2005, J. Renew Energy, Vol. 30, pp. 2163-2178.
126. *A numerical and experimental study on gap compensation and wavelength selection in UV-lithography of ultra-high aspect ratio SU-8 microstructures.* **Yang R, Wang W.** 110, 2005, Sensors Actuators B, pp. 279–88.
127. *Variation of absorption coefficient and determination of critical dose of SU-8 at 365 nm.* **Gaudet M et al.** 88 , 2006, Appl. Phy. Lett., p. 024107.
128. *Fabrication process of high aspect ratio elastic structures for piezoelectric motor applications.* **L. Dellmann, S. Roth, C. Beuret, G. Racine, H. Lorenz, M. Despont, P. Renaud, P. Vettiger, and N. de Rooij.** Chicago : s.n. Proc. Transducers 1997. pp. 641-644.
129. *Microneedles for Transdermal Drug Delivery.* **M.R. Prausnitz.** 2004, Advanced Drug Delivery Review, Vol. 56, pp. 581-587.
130. *A Novel Microneedle Array Integrated with a PDMS Biochip.* **S-J Paik, J-M Lim, I. Jung, Y. Park, S. Byun, S. Chung, K. Chun, J. Chang, D. Cho.** Boston : s.n., 2003. Transducers' 2003 - 12th International Conference on Solid State Sensors, Actuators and Microsystems.
-